QATAR UNIVERSITY

COLLEGE OF ENGINEERING

MICROMODEL STUDY ON COLLOID RETENTION AND MOBILIZATION UNDER DIFFERENT GEO-CHEMICAL CONDITIONS DURING SINGLE AND TWO-PHASE FLOW

BY

SAFNA NISHAD

A Dissertation Submitted to

the College of Engineering

in Partial Fulfillment of the Requirements for the Degree of

Doctorate of Philosophy in Civil Engineering

June 2020

COMMITTEE PAGE

The members of the Committee approve the Dissertation of
Safna Nishad defended on 30-04-2020

Riyadh I. Al-Raoush
Thesis/Dissertation Supervisor

Approved:

Khalid Kamal Naji, Dean, College of Engineering

ABSTRACT

Nishad, Safna, Doctorate: June : 2020, Doctorate of Philosophy in Civil Engineering

Title: Micromodel Study on Colloid Retention and Mobilization under different Geo-Chemical Conditions during Single and Two-Phase Flow

Supervisor of Dissertation: Dr. Riyadh I. Al-Roush.

Understanding the transport of colloids and colloid-facilitated transport of contaminants is essential for efficient cleanup and remediation processes. Various factors and mechanisms contributing to their retention in the porous media have been studied indirectly through laboratory column breakthrough analysis and directly using visualization studies. Micromodels are analogs to porous media that allow the real-time visualization of pore-scale processes that occur at highly controllable physio-chemical conditions in the laboratory scale.

In this thesis, we used a glass micromodel with representative geometry to observe the pore-scale mechanisms during colloid retention and mobilization experiments in a saturated and unsaturated porous media. The focus of this research was to investigate the colloid retention mechanisms under different physio-chemical conditions such as variable colloid type, solution ionic strength, and solution pH. Various colloid retention sites in unsaturated porous media were identified from the captured images and videos during drainage (using CO_2 gas) in a saturated micromodel. Quantitative analysis of colloid mobilization was performed using image-processing algorithms on a Representative Elementary Area (REA) image of the micromodel before and after drainage.

This study also investigated colloid mobilization from AWI during imbibition

in porous media. The impact of colloid hydrophobicity on mobilization was observed in a micromodel. The visual findings explained with the theoretical conceptualization of the forces acting on a colloid at AWSI. The colloid reattachment on SWI found during the dissolution of the gas bubble for hydrophilic colloids due to their greater capillary potential. Whereas, the lifting-capillary forces on hydrophobic colloids resulted in aggregation of excess colloids on AWI.

This study also examined the retention and release of colloids under the influence of perturbations in flow rate and solution chemistry. The retention of three different types of colloids (i.e., favorable, unfavorable, and medium favorable conditions) was observed visually in a micromodel. The pore-scale visualizations reveal the impact of colloid deposition profile on colloid release with an increase in flow rate and solution pH as well as a decrease in solution ionic strength. The results from this study show the dependence of favorability of interaction conditions on colloid deposition profile as well as the colloid release during hydro-chemical perturbations in saturated porous media.

This dissertation accompanied by supplementary material showing video images of the illustrated processes.

DEDICATION

To my little Jennah and my beloved Husband

ACKNOWLEDGMENTS

I would like to express my sincere gratitude to *God Almighty* for all the blessings and mercy for the successful completion of this thesis.

Many thanks to my supervisor, Dr. Riyadh Al-Raoush, for his incredible support, guidance, valuable advice, and constructive criticism throughout the course that led to the successful completion of this work.

I greatly appreciate and acknowledge the support receive from the center for advanced material (CAM) and Qatar University Mechanical workshop for various analysis and fabrication works. I am equally thankful to Mr. Abdul Aziz, Mr. Siju Joseph, Mr. Sivaprasad, and Mr. Sunith, for their technical support during the entire period of my research. I would also like to extend my sincere thanks to my Colleagues Dr. Anchu and Mrs. Reem, for their help in many ways in my research work. I appreciate my research team for their cooperation, support, and positive comments through my research.

I am indebted to the entire department of Civil Engineering at Qatar University for their excellent collaboration and support by providing me lab equipment and facilities to accomplish my research objectives.

I would like to express my deepest gratitude to my family: my father, mother, brother, sister, and in-laws for their immense support and encouragement to achieve this degree. Finally, these acknowledgments would be incomplete without expressing my sincere gratitude to my husband. Without his endless patience, care, support, motivation, encouragement, it would have been impossible to achieve my dream. Special thanks to my Jennah, for being the best daughter in the world. You are there

with me from the beginning through this journey and never complain to me on my busy and late-night works.

TABLE OF CONTENTS

LIST OF TABLES

LIST OF FIGURES

LIST OF ABBREVIATIONS

Abbreviation	**Definition**
SWI	Solid-Water Interface
AWI	Air-Water Interface
AWSI	Air-Water-Solid Interface
DLVO	Derjaguin, Landau, Verwey, and Overbreek
CFT	Colloid Filtration Theory
pH_{pzc}	pH corresponding to point of zero charge
FFSZ	Forward Flow Stagnation Zone

LIST OF NOMENCLATURE

Symbol	Meaning	Unit
η_0	Single collector efficiency	
η_D	Single collector efficiency under diffusion	
η_I	Single collector efficiency under interception	
η_G	Single collector efficiency under sedimentation	
η	Collector efficiency	
P_e	Pacelet number	
k_B	Boltzmann's constant	JK^{-1}
T	Temperature	K
ν	Fluid velocity	m/s
μ	Dynamic viscosity of the fluid	Pa.s
υ	Kinematic viscosity of the fluid	m^2/s
d_c	Colloid diameter	µm
d_g	Grain diameter	µm
g	Acceleration due to gravity	m/s^2
ρ	Density of fluid	g/cc
ρ_c	Density of colloid	g/cc
α	Collision efficiency	
C	Effluent colloid concentration	mg/L
C_0	Influent colloid concentration	mg/L
n	The porosity of the porous medium	
L	Length of the column	m

Symbol	Meaning	Unit
Φ_{tot}	Total interaction energy	J
Φ_{vdW}	Van der Waals interaction energy	J
Φ_{DL}	The double-layer interaction energy	J
Φ_{Born}	Born repulsion energy	J
σ_{Born}	Born collision parameter	nm
Φ_{hyd}	Hydrophobic interaction energy	J
Φ_c	Capillary energy	J
D	Separation Distance	nm
A_{123}	Hamaker Constant for surface 1 and 3 in medium 2	J
r_1 & r_2	Colloid radii for two colloids interacting each other	μm
λ	Characteristic wavelength	nm
r	Radius of colloid	μm
A_{11} A_{22} and A_{33}	Haymaker constants of different medium	J
κ	Inverse Debye Huckel length	m^{-1}
ψ_1 and ψ_2	Surface potentials of two interacting surfaces	mV
ψ_c	Colloid surface potential	mV
ε	The dielectric constant of the medium	
ε_0	The permittivity of free space	$C^2J^{-1}m^{-1}$
e	Electronic charge	C
I	The ionic strength of the solution	Mol/m^3
N_A	Avogadro number	Mol^{-1}

Symbol	Meaning	Unit
c	The molar concentration of electrolyte	Mol/m^3
z	Valence of electrolyte	
a and b	Constants to evaluate force constants for hydrophobic interactions	
θ	Colloid contact angle	Degree
θ_2	The colloid contact angle of the second surface in hydrophobic interaction calculation	Degree
K_{123}	Force constants for hydrophobic interaction	
F_L	Hydrodynamic lift force	N
F_D	Hydrodynamic drag force	N
$\partial v/\partial r$	Hydrodynamic shear at distance r	s^{-1}
F_c	Capillary forces	N
φ	Angle determining the position of GWI on the colloid surface	Degree
σ	Surface tension force	N/m
F_A	Adhesion forces	N
β	Collector dynamic contact angle	Degree
F_f	Frictional force	N
F_N	Net normal force acting on the solid surface	N
μ_f	The friction coefficient of the solid surface	
T_A	The torque due to adhesion forces	Nm
T_D	The torque due to hydrodynamic drag	Nm

Symbol	Meaning	Unit
l_x	Lever arm for adhesion forces	m
l_c	Lever arm for capillary forces	m
l_D	Lever arm for hydrodynamic drag forces	m
K	Composite Young's modulus	$\mu N/m^2$
$\boldsymbol{F_c^x}$	The horizontal component of the capillary force	N
$\boldsymbol{F_c^y}$	The vertical component of capillary force	N
ϕ_{min1}	Primary energy minimum	J
ϕ_{min2}	Secondary energy minimum	J
ϕ_{max1}	Repulsive energy barrier	J
d_0	Separation distance corresponding to the primary minimum	nm
V	AWI velocity	m/s
h	Water thin-film thickness	μm
Ca	Capillary Number	

CHAPTER 1: INTRODUCTION

1.1. Background and Motivation

The fate and transport of colloids through the subsurface have recently attracted significant attention by various researchers due to its importance in different applications, including groundwater recharge and contamination, filtration in water and wastewater treatment process as well as oil and gas production [1–4]. Also, the colloid-facilitated transport of pathogens, pesticides, and radionuclides can significantly enhance the movement of contaminants in subsurface environments [5–7]. The colloid immobilization in the porous media can restrict contaminant transport in the subsurface water bodies. Therefore, identifying the potential colloid retention mechanisms in porous media is essential to predict the groundwater quality and prevent the spread of contaminants.

Besides the retention, colloid release can occur during perturbations in hydro-geochemical properties such as flow rate, solution ionic strength, pH, etc. Moreover, two-phase flow induced by alternate drying and infiltration of the porous media mobilize the retained colloids and transport them along with the interfaces into the groundwater aquifers. Researchers are also interested in multi-phase flow associated with environmental and industrial processes such as enhanced oil recovery (EOR), geological CO2 sequestration, non-aqueous phase liquid remediation, etc. Colloidal transport is an emergent phenomenon that occurs together with the above processes and affects oil recovery, relative permeability, and groundwater quality. Therefore, understanding the colloid transport and release mechanisms in unsaturated or multi-phase systems improve insights in the above industrial applications.

The colloid attachment on collector surfaces was predicted by Colloid filtration

theory (CFT), which was developed based on attachment via interception, sedimentation, and Brownian diffusion [8]. CFT provides a single collector efficiency for favorable colloid-collector interaction. Previously, colloid transport experiments were conducted in laboratory packed columns. The breakthrough concentration curves obtained from column experiments provide colloid attachment efficiency. The breakthrough curves helped to determine the effect of different factors, including flow rate, solution chemistry, type and size of colloids, etc. on overall retention of colloids. The discrepancy in the observed experimental results and CFT predictions under saturated conditions was reported as a straining effect based on the column dissection analysis [9,10]. Straining was defined as retention of larger sized colloids or aggregates in small pore constrictions or grain-grain contacts. Therefore, in saturated porous media, the interaction of colloids with collectors (or Solid-Water Interfaces (SWI)) and other colloids will result in colloid attachment and straining, respectively.

The retention of colloids in unsaturated porous media was complicated by the presence of Air-Water Interfaces (AWI). The elution curves showed higher colloid retention for unsaturated systems compared to saturated porous media. However, the pore-scale mechanisms responsible for colloid retention were not identified from the laboratory column studies but was hypothesized. For example, the retention of colloids on AWI was suggested based on the observation of excessive eluted colloid concentration with the moving AW front during drainage or imbibition [11]. Later on, researchers started pore-scale visualization on sand columns using confocal microscopy. They realized that the colloids were retained on Air-Water-Solid Interfaces (AWSI) and thin water film around the grains and not on AWI [12–14].

The interaction potential of the colloids to various interfaces can be evaluated from the DLVO theory as the sum of van der Waals and electrostatic energies [15,16].

Direct comparison of calculated DLVO energy and pore-scale visualization studies reveal the application of the theory to predict colloid interaction with SWI and other colloids [1,12,17,18]. The inadequacy of the DLVO approach in predicting colloid interaction with AWI, AWSI, and thin films resulted in the inclusion of non-DLVO forces, including hydrophobic and capillary forces in the theoretical evaluations [19–24].

Later on, micromodels fabricated on different materials (like silica, glass, poly-methyl methacrylate (PMMA), polydimethylsiloxane (PDMS), etc.) were adopted to represent two-dimensional porous media [1,18,31,32,23–30]. The transparency of those materials allows the direct visualization of the relevant phenomena that occurred during transport experiments using optical microscopy. Highly controllable physical and chemical environments in the micromodel enhance its applicability to focus on relevant and interested experimental conditions. Several studies have been conducted using micromodels with idealized geometries such as capillary channels, homogenous or triangulation networks of pore bodies, and throats [18,24,26,33,34]. Colloid transport in saturated micromodels was limited to visualization of clogging behavior on homogenous porous media as a function of the relative size of colloid and pore throat size, flow velocity, and ionic strength [27,28,35–40]. Micromodel experiments on unsaturated flow were confined to the mechanisms of colloid attachment on AWI in steady-state flow conditions [1,25,41–43]. The colloid covered surfaces and capillary channels of various cross-sections have been adopted by the researchers to study the mobilization of colloids from SWI by the moving AWI [23,34,44]. Zhang et al. [45] first quantified colloid transport under transient two-phase flow experiments in a micromodel with a triangulated network of pores. The fluorescent intensity of the breakthrough colloids in the outlet channel was measured using a confocal microscope,

and the corresponding concentration was obtained from the calibration charts. The impact of transient flow, hydrophobicity, and interfacial tension were investigated using the breakthrough curves and visual observations [18,31,33]. However, the hydrophobic micromodel with the simplified geometry of their system restricts the direct comparison of their results to natural porous media.

Recently, researchers started to fabricate the micromodels with real sand-stone geometry obtained from computer tomography images to analyze hydrocarbon recovery, CO2 sequestration, and specific biomedical applications [4,46,55,47–54]. Combining the application of physically representative micromodel with colloid transport studies can benefit in upscaling the real pore-scale mechanisms to reservoir scale. Therefore, the micromodel used in this study resembles the geometry of actual sandstone porous media to conduct colloid transport studies in single and two-phase flow systems.

Previous research focused on the impact of several physical and chemical factors such as type of colloid, flow velocity, solution chemistry (i.e., ionic strength, pH), etc. on colloid transport using laboratory column breakthrough curves or mechanistic models. Various retention and mobilization mechanisms were hypothesized in previous studies based on colloid elution curves due to the lack of visualization data. Thus, this proposed research will provide visualization evidence on the mechanisms of retention and mobilization of different types of colloids under the influence of solution chemistry, flow velocity, and two-phase flow.

1.2. Research objectives and significance

The current research provides a better fundamental understanding of colloid interactions in saturated porous media, as shown in Figure 1 under different

geochemical conditions, with emphasis on colloid transport in subsurface soil and sediments. The understanding of the various pore-scale mechanisms responsible for the mobilization of the deposited colloids under the influence of perturbations in solution chemistry, flow rate, and two-phase flow is beneficial to design efficient clean-up and remediation measures. The goal of this study is to obtain visualization evidence on the colloid retention and mobilization mechanisms under different geochemical conditions in porous media.

The specific objectives of the research presented in this thesis are to:

1. Investigate the retention mechanisms of hydrophilic and hydrophobic colloids in a saturated hydrophilic micromodel under different solution chemistry (i.e., ionic strength and pH) and compare with DLVO theory.
2. Evaluate the effect of hydrophobicity, solution ionic strength, and pH on a colloid mobilization by moving AWI during two-phase flow (i.e., drainage using CO_2).
3. Examine the detachment of colloids retained on AWI during imbibition.
4. Explore the colloid deposition profiles and the mobilization mechanisms for different types of colloids under favorable and unfavorable attachment conditions in saturated porous media during perturbations in flow rate and solution chemistry.

The results of this research are significant in advancing the understanding of colloid facilitated contaminant transport in the subsurface.

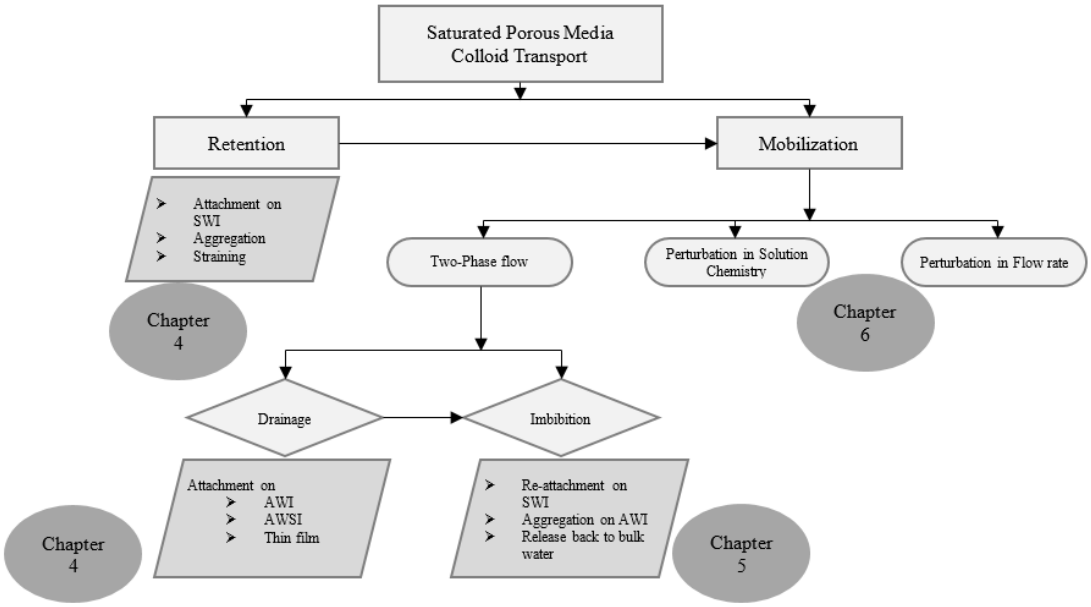

Figure 1. The study plan for this current research, which advances the knowledge of colloid transport in saturated porous media

1.3. Thesis Outline

The thesis consists of 7 main chapters. The details of each chapter are as following:

Chapter 1 introduces the background, motivation, and objectives of the research.

Chapter 2 provides a detailed review of current and relevant literature in the field of colloid transport.

Chapter 3 describe the materials, equipment, and the experimental set up for colloid transport and mobilization study.

Chapter 4 reports the results of an extensive experimental study to explain the colloid retention mechanisms under different geochemical conditions during single and Two-phase flow. The experimental program included the visualization of colloid deposition on a saturated glass micromodel with representative geometry and

mobilization by the moving AWI during drainage with CO_2. Two types of colloids, hydrophilic and hydrophobic colloids, under variable solution ionic strength and pH were studied.

Chapter 5 presents the different mobilization mechanisms of hydrophilic and hydrophobic colloids from the Air-Water interface during imbibition.

Chapter 6 provides pore-scale visualization evidence on the deposition and mobilization profile of different types of colloids in saturated porous media under varying favorability conditions. Three types of colloids were selected based on their interaction with the collector surface; unfavorable, favorable, and medium favorable conditions. Colloid mobilization in response to the perturbations in solution chemistry (i.e., decrease in solution ionic strength, increase in solution pH), and the flow rate was visually studied.

Finally, Chapter 7 presents the summary and conclusion of overall research work.

CHAPTER 2: BACKGROUND AND LITERATURE REVIEW

2.1. Colloid transport and retention in porous media

Colloids are particulate matter typically range in size from 1nm to 10 μm [56]. The subsurface porous media contain organic, inorganic, or biological colloids within soils and sediments. Mineral fines such as clay and oxide precipitates, organic macromolecules, bacteria, viruses, etc. are examples of colloids present in subsurface environments [5,38,57–59]. Relatively higher surface area and unbalanced electrical charges on the surface of these colloids cause the formation of stable complexes with various contaminants, including metals [60,61], pesticides [62], and radionuclides [63,64]. Moreover, some colloids are themselves toxic or pathogens (i.e., bacteria and viruses) [65–68]. Therefore, mobile colloids in the subsurface environments have received considerable attention in the past few decades because of their environmental impact on underground aquifers [69–72]. However, the immobilization of the colloids on various retention sites in the porous media can limit the mobility and outbreak of contaminants towards groundwater sources. Hence, understanding various retention mechanisms of colloids in subsurface environments is important to achieve effective treatment methods.

Previous researchers explained several processes of colloid transport in porous media such as advection, dispersion, physicochemical interactions, and straining. Among the processes, straining and physicochemical interactions play a vital role in the retention of colloids. Straining refers to colloid entrapment in small pore constrictions and grain-grain contacts. The physicochemical processes result in attachment of colloids on the collector surfaces by three primary transport mechanisms: interception, sedimentation, and Brownian diffusion. Attachment of the colloids

moving along the streamline occur on the collector surface by interception due to the zero fluid velocity (i.e., no-slip condition) near the solid boundary. Sedimentation or gravitational settling of the particles occurs due to its higher density than that of the fluid. Brownian diffusion is significant for smaller sized colloids. Physicochemical interaction of colloids can result in attachment on various interfaces, including Solid-Water Interfaces (SWI), Air-Water Interfaces (AWI), and other colloids, as shown in Figure 2. Additionally, more complicated retention mechanisms observed for partially saturated porous media due to the presence of air in the system such as Air-Water-Solid Interfaces (AWSI) and thin water film (enveloping solid grains) in addition to the above [10,13,17,73,74] (Figure 2).

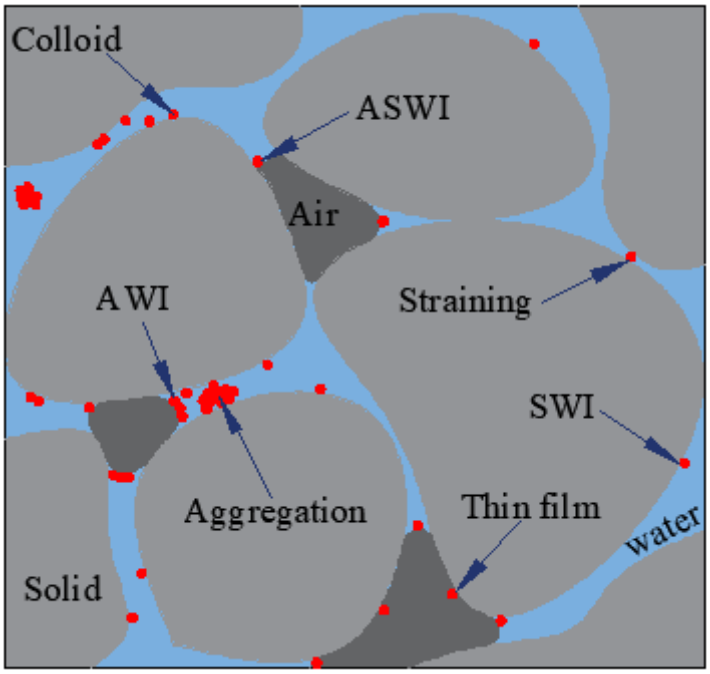

Figure 2. Schematic representation of porous media showing the typical phases (solid, water, air, and colloids) and colloid retention mechanisms (SWI, AWI, AWSI, thin water film, aggregation, and straining)

The physicochemical attachment is directly related to the interaction potential of the colloid with different interfaces. Therefore, theoretical considerations on the major forces acting on a colloid interacting with various interfaces were examined first to give broader knowledge in the colloid retention or mobilization process. Also, a review of current experimental and numerical studies regarding colloid transport, retention, and mobilization in porous media can suggest the necessity for additional work.

2.2. Theoretical considerations

Colloid Filtration Theory (CFT) has been frequently used to quantify colloid retention in porous media [8]. Two processes involved in colloid deposition on collector surfaces: (1) colloids transported towards the collector surface from the bulk fluid; and (2) attachment on the collector surfaces. Three transport mechanisms, including interception, sedimentation, and Brownian diffusion, govern the transport of colloid, as shown in Figure 3. Colloids come closer to the collector surface by the above transport mechanisms are deposited if the interaction potential of the particular interaction (i.e., colloid-colloid, colloid-SWI, and colloid-AWI) is attractive. Traditional DLVO theory (Derjaguin, Landau, Verwey, and Overbreek, [15,16]) considers the force balance between the attractive van der Waals force and repulsive electrostatic double-layer forces to determine the interaction potential. However, the failure of classical DLVO theory in predicting the retention of colloids on AWI explains the existence of non-DLVO forces, as reported in previous experimental studies [2,22]. Hydrophobic forces, Born repulsion, and steric forces are considered in colloid attachment or deposition study, whereas hydrodynamic and capillary forces are considered in colloid detachment or desorption study. Torque balance considerations were adopted to evaluate colloid

detachment from the collector surfaces theoretically. Colloid Filtration Theory, DLVO theory, major non-DLVO forces, and torque balance are explained in the following sections.

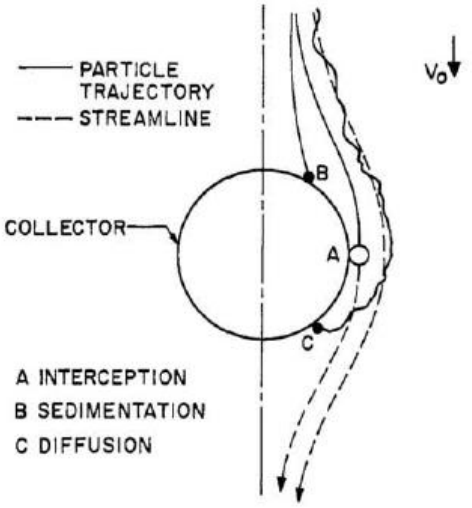

Figure 3. Schematic of the three colloid filtration mechanisms [8]

2.2.1: Colloid Filtration Theory (CFT)

Colloid filtration theory was based on a single spherical collector surrounded by an infinite fluid [8]. The collector efficiency (η_0) was defined as the fraction of the transported colloid that was captured on the collector surface via three transport mechanisms: interception, Brownian diffusion, and sedimentation, as shown in Figure 3. The single spherical collector efficiency can be calculated as the sum of individual collector efficiency under diffusion (η_D), interception (η_I), and sedimentation (η_S).

$$\eta_D = 4.04 {P_e}^{-2/3} = 0.9 \left(\frac{k_B T}{\mu d_g d_c \nu} \right)^{2/3} \quad (1)$$

$$\eta_I = \frac{3}{2} \left(\frac{d_c}{d_g} \right)^2 \quad (2)$$

$$\eta_G = \frac{(\rho_c - \rho) g d_c^2}{18 \mu v} \quad (3)$$

$$\eta_o = \eta_D + \eta_I + \eta_G \quad (4)$$

Where P_e is the Paclet number, μ is the fluid viscosity, ν is the interstitial fluid velocity, d_c is the colloid diameter, d_g is the collector diameter, ρ is the density of the fluid, ρ_c is the density of the colloid, k_B is the Boltzmann's constant, T is the temperature, and g is the acceleration due to gravity.

The fraction of transported colloid that was captured on the collector surface was related to the fraction that contacts the collector surface using the term collision efficiency (α).

$$\eta = \alpha \eta_o \quad (5)$$

For favorable interaction, collision efficiency was taken as unity and for unfavorable conditions; collision efficiency can be calculated by analyzing particle breakthrough curves from column experiments by:

$$ln \frac{C}{C_0} = -\frac{3}{2}(1 - n) \alpha \eta_o \left(\frac{L}{d_g}\right) \quad (6)$$

Where C and C_0 are the effluent and influent colloid concentration, respectively, n is the porosity of the sand column, L is the column length, and d_g is the individual collector diameter.

Rajagopalan and Tien, (1976) modified the CFT using the Happel sphere-in-cell model incorporating van der Waals forces and hydrodynamic retardation to the mechanisms of interception and sedimentation, whereas diffusion was treated as in CFT. Later, several researchers modified CFT to obtain correlation functions under specific conditions [75–79].

2.2.2: DLVO theory

According to the DLVO theory, the interaction energy of a colloid interacting

with other interfaces such as SWI, AWI, and other colloids can be calculated as the sum of van der Waals and electrostatic double-layer energies [15,16].

$$\phi_{tot}(D) = \phi_{vdW}(D) + \phi_{DL}(D) \quad 7$$

Where ϕ_{tot}, ϕ_{vdW}, and ϕ_{DL} are the total, van der Waals and double layer energies respectively, and D is the separation distance between the colloid and the interface.

The attractive interaction between two closely spaced surfaces due to the intermolecular forces arising from spontaneous polarization of the molecules into dipoles is generally called the London-van der Waals force. The retarded van der Waals interaction energy can be determined using the expression [80] for two spheres of radius r_1 and r_2:

$$\phi_{vdW}(D) = -\frac{A_{123} r_1 r_2}{6D(r_1+r_2)}\left(1 + {}^{14D}/_{\lambda}\right)^{-1} \quad 8$$

Where A_{123} [ML^2T^{-2}] is the complex Hamaker constant for surfaces 1 and 3 (i.e., colloid and collector) in medium 2 (i.e., aqueous solution) and λ is the characteristic wavelength that is often taken as 100 nm [80]. For the sphere-plate interactions $r_1 r_2/(r_1 + r_2)$ in Equation [8] is replaced by r, which is the colloid radius.

The complex Hamaker constant can be estimated from the Hamaker constants of each medium using the expression given by [81]:

$$A_{123} = \left(\sqrt{A_{11}} - \sqrt{A_{33}}\right)\left(\sqrt{A_{22}} - \sqrt{A_{33}}\right) \quad 9$$

Where A_{11}, A_{22}, and A_{33} are the Hamaker constants of the colloid, collector, and the aqueous solution, respectively. The Hamaker constants of polystyrene latex, glass, water, CO_2, and air are reported to be 6.6 x 10^{-20}, 6.34 x 10^{-20}, 3.7 x 10^{-20} J, 6.2 x 10^{-22} J and zero, respectively [81]. Hence, A_{123} is equal to 3.84 x 10^{-21} J for polystyrene-water-glass systems, 4.17 x 10^{-21} J for polystyrene-water-polystyrene systems, -1.24 x 10^{-20} J for polystyrene-water-air systems and -1.08 x 10^{-20} J for polystyrene-water-CO_2

systems indicating attractive van der Waals interaction of colloids with other colloids and glass systems, whereas repulsive interaction for colloid-AWI/GWI interactions.

Dispersed colloid particles are surrounded by clouds of ions in a double layer consisting of the Stern layer and the Diffuse layer. The stern layer comprised of ions of opposite polarity of the colloid surface, and the diffuse layer consists of loosely bound ions having the same polarity of the colloid surface. Debye length describes the thickness of the diffuse double layer measuring from the surface of the colloid to the outer edge of the diffuse layer. The diffused double layers formed around the colloid and the interacting surface in the electrolyte medium exert an attractive or repulsive force between two surfaces depending on the surface charges. The attractive force between two unlike-charged surfaces results in favorable interaction, and repulsive interaction of two like-charged surfaces induce unfavorable interaction. The electrostatic double-layer forces generated between two charged colloid surfaces due to the overlap of diffuse double layers can be determined from the following expression [82].

$$\phi_{DL} = \frac{\pi\varepsilon\varepsilon_0 r_1 r_2}{r_1+r_2}\left\{2\psi_1\psi_2 \ln\left[\frac{1+\exp(-\kappa D)}{1-\exp(-\kappa D)}\right] + (\psi_1^2+\psi_2^2)\ln[1-\exp(-2\kappa D)]\right\} \quad 10$$

where ε is the dielectric constant of the medium; ε_0 is the permittivity of free space; r_1 and r_2 are the radii of the two colloids; ψ_1 and ψ_2 are the surface potential of the colloids, and κ is the inverse Debye-Huckel length calculated from the following equation [81].

$$\kappa^{-1} = \sqrt{\frac{\varepsilon\varepsilon_0 k_B T}{2e^2 I N_A}} \quad 11$$

where the constants are listed in Table 1, and I is the ionic strength of the solution given by

$$I = \frac{1}{2}\sum_{j=1}^{n} c_j z_j^2 \quad 12$$

where c is the molar concentration of the electrolyte, and z is the valence of the electrolyte.

Table 1. Values of constants used for DLVO energy calculations

Parameter	**Value**
The dielectric constant of water, ε	80.4
Permittivity of free space, ε_0, ($C^2J^{-1}m^{-1}$)	8.85 x 10^{-12}
Electronic charge, e, (C)	-1.602 x 10^{-19}
Avogadro Number, N_A, (mol^{-1})	6.022 x 10^{23}
Boltzmann's constant, k_B, (JK^{-1})	1.381 x 10^{-23}
Absolute temperature, T, (K)	298

The colloid-SWI/AWI interactions are treated as sphere-plate interaction, and a similar expression can be obtained after replacing $\frac{r_1 r_2}{(r_1+r_2)}$ as the radius of the colloid, r. ψ_c is the surface potential for the colloid.

Measured zeta potentials of the colloids are used in place of their surface potential in earlier studies [83]. Zeta potentials of glass surface typically range between -10 mV to -85 mV depending on the ionic strength and pH of the electrolyte solution [84–86]. The reported zeta potential values of AWI range between +20 to -120 mV [42,87].

The net energy versus separation distance for a collector and colloid interaction can be drawn, as shown in Figure 4 [88]. The attachment occurs for negative interaction energy whereas, colloids repelled from the surface for positive interaction energy. For favorable interaction (silver colloid – iron oxide), the DLVO energy is negative at all separation distance. However, the effect of short-range van der Waals attraction and long-range double-layer repulsion results in two energy minima (i.e., primary energy minima and secondary energy minima) and one energy maxima (i.e., energy barrier)

for unfavorable interactions. The repulsive barrier for unfavorable interaction (silver colloid – quartz) limits the colloidal attachment to the surface at primary minima. However, a secondary minimum exists where colloids may attach to the surface at separation distances tens of nanometer from the collector surface. The depth of secondary minima changes with the solution chemistry as the double layer forces are affected. The colloids attached at the secondary minimum may elude from the porous media as it is sensitive to solution chemistry and fluid flow [89].

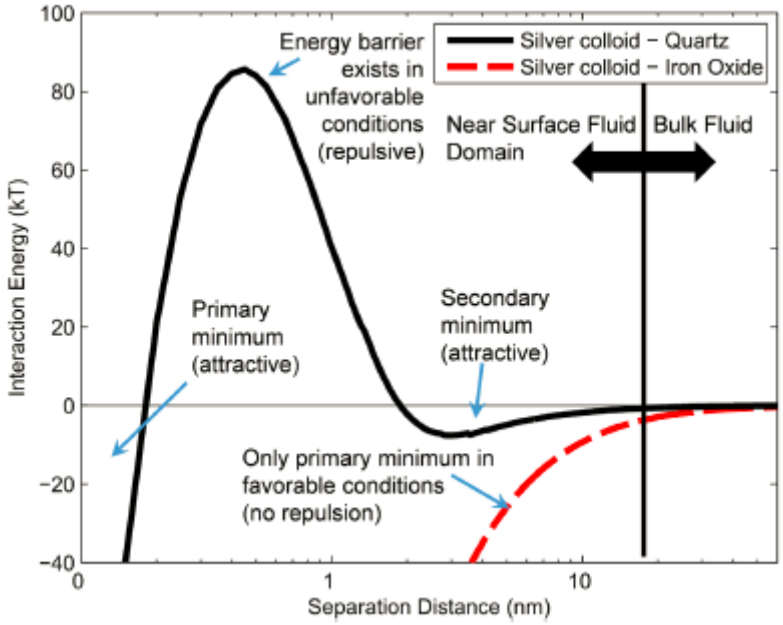

Figure 4. The distribution of colloid surface interaction potential with separation distance for favorable and unfavorable interaction [88]

Previous studies revealed some discrepancies between the predicted DLVO energy and the observed retention behavior of colloids in the column as well as micromodel experiments [90,91]. Non-DLVO forces such as hydrophobic forces, born repulsion, and capillary forces are introduced in the potential energy calculation in

addition to the classical DLVO forces. These forces are described in the following sections.

2.2.3: Hydrophobic forces

The hydrophobic force is attractive between two hydrophobic surfaces [19,20]. Hence, the hydrophobic forces can affect the interaction of hydrophobic colloids with AWI and other colloids since AWI is superhydrophobic [92,93].

The hydrophobic interaction energies between the particles and the interfaces can be calculated based on the respective contact angles. The following empirical correlation can be used to quantify the hydrophobic energy for a sphere-plate system [94].

$$\emptyset_{hyd}(D) = -\frac{K_{123}r}{D} \quad 13$$

where K_{123} is the force constant for the asymmetric hydrophobic interaction between macroscopic bodies 1 and 2 in medium 3. The value of K_{123} can be determined as [94]

$$logK_{123} = a\left(\frac{\cos\theta+\cos\theta_2}{2}\right) + b \quad 14$$

where θ is the contact angle on the colloid surface (Table 1) and θ_2 is the contact angle of the second surface. The contact angle of AWI was reported as 180^0 [94]. The terms *a* and *b* are system-specific constants and are reported as a = -6 and b = -22 for polystyrene colloids and AWI [2], a = -5 and b = -20 for bacteria and AWI [94], and a = -7 and b = -18 for silanated glass sphere and silanated glass plate [95].

2.2.4: Born repulsion

Overlap of electron clouds of atoms of two interacting surfaces exerts a short-range repulsive force called Born repulsion. This force is dominant at a separation distance less than 1 nm, and it is insignificant for larger distance compared to the DLVO

forces. Born repulsive energy can be calculated for a sphere-plate interaction using the following expression [96,97].

$$\emptyset_{Born}(D) = \frac{A_{123}\sigma_{Born}^{6}}{7560}\left[\frac{8r+D}{(2r+D)^{7}} + \frac{6r-D}{D^{7}}\right] \quad 15$$

Where σ_{Born} is the Born collision parameter and is usually taken as 0.5 nm [96,98]. The value of the collision parameter was observed to change only the depth and location of primary minima and did not affect the energy maxima and secondary energy minima [99,100]. Some researchers depicted Born repulsion energy as a vertical straight-line located around 0.136 nm from the origin due to its steep decay nature with separation distance [19]. Ryan and Gschwend (1994) have increased the collision parameter to 2 nm to remove the energy barrier in the calculated DLVO profiles and to explain the observed detachment behavior of colloids. In some studies, the collision parameter was set to 0.26 nm to achieve a distance of 0.157 nm for the primary minimum depth [19,102].

Born repulsion due to the positive value of Hamaker constant hinders colloid deposition or aggregation along with the electrostatic repulsion. However, for negative values of Hamaker constant as in the case of polystyrene colloid-AWI interaction, Born interaction can be attractive and promote attachment [103].

2.2.5: Hydrodynamic forces

The colloid particles subject to hydrodynamic forces in a flowing fluid. Hydrodynamic forces are mainly considered in the detachment studies where the drag and lift forces result in the release of the deposited colloids.

For laminar flow in the porous media, lift and drag forces can be calculated from the following expressions [104–107]:

$$F_L = \frac{81.2\mu(\partial v/\partial r)^{1.5} r^3}{\upsilon^{0.5}} \quad 16$$

$$F_D = 10.205\,\pi\mu\,(\partial v/\partial r) r^2 \quad 17$$

Where ν is the pore water or AWI velocity, $(\partial v/\partial r)$ is the hydrodynamic shear at a distance r from the collector surface, μ and υ are the absolute and kinematic viscosity of the fluid. Because the drag force derived for a fully submerged particle in a linear shear flow, the drag force on a partially submerged particle will be smaller [23,34,108]

2.2.6: Capillary forces

When the colloids interact with AWI in unsaturated porous media, the deformation of the interface meniscus occurs as shown in Figure 5. The capillary force, which is also termed as surface tension force, exerts on the colloid surface in response to the rupture of AWI and formation of a three-phase contact line around the colloid particle [109–111].

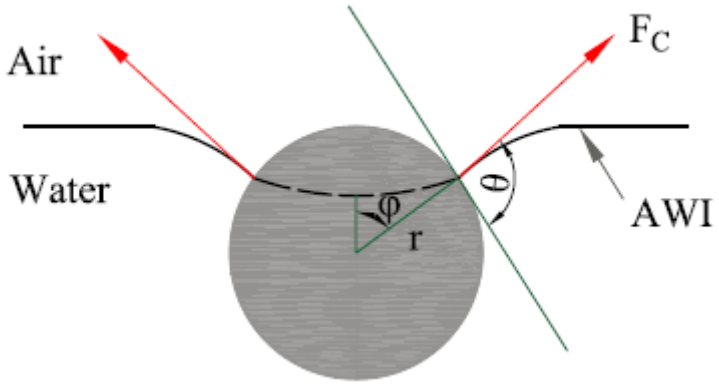

Figure 5. Colloids interacting with AWI; the deformation of the meniscus causes the development of capillary forces on the colloid

The surface tension force (σ), particle hydrophobicity (or contact angle, θ), size

of the particle (particle radius, r), and the angle determining the position of the interface on the colloid (φ) determine the direction and magnitude of the capillary force acting at AWI. The capillary force acting normal to the interface orientation can be determined as [24,112]

$$F_c = 2\pi r\sigma \sin\varphi \sin(\theta - \varphi) \quad (18)$$

The energy required to remove the particle retained by capillary force can be calculated as [113]

$$\phi_c = \pi r^2 \sigma (1 - \cos\theta)^2 \quad (19)$$

Besides the interaction with AWI, colloids on AWSI also interact with solid surfaces resulting in a complex behavior [14,26,42]. Colloid adhesion force, as well as hydrodynamic force, will be acting on the contact line in addition to the capillary force. Moreover, the capillary force vary on a moving AWI with the interface position on the colloid (φ) as shown in Figure 6, and two magnitude maxima can be obtained for the capillary force as below [18,34]:

$F_c = 2\pi r_c \sigma \, sin^2(\theta/2)$ for $\varphi < \theta$, directed towards the air-phase, (20)

$F_c = -2\pi r_c \sigma \, sin^2(90 + \theta/2)$ for $\varphi > \theta$, directed away from the air-phase, (21)

The negative sign indicates the direction of the capillary force, acting away from the air-phase.

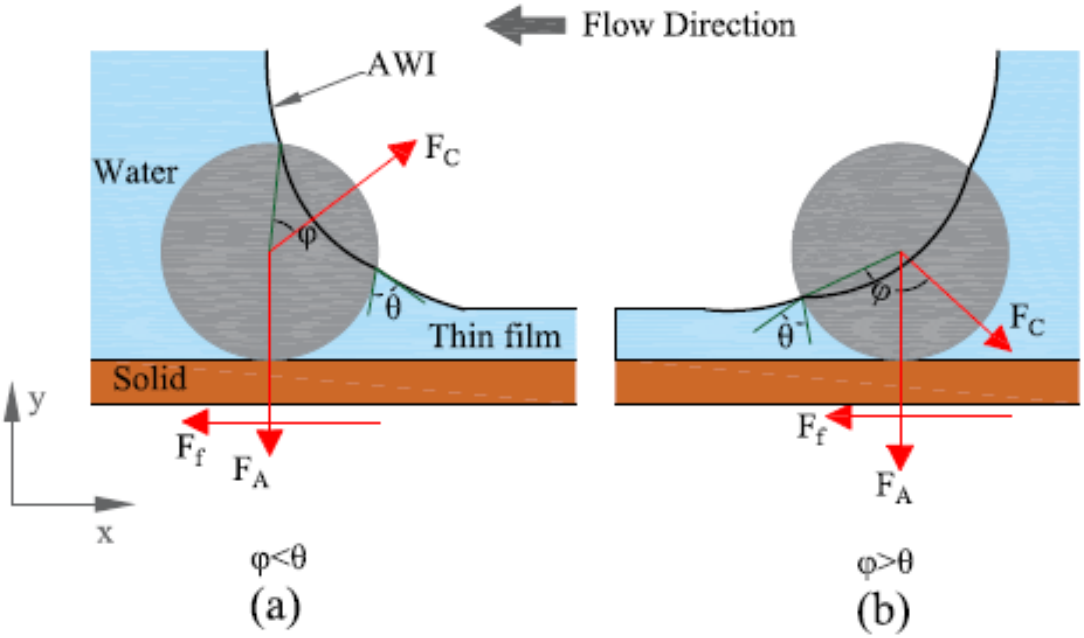

Figure 6. The forces acting on the colloid at two magnitude maxima (φ < θ and φ > θ) of capillary force [34,114]

For a particle on AWSI, the components of maximum capillary force also depend on the collector dynamic contact angle (β) and are calculated as:

For φ < θ,

$$F_c^y = 2\pi r\sigma \, sin^2(\theta/2)\cos\beta \quad (22)$$

$$F_c^x = 2\pi r\sigma \, sin^2(\theta/2)\sin\beta \quad (23)$$

For φ > θ,

$$F_c^y = -2\pi r\sigma \, sin^2(90+\theta/2)\cos\beta \quad (24)$$

$$F_c^x = -2\pi r\sigma \, sin^2(90+\theta/2)\sin\beta \quad (25)$$

2.2.7: Force and Torque balance

Colloid attachment to and release from the collector surfaces depends on the balance of hydrodynamic, capillary, and surface interaction forces as well as torques. Torque balance was mostly used to estimate the detachment of colloids from the

collector surface. Three mechanisms observed for particle movement in response to the hydrodynamic forces and capillary forces in saturated and unsaturated flow conditions, respectively. (1) a net vertical force causes particle **lifting**, (2) a lateral hydrodynamic force or capillary force tangential to the collector surface results in **sliding** of the particle, and (3) a torque about the contact point causes **rolling** of the particle on collector surface.

A friction force acts on the colloid contact point (with the collector surface), which is proportional to the net normal force [115].

$$F_f = \mu_f F_N \quad 26$$

where μ_f is the coefficient of static friction, which varies between 0.1 and 2 [116]. For a smooth glass substrate, μ_f can be considered as 1 [34].

The hydrodynamic drag and lift forces and capillary forces can be estimated as per section 2.2.5 and 2.2.6. Net surface interaction force (i.e., adhesive forces) was calculated as the summation of DLVO forces, hydrophobic, steric, and Born forces. The force and torque balance for colloids in saturated and unsaturated flow are described separately in the following sections:

2.2.7.1. Saturated flow conditions:

The mobilization mechanisms can be derived based on the forces acting on the colloid, as shown in Figure 7. Colloid lifting occurs when the hydrodynamic lift force exceeds the adhesive force. The attached colloid begins to slide when the hydrodynamic drag force exceeds the frictional force generated by the net normal force at the interface. Finally, rolling of colloid occur on the collector surface when the adhesive torque (i.e., resisting torque) overcome by the applied hydrodynamic torque.

$F_A < F_L$ for lifting

$F_F < F_D$ for sliding

$T_A < T_D$ for rolling

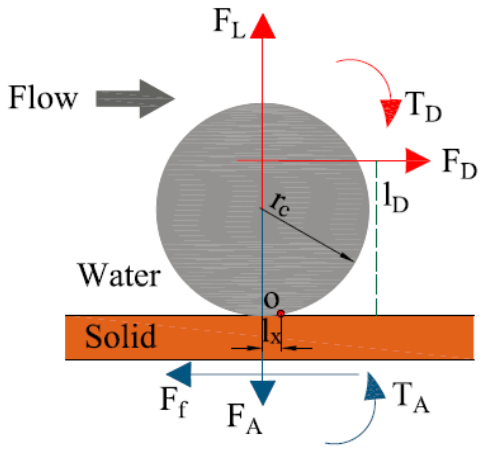

Figure 7. Forces and torques acting on a deposited colloid in saturated flow conditions

Rolling was reported to be the predominant mechanism of colloid release under laminar flow conditions in the porous media [106,116]. The fluid velocity increases from the collector surface, and the effective drag force acts at the height of 1.4 r. Thus, the drag force generates torque by operating at a lever arm of 1.4 r

$$T_D = 1.4rF_D \quad (27)$$

The adhesive force (F_A) was estimated as ϕ_{min}/d_0, where ϕ_{min} is the absolute value of primary or secondary minima, and d_0 is the corresponding separation distance. The adhesive or resisting torque can be calculated as [102].

$$T_A = F_A l_x \quad (28)$$

Where l_x is the lever arm, which is the radius of the colloid-surface contact area. The colloid and collector are not physically contacted while interacting at primary or secondary energy minima. Therefore, the contact radius on a smooth surface is given by [117]

$$l_x = \left(\frac{4F_A r}{K}\right)^{1/3} \quad (29)$$

Where K is the composite Young's modulus. Bergendahl and Grasso (2000) used a value of 4.014×10^9 Nm^{-2} for a glass surface and a polystyrene colloid suspension.

2.2.7.2. Unsaturated flow conditions:

A colloid deposited on AWSI was subjected to capillary, hydrodynamic, and adhesive forces. Hydrodynamic drag forces were reported to be negligible in unsaturated flow conditions compared to adhesion and capillary forces [23,34,108]. The vertical and horizontal components of capillary forces affect the equilibrium of colloid along with the adhesion forces (

Figure 8).

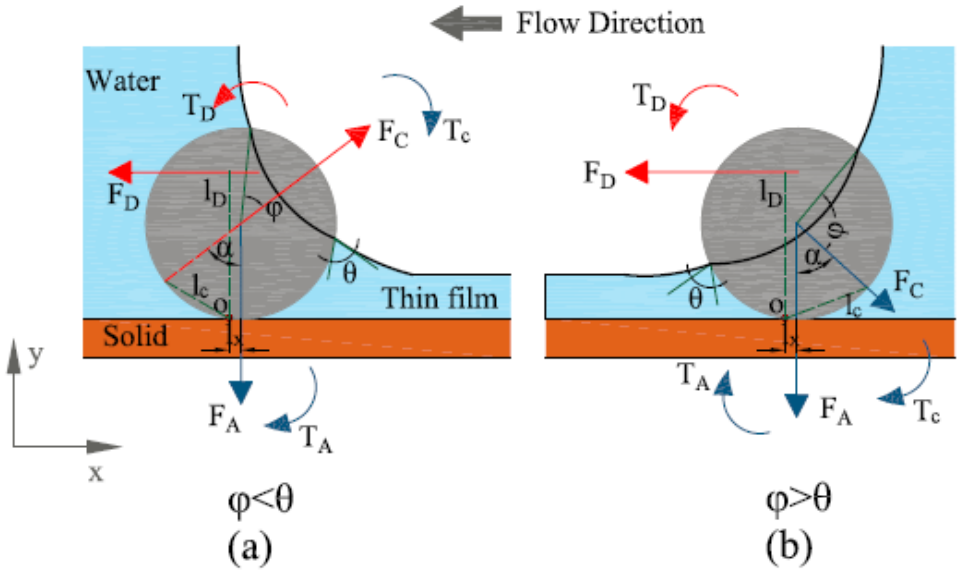

Figure 8. Forces and torques are acting on a colloid at AWSI for φ < θ and φ > θ in unsaturated flow conditions.

Colloid lifting occurs when the net vertical force act in the upward direction (i.e., the sum of the vertical component of capillary force, F_c^y and adhesion force, F_A).

$$F_c^y + F_A > 0 \quad (30)$$

Sliding of attached colloids occur when

$$F_c^y + F_A < 0 \; and \; F_c^x + F_D > F_f \quad (31)$$

Rolling occurs when the applied torque by the capillary forces exceeds the resisting torque due to adhesion forces.

$$T_A < T_c \quad (32)$$

Where T_A calculated similar to saturated conditions T_c is the torque due to capillary forces [34]

$$T_c = F_c l_c \quad (33)$$

$$\text{where } l_c = r \sin \alpha \quad (34)$$

2.3. Factors affecting colloid deposition and release

Various physicochemical and hydrodynamic factors affect the attachment, mobilization, or transport of the colloids in the porous media. Earlier experimental, theoretical and numerical studies examined the impact of several parameters including flow rate, water content and transient flow [14,67,118,119]; solution chemistry, such as pH and ionic strength [46,71,97,120–122]; size, concentration and type of colloids (i.e., hydrophilic or hydrophobic) [25,35,36,42,123], and the properties of porous medium such as wettability and surface roughness [13,41,121,124–126]. In this section, only the factors affecting colloid retention and release that addressed in this dissertation will be discussed, including ionic strength, pH, flow rate, and type of colloids.

2.3.1: Ionic strength

When suspended in an electrolyte solution, colloidal particles are surrounded by two layers of ions, each with opposite polarities attracted via electrostatic and diffusive forces, which is called a double layer. The surface charge of the colloid is

balanced by the clouds of ions in the double layer [127]. The potential energy that arises from the double layer is proportional to its thickness. As the ionic strength increases, a thin double layer can balance the surface charge because the ion concentration in the electrolyte is high; conversely, low ionic strength will produce thick double layers. At low ionic strength, electrostatic potential energy dominates due to the thick double layer, and the repulsive energy barrier prevents the colloids from interacting with the surfaces. At high ionic strength, the double layer compress to a thin layer, and van der Waals attraction prevails over electrostatic repulsion resulting in the absence or negligible energy barrier.

According to the DLVO theory, increasing ionic strength increases the secondary energy well and decrease the energy barrier. At higher ionic strength, the energy barrier disappears, leaving only the primary minimum well. Accordingly, colloids deposited on primary and secondary minima for high and low ionic strength, respectively [128]. At some intermediate ionic strength, the coexistence of primary and secondary minimum attachment can be possible where the secondary minimum is deep enough [129]. A fraction of colloids deposited at a secondary minimum might be able to jump over a comparatively smaller energy barrier and deposited at the primary minimum. Energy barrier less than 15 kT can overcome by the colloids in the secondary minimum by Brownian diffusion [130,131].

The impact of ionic strength on colloid deposition has been extensively studied in previous literature based on laboratory column experiments and mathematical modeling. In general, the favorability of colloid interaction with other colloids and collector surfaces increases with an increase in ionic strength. Therefore, colloid removal efficiency increases with ionic strength in porous media. However, the impact cannot be generalized for different types of colloids under various physicochemical

conditions, and this necessitates the study of coupled nature of other factors influencing colloid retention, including pH, type of colloid, and flow rate.

2.3.2: pH

The surface charge of the colloids is affected by the pH of the solution. For most of the colloids, there exists a point of zero charges (pH_{pzc}) below which the surface charge turns positive. Different pH_{pzc} of the two interacting surfaces can pose opposite surface charges and favorable interaction. On the other hand, if two interacting surfaces possess the same charge, unfavorable interaction persists due to the repulsive electrostatic potential. With the increase in pH, the surface charge becomes more negative for the colloid and collector, resulting in electrostatic repulsion [132].

Previous studies reported greater attachment of kaolinite compared to illite with a decrease in pH [133]. The sensitivity of the edge sites of kaolinite particles to pH can enhance the attachment on the collector surfaces as the edge sites become positively charged with a decrease in pH [134]. Although Illite has the pH-dependent charge for the edge sites, the higher permanent charge, aspect ratio, fewer planar edge sites, and a lower pH_{pzc} compared to kaolinite were attributed to its negligible impact on pH [73].

2.3.3: Flow rate

The fluid flow rate in the porous media has a significant impact on colloid deposition on the collector surface. Increased colloid depositions rates were reported from the laboratory column experiments with an increase in flow rate under favorable conditions [135]. In contrast, under unfavorable conditions, colloid deposition reduced with an increase in flow velocity [136]. This observed behavior was explained with the mitigating effect of hydrodynamic drag forces on colloid deposition in the presence of an energy barrier [136]. Additionally, colloids attached at a secondary minimum can be

detached and translated along the collector surface via hydrodynamic force [137]. Therefore, the relative increase in the detachment rate under unfavorable conditions with the flow rate than under favorable conditions explains the changes in the type of colloid deposition under favorable and unfavorable conditions. These differences suggest the relative importance of colloid interaction potential on deposition under various hydrodynamic conditions. While colloid interaction with collector surfaces occurs via primary minimum under favorable conditions, secondary minimum deposition has been considered as a vital retention mechanism under unfavorable conditions.

The relative significance of adhesion forces over hydrodynamic forces was studied by Torkzaban et al. [105] by solving the fluid flow field around a single collector. The theoretical force and torque calculations were identified three conditions, namely: (1) 'favorable' conditions when the adhesive torque was greater than the hydrodynamic torque over the entire collector surface, (2) 'unfavorable' conditions when the adhesive torque was less than the hydrodynamic torque over the majority of the collector surface, and (3) 'partially favorable' conditions when the applied hydrodynamic torque was less than the adhesive torque near the front and rear flow stagnation zones but was greater near the collector center. This condition exists for colloids that are weakly associated with the collector surface via a secondary minimum. The solution ionic strength, pore water velocity, size, and shape of the colloid and collector affects the partially favorable conditions. At higher flow velocity, smaller colloids attach more rapidly than larger colloids due to the larger lever arm of larger colloids that increase the hydrodynamic torque and oppose attachment [138]. At higher flow rates, colloidal particles are transported deep into the porous media as the mobility increased due to higher hydrodynamic shear than adhesive forces under unfavorable

conditions [139,140].

2.3.4: Types of colloid

The natural porous media contains negatively charged collector surfaces. The surface charge and hydrophobicity of the interacting colloid play a vital role in the attachment or transport behavior in the porous media. The colloids with positive surface charge pose a favorable interaction condition, whereas negatively charged colloids experience unfavorable conditions for attachment. Therefore, the above-discussed factors that influence colloid retention mechanisms in the porous media affect differently under favorable and unfavorable conditions. For example, under favorable conditions, colloid deposition increases with an increase in flow rate, whereas it decreases under unfavorable conditions. Moreover, under favorable conditions, the impact of solution chemistry (such as ionic strength and pH) are negligible on colloid attachment on SWI.

Previous studies reported colloid retention on AWI and aggregation of hydrophobic colloids due to the attractive hydrophobic interaction force between two hydrophobic surfaces [12,13,17]. In addition, the capillary force acting on a hydrophilic particle at AWSI, which causes the pinning of colloid on a solid surface, is more significant than hydrophobic particles. Therefore, hydrophilic colloids retain more on AWSI and thin films in an unsaturated media compared to hydrophobic colloids [17,21,141]. Moreover, colloid mobilization mechanisms also vary for different types of colloids under saturated and unsaturated conditions. Therefore, the effect of colloid type on colloid retention and mobilization mechanisms should be considered.

2.4. Colloid retention mechanisms in porous media

Traditional colloid filtration theory describes colloid attachment on the collector

surface in response to Brownian diffusion, settlement, and interception [8,9,75]. However, discrepancies between the experimental results and theoretical predictions were reported because of colloid straining or retention in grain-grain contacts under saturated conditions [142,143]. Straining of colloid aggregates under favorable colloid-colloid interaction was proposed in addition to individual colloid straining in small pore constrictions [10,142,144]. Moreover, recent studies demonstrated the retention of colloids on AWI, AWSI, and thin films under unsaturated conditions [2,25,43,87,145,146]. Breakthrough curve analysis, pore-scale visualization studies on sand columns, and micromodels reported various retention mechanisms under saturated and unsaturated porous media and are discussed in the following sections.

2.4.1: Colloid – SWI interactions

Colloids transported through porous media collide with collector surfaces or SWI because of interception, Brownian diffusion and sedimentation, and consequently attachment. The relative size ratio between the colloid and solid grain and porosity affects the collision by interception. In addition, at higher flow velocity, the colloids following streamlines diverted from the grain surfaces, and thus the interception was less probable. Interception is negligible for smaller colloids less than 1 μm, while diffusion promotes collision on collector surfaces irrespective of the flow velocity. Colloids accumulate in immobile water zones in the porous media such as grain-grain contacts, dead-end pores, pore walls of wider pores, etc., and are more likely to diffuse into collector surfaces. Sedimentation of colloids by gravity is important only for dense particles such as clay minerals, or for low flow velocities of buoyancy neutral colloids.

Once the colloids collide with SWI, van der Waals and electrostatic interactions, as predicted by DLVO theory controlled the attachment. Depending on the DLVO

energy profile, colloid-SWI interaction can be either favorable with strong primary energy minima or unfavorable with energy barriers that prevent or limit colloid attachment onto SWI [89]. Under favorable conditions, colloids physically attach and permanently retain on the collector surface since the adhesion forces exceed the hydrodynamic forces [106]. However, favorable conditions are unusual in the natural environment as the grain surfaces and colloids usually exhibit negatively charged surfaces. Electrostatic repulsive force prevailing between two negatively charged surfaces pose unfavorable conditions for an interaction. Nevertheless, previous column experiments revealed colloid retention under unfavorable conditions. This retention was attributed to different mechanisms, including secondary minimum attachment, straining at grain-grain contact points, retention at physiochemical heterogeneities on the grain surface (i.e., surface roughness and surface charge heterogeneities) [86,91,102,147,148]. Several mechanisms are hypothesized in previous studies to explain colloid retention under unfavorable conditions based on breakthrough curves. For example, increased breakthrough concentration over time (steep ascending limb on the colloid breakthrough curve for ionic strength higher than 0.01M in Figure 9) indicates progressive filling of available retention sites (i.e., blocking) [149–152]. Similarly, decreased elution concentration suggests the presence of additional retention sites by the retained colloids (retention on surface heterogeneity) due to the favorable colloid-colloid interaction (also called ripening) [136,153,154].

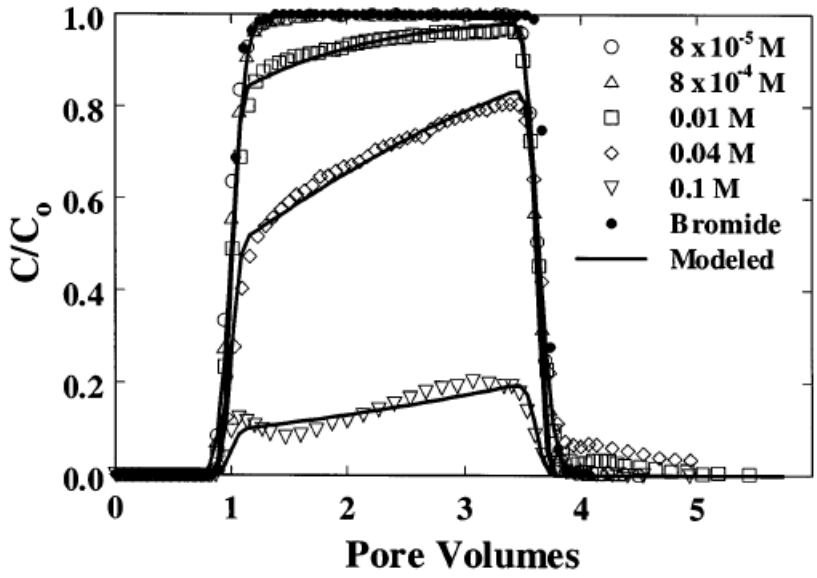

Figure 9. Measured breakthrough curves for the transport of silica colloids at different ionic strength [155]

Under unfavorable conditions, the solution chemistry greatly influenced the colloid attachment on SWI. At lower ionic strength, weak secondary minimum interaction of colloids occurs at a separation distance of few nm from SWI. These colloids can enter into primary minimum and physically attach to the collector surface when the colloids possess enough energy to overcome the energy barrier. The absence of primary or secondary energy minimum prevents the colloids from interacting with the collector surface. However, some visualization studies were observed colloid attachment under repulsive interaction conditions [30,156]. Colloid attachment on concave regions on a rough surface favor colloid attachment for those conditions, as shown in Figure 10.

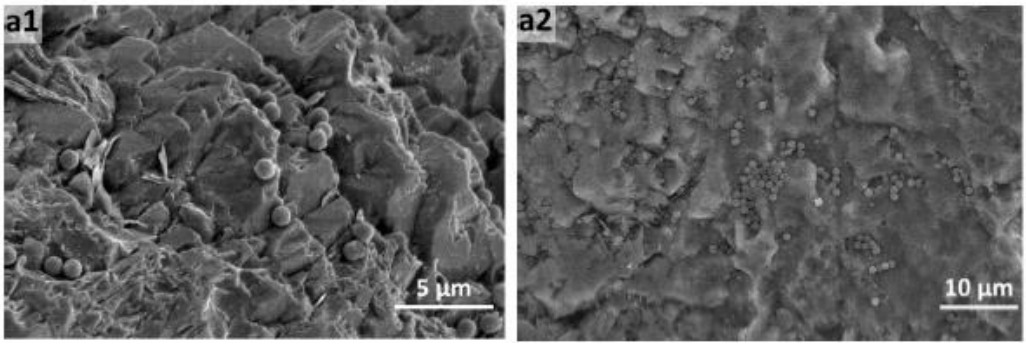

Figure 10. SEM images of sand surface taken after elusion with DI water; colloids were injected at different ionic strengths (1) 1 mM, and (2) 200 mM [156].

Colloid deposition on SWI occurs in saturated as well as unsaturated porous media. Colloid partitioning on SWI and AWI in unsaturated porous media depends on the degree of water saturation and solution ionic strength. At higher ionic strength, colloids interact predominantly with SWI than AWI, although colloid accessible SWI area was more sensitive to the water content. With the decrease in water content and ionic strength, colloid-AWI interaction dominates over colloid-SWI interaction.

2.4.2: Straining and Colloid – Colloid interactions

Straining refers to the entrapment of colloids at grain-grain contacts or small pore throats [157]. Colloids with size larger than the pore throat cannot move in the pore space and were mechanically removed by pore blocking or straining [9,10]. The ratio of colloid diameter to the grain diameter was reported to be critical within a range of 0.002 to 0.05 [9,158]. The permeability of the porous media will be affected when the ratio is higher than the critical value. As the colloid size increases or grain size decreases, laboratory column experiments noticed a decline in breakthrough concentration [9]. The colloid mass recovery obtained after dissection of the column shows straining was spatially-distributed with a higher intensity near the inlet

[10,159,160]. Bradford et al., (2003) reported the critical ratio for straining was 0.002 and above which straining rates increased exponentially. However, Xu et al. (2006) suggested a threshold value of 0.008, and the straining rate increased linearly with a colloid diameter under unfavorable conditions. The disparity between these studies suggests other possible factors, including hydrodynamics, solution chemistry surface roughness, etc. on straining [161–163].

Equally crucial as single-particle straining in the porous media is colloid aggregate straining. The DLVO theory predicts colloid aggregation for those colloids exhibiting favorable colloid-colloid interaction. Previous studies suggested that the hydrophobic colloids form aggregates due to the attractive hydrophobic forces [12,17]. Numerous studies have been conducted to understand the mechanics of aggregate formation in an aqueous environment [164–169]. Primary particles in the colloid suspensions interact spontaneously to form colloid aggregates or clusters or flocs under unstable conditions. The instability can occur due to the higher ionic strength, lower pH, the hydrophobicity of the particle, and/or adding coagulants [164,167]. In contrast, colloids in a stable suspension (i.e., low salt concentration or addition of stabilizers) may remain suspended in the solution for long periods. The aggregation is limited either by diffusion or by a reaction in an unstable suspension. The diffusion-limited colloid aggregation (DLCA) is faster compared to reaction limited colloid aggregation (RLCA) [170,171]. The greater sticking probability of the colloids would result in DLCA and form aggregates with fractal structure, as shown in Figure 11 [172]. In other words, attractive colloid-colloid interaction at all separation distances may cause DLCA, whereas, the presence of the energy barrier limits the sticking probability and result in RLCA [173]. However, colloids overcoming the energy barrier by specific reactions (i.e., thermodynamically) will aggregate in the later stages.

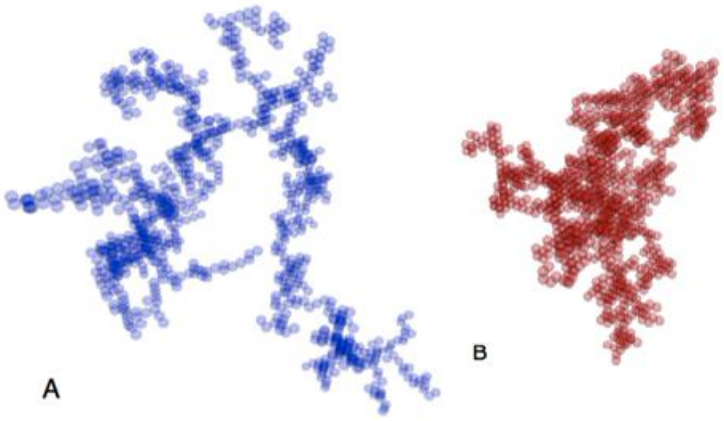

Figure 11. The fractal nature of colloid clusters formed by (A) DLCA, and (B) RLCA [172]

Colloid clusters in the porous media can either attach to the collector surfaces or can be strained in pore throats [2,22]. Additionally, favorable colloid-colloid interaction can result in ripening (i.e., aggregation around solid grains) followed by pore blocking and clogging in porous media [174]. Under unfavorable conditions, a lower colloid breakthrough from the laboratory column experiments was attributed to straining rather than physiochemical attachment based on theoretical predictions [163]. However, to date, no visualization evidence is available on the impact of different factors on colloid aggregation followed by straining in porous media.

2.4.3: Colloid – AWI interactions

The presence of AWI in unsaturated porous media provides additional retention mechanisms, including AWI, AWSI, and thin water films. Several column breakthrough analysis was conducted to prove the increased retention of colloids under unfavorable conditions in unsaturated porous media compared to saturated porous media [42,118,141]. Colloid capture at AWI has been invoked as a dominant process

for colloid retention in unsaturated porous media. Colloid retention at AWI was found to be irreversible, and the captured colloids move along with the infiltration front as the capillary forces holding the particles on AWI are so strong [25,118,175–178]. The water saturation determines the extent of available sites for retention, and it increases with a decrease in water content [118,179,180].

Wan and Wilson (1994) proposed AWI as a potential colloid retention site in unsaturated porous media by conducting micromodel experiments. They reported the retention of latex particles, clay colloids, and bacteria on AWI in a glass micromodel using fluorescent microscopy. Positively charged colloids retained more on negatively charged AWI compared to negatively charged colloids due to the attractive electrostatic force. Moreover, hydrophobic interaction between the hydrophobic colloids and superhydrophobic AWI surfaces resulted in greater retention than hydrophilic colloids. However, Chen and Flury (2005) did not observe any mineral colloids on AWI, and the increased retention under unsaturated conditions was hypothesized to be on thin water films around the grains. Moreover, Crist et al. (2005, 2004) did not found hydrophilic and hydrophobic latex particles on AWI; instead, the hydrophilic colloids deposited at the AWS interface.

Micromodel experiments showed that the colloids retarded near AWI due to the restricted flow and are migrated towards the interface by diffusion or advection. Once the colloids come closer to the interface, the attractive forces or collisions will result in the final attachment on the interface [181]. Mobilization of colloids from AWI was not observed during the dissolution of the air bubble, and colloid clusters were formed after complete dissolution. Theoretical calculations indicated the formation of aggregates is due to higher energy for colloid-AWI interactions than the energy barrier for colloid aggregation.

Previous studies reported partitioning of colloids on SWI and AWI for unsaturated systems [17,73,179]. Some of them suggested preferential partitioning at AWI, while others observed greater retention on SWI under specific cases such as higher ionic strength or heterogeneous porous media [17,73,179].

2.4.4: Colloid – AWSI/Thin film interactions

Previous studies reported colloid attachment on AWSI, where AWI meets the solid surface at which the film thickness is smallest [2,13]. The hydrodynamic flow-field in the porous media is significantly affected by the pore geometry, and low shear forces occur at junctions of SWIs or AWIs. The colloids veering off from the high-velocity pathways in the middle of the pore due to the centrifugal motion within the curved pendular ring will reach the low-velocity zones and are filtered at AWSIs [2]. The kinetic energy associated with those moving colloids deform the AWI meniscus and exert a capillary force. The vertical component of capillary forces, together with colloid surface forces, will result in developing frictional forces against the lateral component of the capillary force, thus holding the particles on the grain surface near AWSI [13,26,34]. Real-time pore-scale visualization on sand columns suggested retention of hydrophilic colloids by trapping at the AWS interface in hydrophilic porous media [2,17]. The higher capillary potential of hydrophilic colloids explains this greater retention [13]. However, inactivation of hydrophobic virus particles was reported near AWS in hydrophobic porous media [182,183].

Film straining is another colloid retention mechanism in unsaturated porous media, which occurs below critical water saturation where the pendular rings become disconnected [13]. The entry to the nearby pendular rings was restricted by thin films surrounding the grain surface that are too thin to move the colloids effectively [184].

This scenario is possible only with hydrophilic grains where thin water film exists. The thickness of water film varies with matric potential (i.e., water saturation). With a decrease in water saturation, the water film thickness around the grain surface falls below the colloid diameter, thereby strain in thin films.

A rapid increase in colloid immobilization was noticed as water content dropped below critical water saturation, and it was related to thin-film straining [184]. In addition, mechanistic models predict the film straining efficiency is proportional to the ratio of colloid diameter to film thickness and flow velocity (or saturation), and it was consistent with column experiments. Veerapaneni et al. [185] further explained the film straining using inclined film flow experiments. When the diameter of the particle is less than the film thickness, particle velocity increases linearly with a particle size as the larger particles are expected to move along the higher velocity regimes. However, colloid size greater than film thickness will result in approaching the fluid interface and pinning by capillary forces thereby restrict further movement.

2.5. Colloid Mobilization

Colloids retained in the porous media are immobile under constant hydro-geo-chemical conditions. However, colloid detachment can occur due to Brownian diffusion when the depth of energy minima is less than the average kinetic energy of the colloid, which is about 15 kT [48,128,186]. Only small amounts of colloids are detached by diffusion. Significant detachment is likely to occur under certain circumstances such as perturbations in groundwater chemistry or flow rate induced by various conditions, including massive rainfall infiltration and injection of water for oil recovery [147,187,188]. The released colloids are either transported with flowing water or may deposit in the downstream by clogging small pore constrictions resulting in

permeability reduction [59,147]. The relative strength of adhesive, hydrodynamic drag, diffusive, and capillary forces affects the colloid release [34,65,105]. Colloid release was predicted by DLVO theory in response to decreasing the ionic strength or increasing the pH of the solution due to the reduction in adhesive force [102,136,187,189]. Additionally, the elevated hydrodynamic drag at higher fluid velocity mobilizes the deposited colloids [30,118,135,190]. Moreover, in unsaturated porous media, capillary forces play a vital role in the release of colloids during drainage and imbibition [14,21].

2.5.1: Perturbation in flow velocity

Colloid release was observed with an increase in flow velocity, but the rate and amount of release show complex behavior. For example, Bradford et al. [191] reported negligible colloid release with flow perturbations, while Bedrikovetsky et al. [192] described greater colloid release with an increase in flow velocity. The shear stress imposed by the mechanical energy of moving water causes the mobilization of colloids from saturated porous media. The increase in shear force due to the higher flow velocity exceeds the attachment force of the colloids and consequently lead to colloid release from the solid surfaces [64]. The increase in flow velocity beyond a critical hydrodynamic shear has a negligible impact on colloid release. This insignificant release behavior can be attributed to the spatially distributed hydrodynamic shear, roughness, deposited colloids on sand grains, and the variations in the adhesive forces of deposited colloids in the porous media [115,193]. It has been reported that the detachment of colloids from porous media of relatively higher porosity and permeability was more susceptible to the hydrodynamic perturbations [194].

Under favorable attachment conditions, hydrodynamic forces will have a

negligible impact on colloid mobilization because of higher adhesive force acting on colloids attached via the primary minimum. The insensitivity of colloid release with the velocity perturbations under native groundwater conditions from a core sample was reported due to favorable attachment conditions [147]. Conversely, colloid attachment occurs via secondary minimum under unfavorable conditions. The force and torque associated with hydrodynamic forces were found to be greater than the adhesive forces and torques acting on colloids retained at a secondary minimum [135,143]. On the other hand, colloids that are weakly associated with the collector surface via secondary minima are expected to be more susceptible to release than those attached via primary minima during hydrodynamic perturbations [147]. However, detachment of colloids from the primary minimum can also occur under the influence of hydrodynamic shear. For instance, a shallow primary minimum was reported for colloids interacting with nanoscale surface asperities and are susceptible to release [3,138].

A sharp increase in colloid release and permeability of the core samples was reported with an increase in flow velocity because of the dislodging of hydrodynamic bridges at small pore constrictions [105,179]. The simultaneous arrival of multiple colloids at small pores may form bridges against the pore entrance. These colloids can freely diffuse in and out of the pore by flow interruptions in the porous media. The greater breakthrough of colloids and increased permeability associated with flow interruption can explain the role of hydrodynamic bridging for porous media with smaller pore sizes [147].

Theoretical calculations show that, with the increase in flow velocity, the release of smaller particles was more difficult compared to larger ones because the hydrodynamic forces and torques decrease more rapidly than the adhesive forces and torques with a decrease in colloid size [106]. The detachment of sheet-shaped graphene

nanoparticle was not observed with an increase in flow rate due to its enhanced adhesive forces compared to hydrodynamic shear [138]. Moreover, an increase in the flow rate restrained the release of mine tailings from the packed sand columns [195]. Conversely, with the reduction in the flow rate, smaller tailing particles were released in significant quantity. This release of submicron particles (1 nm – 1 μm, Brownian) is mainly controlled by the diffusion of detached particles to the bulk fluid [196]. The longer residence time of the infiltration fluid in the packed column at lower velocity was attributed to the diffusion-controlled release of smaller particles with a reduction in the flow rate [197].

Nevertheless, in some studies, increased release of nanoparticles with an increase in flow velocity was noticed [139,198]. There are several explanations available in the literature such as nanoparticles attached at secondary minimum or nanoscale protruding asperities etc. are released due to weak adhesion forces between the colloids and other surfaces compared to hydrodynamic forces [102,193]. However, to date, no systematic visualization studies have been conducted to investigate the role of flow rate on colloid release from porous media under favorable and unfavorable interaction conditions.

2.5.2: Perturbation in solution chemistry

Previous studies have shown that perturbations in solution chemistry, such as decreasing ionic strength or increasing pH, favor colloid release [186,199–201]. A decrease in ionic strength can detach the retained colloids and release them back to the aqueous phase. In addition, colloid aggregates are dispersed in response to the change in ionic strength and promote transport [202]. The long-range van der Waals attraction force extends to greater distance compared to the short-range electrostatic

repulsive force, and thereby a zone of weak attraction (i.e., secondary minimum) may occur beyond the repulsive barrier. Deep energy wells exist at higher ionic strength, and the intensity decreases or vanishes at lower ionic strength, as shown in Figure 12 [7,203]. Under unfavorable conditions, colloid retention occurs via secondary minimum interaction. Therefore, the colloid release was expected with a decrease in ionic strength [203,204].

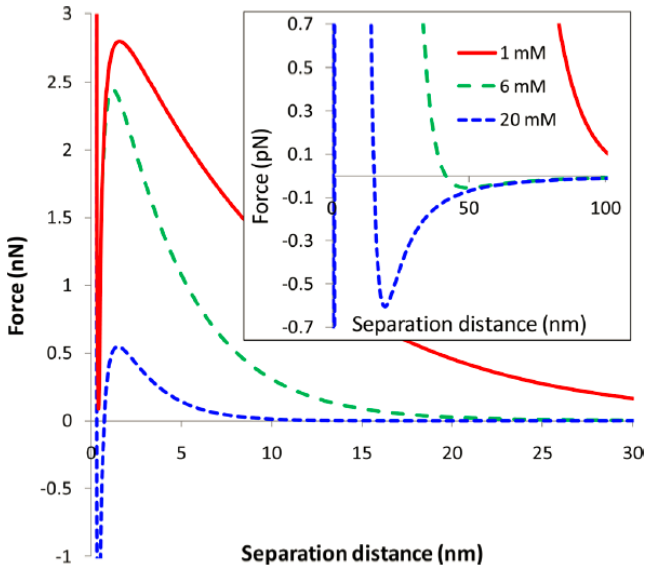

Figure 12. DLVO force profiles for 1.95 μm colloids under different ionic strength conditions (1, 6, 20 mM) [203].

It must be noted that colloids retained via secondary minimum are not expected to immobilize on the collector surface due to the weak and non-contact nature of the adhesion forces [203]. The colloids translating on flat surfaces, as observed from impinging jet experiments were demonstrated the secondary minimum association of colloids on the collector surface [136]. In general, the primary and secondary minimum attachment cannot directly distinguish from indirect observation experiments such as

packed sand column experiments [205]. Nevertheless, the released colloids with the reduction in ionic strength were believed to be retained on the secondary minimum. Colloid release was only observed when the perturbing ionic strength reached a threshold value (i.e., critical release concentration, CRC), regardless of the solution chemistry at which the colloids deposited initially [101,187]. A decrease in ionic strength beyond CRC has mobilized the colloids as the secondary minima disappear at CRC.

However, numerous deviations are reported from the predicted behaviors [193,206]. For example, only a fraction of deposited colloids was mobilized by lowering the ionic strength in sand column experiments under unfavorable conditions [102,155,188,206]. These deviations from the theoretical predictions suggest that considerable colloid retention occurs in the primary minimum, even though a higher energy barrier was predicted for attachment, based on the DLVO theory. The primary minimum depth is independent on IS, whereas the secondary well depth decreases with a reduction in ionic strength. Therefore, those colloids attached to a secondary minimum released during a decrease in ionic strength. The primary minimum attachment was considered as irreversible to ionic strength reduction. However, in some studies, the detachment was observed for colloids retained via primary minimum at higher IS (where energy barrier is absent, and deep primary minimum exist) with a reduction in IS. The infinite depth of energy barrier for detachment was accounted for with the addition of short-range Born repulsion forces in classical DLVO theory [207]. With this modification, particles attached in the primary minimum are shown to have a finite energy barrier for detachment [44,193,208–210]. Although the colloid-collector interaction becomes repulsive with changes in solution chemistry, complete colloid removal was not observed in previous studies [148,188]. This deviation was attributed

to the transfer of colloids to low-flow regimes (i.e., grain-grain contacts, surface roughness, etc.) and nanoscale heterogeneities of the grain surface (i.e., surface roughness and charge heterogeneities) in the natural porous media. Those colloids were not necessarily released with the reduction in ionic strength, as the hydrodynamic forces were less significant at those locations.

Moreover, microscopic heterogeneities (i.e., surface roughness, charge heterogeneities due to the presence of different types of minerals on the collector surface) in the porous media may reduce energy barriers locally and act as favorable sites for attachment [100,148,188,193]. Removal of colloids from primary minima would be more difficult during perturbations in solution chemistry. For instance, SEM images of the sand grains before and after ionic strength reduction in sand columns indicate the release of colloids attached to the protruding asperities (i.e., convex surface) with charge heterogeneity [156]. However, because of the greater adhesive force and torque (smaller hydrodynamic force and torque), the colloids irreversibly attached to the concave regions.

Determining the impact of nanoscale surface heterogeneities on colloid retention and release is an active area of research that has been addressed significantly for unfavorable interaction conditions [41,102,211,212]. The interaction energy of the colloids near these heterogeneities may vary in magnitude depending on the electrostatic zone of influence (ZOI) [213,214]. As the electrostatic interactions decay with the Debye length and the curvature of the particle, electrostatic interactions outside the ZOI do not contribute to colloid-collector interaction, where ZOI is proportional to the square root of the product of colloid radius and the Deye length [213,215]. The radius of ZOI increases with an increase in colloid size and a decrease in solution ionic strength, as shown in Figure 13 [216]. Colloid interaction over the heterodomain under

bulk repulsive conditions can be attractive or repulsive, depending on the relative size of heterodomain over the ZOI [217]. When the ZOI is much larger than the nanoscale asperities, net repulsion persists for colloids interacting with the heterodomain [203]. Therefore, a widely distributed strength and locations of colloid attachment in heterogeneous porous media resulted in a fractional colloid release in response to perturbations in solution chemistry and flow rate [203].

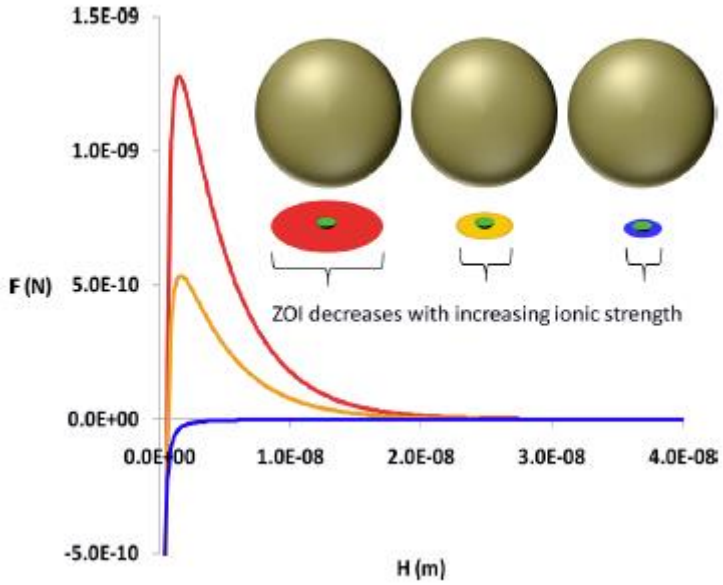

Figure 13. DLVO force profiles for 1.1 µm colloids under different ionic strength conditions (6, 10, and 20 mM shown in red, yellow, and blue colors, respectively). The colored disc represents the ZOI, and the inner green disc is the heterodomain. The size of ZOI decreases with an increase in ionic strength, and the heterodomain occupies the sufficient fraction of the ZOI at higher ionic strength. [216].

Permeability decline in the laboratory column experiments with the perturbations in solution chemistry has been extensively studied [106,147]. Significant and sudden clogging of the pores by the transported colloids in the porous media (with

a higher percentage of colloids and smaller pore sizes) was attributed to this permeability reduction. Clogging of pores affects the permeability of the reservoir rocks, followed by injectivity decline and formation damage [98,218]. Moreover, permeability decline was also reported to be more significant at pH greater than 7 or 8, as many mineral colloids are negatively charged over this pH range [106]. Low salinity water flooding in oil reservoirs for enhanced oil recovery was studied in detail considering colloid release and associated oil recovery [4,50,121,124,219–223]. Moreover, facilitated transport of contaminants into the groundwater aquifer during rainwater infiltration (i.e., low ionic strength and high flow rate) impacts the water quality [127,224].

Previous studies mostly focused on indirect observations on the colloid deposition or release behavior based on the laboratory column breakthrough curve [59,115,147,148,152,225]. The mass of colloids retained was analyzed in response to the changes in colloid or collector size and surface properties (changed by varying solution chemistry), and fluid flow rate. The indirect observations based on the theoretical considerations infers the pore-scale processes that influence colloid retention [100,105,226]. However, the changes in the breakthrough or retention may often occur due to multiple mechanisms in the column including straining (grain-grain contacts, small pore throats), size exclusion, ripening, bridging, clogging, attachment on nanoscale surface heterogeneity, etc. [100,147,193,227]. Moreover, colloid release and further re-deposition in the porous media were also interpreted indirectly in the previous studies. For instance, the negligible release of colloids with a decrease in ionic strength was explained by the solid phase colloid mass transfer to low-velocity regions (grain-grain contacts) where the hydrodynamic forces are insignificant to release them back to bulk water [105,115,228].

Direct visualization studies on colloid release with perturbations in solution chemistry and flow rate are minimal and many of them are focused on the impinging jet experiments where the colloids attach on a flat surface only. The real pore-scale processes cannot be directly compared with those studies, as they do not show multiple mechanisms, as explained above. Also, the impinging jet experiments not recreated the spatially distributed hydrodynamic forces (because of pore-scale velocity distributions) in the actual porous media [115,193]. Systematic direct visualization studies are required to determine the coupled effects of various factors that influence the colloid retention and release in saturated porous media.

2.5.3: Two-phase flow

The unsaturated subsurface soil in the vadose zone consists of two fluid phases, air, and water. The movement of fluid interfaces often occurs during rainwater infiltration or drainage. Additionally, capillary fringe fluctuations in the vadose zone also contain moving fluid interfaces. This moving AWI can mobilize previously deposited colloids in the porous media either on SWI or on AWI [29,44,71,114,175,229]. El-Farhan et al. [11] and Saiers et al. [230] were the first to highlight the significance of moving AWI in colloid mobilization during transient flow events in soil porous media (i.e., drainage and imbibition). Although electrostatic repulsion prevails between the negatively charged clay colloids and AWI in their study, clay partitioning was observed on AWI. A strong capillary force arises when an AWI intercepts and is deformed by the colloid deposited on SWI, as shown in Figure 5. Previous calculations for the capillary force acting on idealized systems reveal that the capillary force exceeds the adhesion force that binds the colloids on SWI by several orders of magnitude [21,118,231]. Therefore, colloid deposition on AWI was believed

to be irreversible.

Colloid detachment by the moving AWI was found to be affected by the solution ionic strength [230]. The lower colloid breakthrough concentration with the increase in ionic strength was linked to the colloid deposition morphology. In other words, the colloid aggregates formed at higher ionic strength were less susceptible to detachment by moving AWI. The larger aggregates pose greater resistance to detachment due to the magnified van der Waals attraction on SWI [111]. However, the capillary force increased with an increase in colloid size, surface tension, colloid hydrophobicity, and a decrease in interface velocity [44,110,111]. Therefore, the capillary retention of colloid aggregates can occur significantly greater than individual colloids. Later on, capillary pinning at AWSI and thin water films of the colloids at higher ionic strength was reported due to its greater affinity to SWI [13,24,141]. Accordingly, the breakthrough concentration reduces with an increase in ionic strength in unsaturated porous media.

An increase in interface velocity decreased the colloid scavenging by moving AWI on a flat surface [44,111,114,232]. At elevated velocities, the colloid-AWI contact time was too short to permit the colloid attachment on AWI followed by interception, liquid film thinning (around the colloid), and stabilization of the colloid on AWI. The colloidal particles become attached to AWI only if the contact time was larger than the time required to form a three-phase contact line and interfacial interactions [44,111,232]. Moreover, water film thickness plays a significant role in the mobilization of wet deposited colloids. For example, Aramrak et al. [114] explained the detachment for colloids with a size greater than the thin-film thickness. For a larger film thickness, the colloids do not form a three-phase contact line with the air bubble, and consequently, no colloids will be removed due to the absence of capillary force

[44,114]. The thin film thickness can be related to interface velocity (V) at larger flow velocity (Capillary number, Ca between 5 x 10^{-3} and 10^{-5}) as given below [34,114,233,234]:

$$h = 1.34r\left(\frac{\mu V}{\sigma}\right)^{2/3} \quad 35$$

However, at smaller flow velocity, the water film thickness was not dependent on the flow velocity or capillary number (Ca < 10^{-5}). The film thickness is only affected by the surface tension force and can be calculated as [34,235]:

$$h = (-A_{123}r/6\pi\sigma)^{1/3} \quad 36$$

On the contrary, laboratory column experiments showed an increased colloid breakthrough concentration with an increase in air-flow velocity [44,230]. The reduced release of colloids at a lower flow rate was explained by Saiers et al. [230] as the mobilized colloids were redeposited on SWI because of longer contact time between the colloids on AWI and SWI. Conversely, the increased water flow-velocity directly increases the pore saturation and which in turn provides more connectivity to the water flow by increasing the water film thickness. The capillary force holding the particles at thin-water films and AWSI vanish with an increase in pore saturation and are released back to bulk water resulting in higher colloid breakthrough with an increase in flow rate in unsaturated porous media [118,133].

When the interface moves over the SWI, depending on the position of AWI on the colloid surface, the capillary forces can either pin the colloids on SWI or cause detachment and accumulation on AWI [236,237]. Several experimental and theoretical studies on detachment by moving AWI showed that the removal was effective for unfavorable interaction between colloid and SWI compared to favorable conditions. Similarly, the detachment was increased with an increase in surface tension, colloid

size, and colloid hydrophobicity, decrease in interface velocity [44,110,111]. Additionally, advancing interfaces were reported to detach more colloids than receding interface due to greater capillary potential owing to the smaller contact angle [114]. Sensitivity to interface velocity was mostly observed under favorable conditions rather than unfavorable conditions [44].

Theoretical conceptualization of the forces acting on a colloid at the contact line with the advancing and receding interface was used to predict the mobilization from the collector surface [108,112,231]. The forces include the capillary force, colloid adhesion force on a solid surface, and hydrodynamic drag force. Among these forces, the capillary force was identified as the dominant force responsible for colloid detachment from the solid surface [18,23]. The force and torque balance at the contact line consider various mobilization mechanisms, including lifting, sliding, and rolling [21,238]. Lazouskaya et al. [34] derived theoretical criteria for colloid mobilization for hydrophilic and hydrophobic colloids and substrates with drainage and imbibition fronts. The imbibition and drainage fronts mobilize colloids differently because of their different dynamic contact angles and thin-film configurations [34]. The colloid release was more pronounced during imbibition than drainage. Because of contact angle hysteresis, advancing contact angle exceed receding contact angle. As a result, the capillary potential will be higher for imbibition resulting in detachment rather than pinning on SWI [23,29,34,193]. Moreover, a lower colloid detachment was observed during imbibition at higher ionic strength due to the strong adhesion forces on SWI [44,122,239].

The colloid breakthrough curves from sand column experiments have shown that colloids mobilize from sediments during drainage and imbibition events [71,87]. The moving AWI associated with drainage and imbibition can mobilize or immobilize

colloids according to the force balance at the contact point (i.e., AWSI). Previous studies reported that drainage cause retention or release of colloids, whereas imbibition promotes detachment [29,70,239,240]. The changes in AWI configurations and an increase in water flow velocity associated with imbibition was attributed to the release of trapped colloids in thin water films and pendular rings. Moreover, colloids stored in the stagnant water zones were released during imbibition as water displaces the air, and the immobile water zones are reconnected to the bulk water flow [14]. The increased hydrodynamic drag forces impose higher shear stress on the attached colloids and may contribute colloid release during infiltration [72,241]. Although shear rates associated with colloids in partially saturated porous media are less significant than colloids attached to SWI, dissolution of the air-bubbles release colloids retained on AWI [1,43]. Therefore, colloid release suing imbibition can increase with the increase in the rate of infiltration [71,122,229].

Direct visualization of colloid mobilization by drainage and imbibition fronts in a capillary channel was observed the detachment of deposited colloids at the contact line and are transferred to the AWI. Colloid and surface contact angles, as well as the number of colloids available to interact, can affect the overall mobilization efficiency of drainage and imbibition fronts [23]. Colloid mobilization study on deposited colloids on flat surfaces and capillary channels have been investigated different factors and mechanisms responsible for colloid detachment by direct visualization. However, to date, no direct visualization study has been conducted to evaluate the coupled effects of solution chemistry, colloid type, and pore geometry on colloid mobilization during drainage and imbibition.

CHAPTER 3: MATERIALS AND METHODS

3.1. Materials

The colloid transport and mobilization experiments were conducted in a micromodel (Microfluidic chip). Micromodels enable the real-time direct visualization of flow and associated mechanisms through a physically representative two-dimensional porous medium. Recent advances in the field of Microfluidic has reached up to its facile availability in the scientific community. We have purchased Microfluidic chips from Micronit Microtechnologies B. V. (Enschede, Netherlands) with physically representative geometry. Details on the micromodel, different types of colloids, and fluids are described in the following sections.

3.1.1. Micromodel

The microfluidic chip consists of an etched area, 20 mm x 10 mm, on a borosilicate glass with a pore depth of 20 μm. The properties of the micromodel, including porosity, pore-volume, and contact angle, were measured from image processing techniques as discussed later and were obtained as 0.58, 2.3 μL, and $23^0 \pm 3.2^0$, respectively. The permeability of the etched geometry was 2.5 Darcy (Manufacturer's Data). The microfluidic chip has one inlet and one outlet, each can be connected to 1/16" OD (outer diameter) tubing after inserted into the holder with the nuts and ferrules supplied by the Manufacturer. The microfluidic chip, holder, connections, and etched geometry are shown in Figure 14.

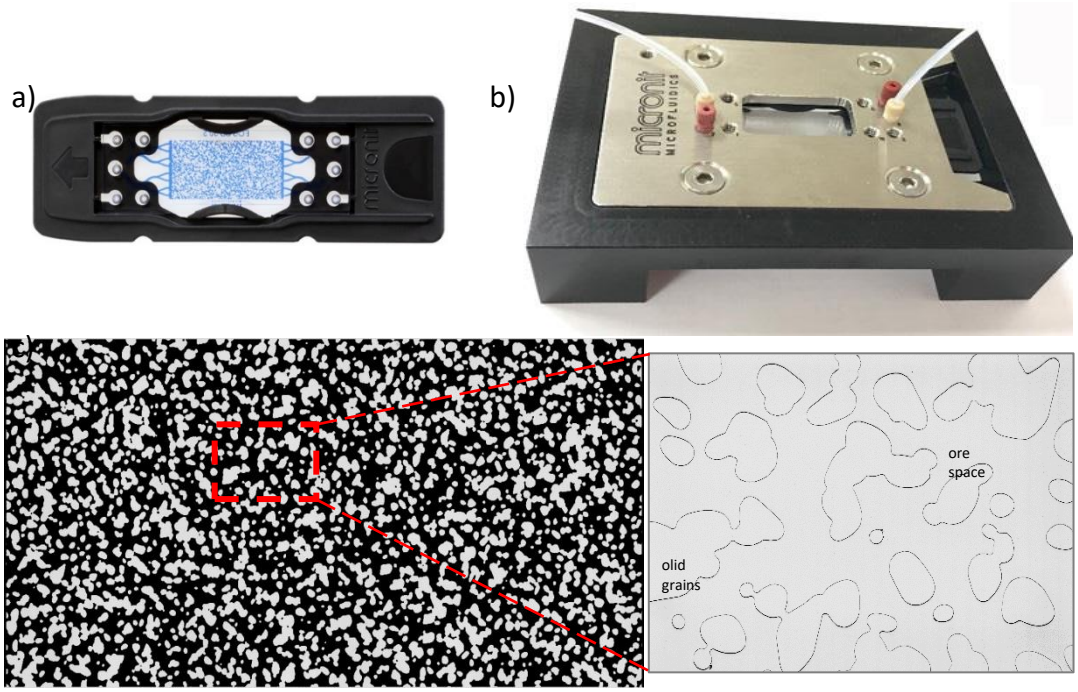

Figure 14. (a) The microfluidic chip, (b) holder and connections and (c) etched geometry

3.1.1.1. Cleaning of micromodel

The micromodel was thoroughly cleaned after each transport experiments and are re-used. Alternate injection of 0.1M NaOH solution and air for multiple pore volumes can dislodge the attached colloids from the solid grains and micromodel bottom. The strong interfacial tension between the liquid and air could sweep away the colloids detached by a higher pH of alkaline solution. However, colloids retained in the low flow zones are difficult to remove, as air cannot invade those pores. The images of the micromodel before the colloid transport experiment were taken for each case so that the previously attached colloids can be subtracted during image processing. Further injection of 100 Pore Volumes (PV) of ethanol followed by 500 PVs of deionized water can remove unnecessary ions and organic contaminants. Then the micromodel was

dried at 80^0C for 48 hours before using for the next experiment.

3.1.2. Colloids

The colloids used in this study were Polystyrene (PS), Carboxylate Modified PolyStyrene (CMPS), and Aminate modified Polystyrene (AMPS) microspheres (Magsphere Inc., Pasadena, CA) with a mean diameter of 5 µm and a density of 1.05 g/cc. Colloid suspension of 0.5% concentration was prepared by diluting the stock solution (10% solids) in brine to obtain approximately 7.3x 10^7 colloids/mL. The diluted suspension was sonicated in a water bath using an ultrasonic processor (SONICS, Vibra cell) to obtain a monodispersed colloidal suspension for up to 30 minutes prior to each experiment. The zeta potential of the colloids in different brine solutions used in this study was measured with Zetasizer (Nano ZSP, Malvern Panalytical, Southborough, MA) at 21^0C in triplicates and the average values are noted.

3.1.1.2. Colloid hydrophobicity determination

A thick layer of colloid particles on a glass slide was obtained by evaporating a concentrated colloid suspension. The contact angle was measured from a drop of distilled water placed on top of the dried colloids. The measured contact angles are macroscopic and may differ from microscopic contact angles [108,238].

3.1.3. Fluids

Brine, CO2, and air were the immiscible fluids used in this study. The ionic strength was changed by adding NaCl, and the pH was adjusted by adding 0.1 M HCl or 0.1 M NaOH. The higher pH solution used for mobilization studies in saturated micromodel was 1 mM NaOH solution (pH 11).

3.1.4. Visualization system

An industrial microscope (Leica Z6 APO) equipped with a Charged Coupled

Device (CCD) camera (Leica MC170 with a resolution of 5 Mpixels) was used to capture images and videos of colloid transport experiments in the micromodel (Figure 15). The transmitted light base of the microscope allows the clear visualization of fluids and colloids in the micromodel. The sensor size of the camera was 6.1 mm x 4.6 mm, with a pixel size of 2592 x 1944. The exposure time varied from 0.5 msec – 500 msec.

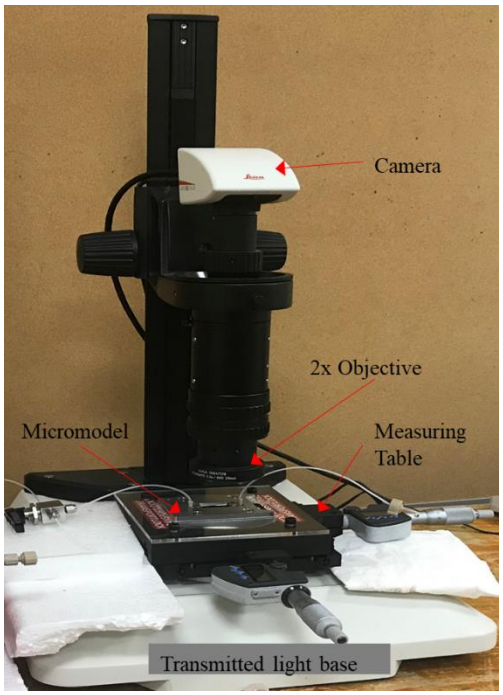

Figure 15. The visualization system used in this study

Additionally, live images captured at 30 fps (frames per second) at a pixel size of 1920 x 1080 pixels. The level of magnification can be adjusted from 0.57x to 3.6x with a 2x objective lens, which provides a final resolution of 4.1 to 0.66 µm/pixel. A digital measuring table was attached to the microscope stage to move the micromodel horizontally or vertically for a known distance up to 25 mm at an accuracy of 1 µm. Multiple images can be captured at each phase of the experiment and stitched together to achieve Representative Elementary Area (will be discussed in section 3.3.2). Leica

Application Suite (LAS EZ) software was used to capture the images and was stored in a computer (DELL 7460) for further analysis.

3.2. Experimental setup

A precision syringe pump (Kats Scientific, NE-1010) was used to inject colloids and colloid-free brine solution into the micromodel using a 10 mL disposable syringe (Cole Parmer). CO_2 was inoculated using a high-pressure Teledyne ISCO pump (500 HP) connected to a commercial CO_2 cylinder (Buzwairgas, 99.99%). Constant pressure mode was adopted to inject CO_2 to eliminate the effect of pressure changes on colloid mobilization. A pressure of 10 ± 1 kPa was maintained during drainage tests. The minimum pressure that can be controlled by the ISCO pump was limited to 70 kPa, and it was reduced to 10 kPa using a high-sensitivity diaphragm-sensing pressure-reducing regulator (Swagelok co). Pressure transducers (OMEGA PX309-100GV) were used to monitor the pressure during the test. To prevent the flow of colloids to the pressure transducer and regulator, an inline filter (Swagelok co) was connected to the micromodel.

3.3. Image processing and analysis

3.3.1. Image Stitching

The images were captured at a magnification of 2.5x to achieve a resolution of 0.94 μm/pixel (image size of 2.43 mm x 1.82 mm). Therefore, an individual colloid can be resolved clearly up to around 5-pixel size. The entire chip imaged by moving the microscope stage for the image size in that direction. A specific overlap of approximately 17% was maintained between two consecutive images to have flawless stitching. For example, 2.0 mm in the horizontal direction or 1.5 mm in the vertical direction. Therefore, the entire chip can be imaged in 7 rows and 10 columns. The

images stitched using the grid/collection stitching plugin in ImageJ software. The stitched images of the entire chip were explicitly used for two purposes; (1) estimating porosity and pore size distribution, (2) evaluating Representative Elementary Area (REA) for porosity. Images during transport experiments are captured only for REA.

3.3.1.1. Porosity and Pore size distribution

Segmentation of the pore space from the solid grains was difficult by intensity thresholding due to the similar intensity of both phases. Therefore, the images were captured after injecting red-dyed water. The red-dyed image of the pore network was segmented into solid and pore space using a threshold value identified by Otsu's algorithm in Matlab. The resulting binary image was used to count the pixels corresponding to solid and pore phases. The ratio of the number of pore pixels to the total pixels represents the porosity of the micromodel, and the estimated value was 0.58.

A distance map was created from the binary image (i.e., segmented image) to generate pore size distribution employing a pixel-based distance transform. Each pixel in the pore space was given a value of the shortest distance to the solid pixels (i.e., pore walls). The medial axis was identified from the distance map, which is the pixels along the center of the channels that are equidistant from the pore wall. The pore size was then obtained from the value of the distance transform at the pixels that form the medial axis. Figure 16 shows the histogram of the pore size assigned to the medial pixels of the image of the micromodel. The mean and median pore widths obtained are 88 and 85 µm, respectively.

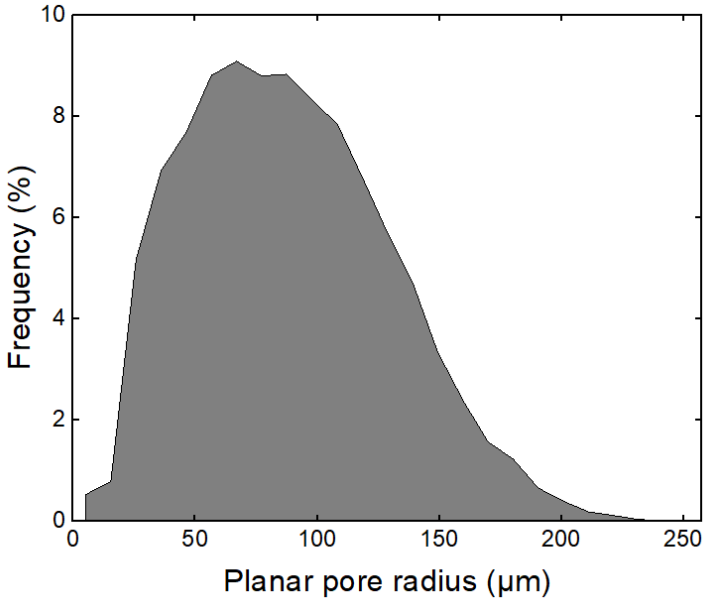

Figure 16. The statistical distribution of radii of inscribed circles of the network model

3.3.1.2. Representative Elementary Area (REA) for porosity

Instead of imaging the whole area of the micromodel, images were captured only for the Representative Elementary Area (REA) during transport experiments. REA was determined by calculating the porosities associated with rectangular areas of the base image, as shown in Figure 17-a. The base image was created by segmenting the entire image of the micromodel, as discussed later. The porosities were plotted for the area of the rectangular sampling areas, as shown in Figure 17b. The porosities of domains larger than an area of 20 mm^2 were calculated as 0.58, which was the porosity of the entire flow network. A stitched image of three rows and three columns of images at 2.5x magnification with a 2x plan apochromatic objective (0.234 numerical aperture, 0.94 µm/pixel resolution) corresponds to an image area of 29.6 mm^2 (4.7x 6.3 mm^2), which is REA.

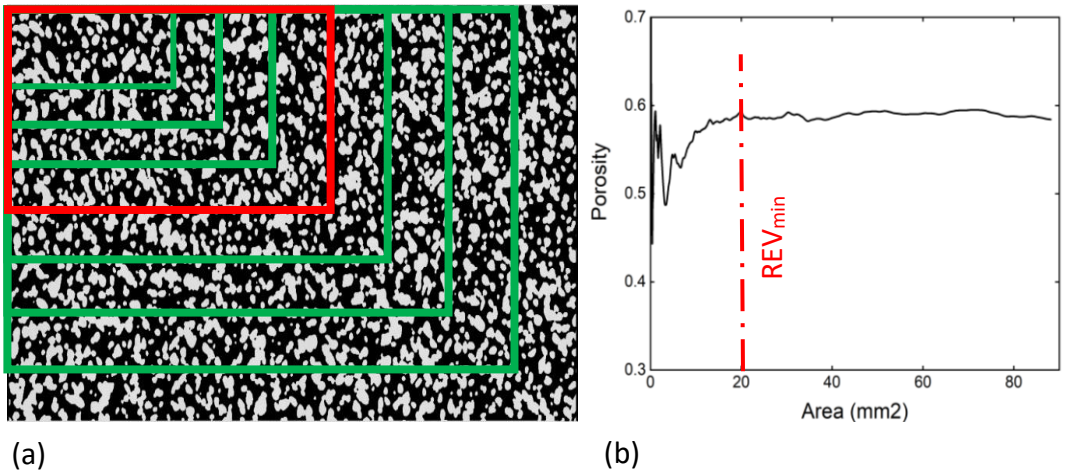

Figure 17. REA calculations: (a) The REA was determined by increasing the sampling area of the base image by 3.5 µm width and 1 µm depth until the porosity values converged, (b) the area of REA was found to be ~ 20 mm^2.

3.3.2. Image Registration

The images captured at various stages of transport experiments, including before and after colloid injection, after colloid mobilization by perturbations in solution chemistry, flow rate, and two-phase flow. The manual movement of the stage to acquire the images at various phases of the experiment and the automated grid stitching can misalign the images even though there was no change in relative position and magnification between the camera and the object. This requires the registration of the group of images for each set of experiments. Image registration is the process of aligning two or more images of the same sections. This process involves applying geometric transformation or local displacements to the distorted image with respect to the reference image (also called fixed image or original image). Automated feature detection and matching algorithm in Matlab Computer Vision Toolbox was used for image registration in this study. Images of the micromodel saturated with water were

considered as the reference image; other images at different phases of the experiment were registered and saved after cropping the boundary pixels. These images are used for further analysis.

3.3.3. Image Filtering

The images after registration may contain artifacts and noise from the low exposure of the camera and cause uneven contrast. The choice of filters from the available filter sources is based on the end-use of the images. Since the filtered images are used for binarization (or segmentation), the best filter should preserve the phase edges while unify or blur the intensity values inside the phases. A combination of bilateral filtering with Gaussian kernels and median filtering was found to yield the best results considering the quality and computational time. Bilateral filters preserve the high contrast regions (i.e., edges) and assign convolutions of blurred scalar values to the neighboring pixels with small variance resulting in conserved edges with blurred noise inside the phases. The median filter replaces the pixel intensity with the median value of the neighboring pixels and removes the impulsive noises in the images while preserving the edges.

3.3.4. Image Segmentation

Segmentation is the process of partitioning an image into multiple regions and assigning specific, meaningful values to it. Automatic and manual thresholding methods were utilized in this study. Automatic thresholding using Otsu's algorithm returns a single intensity threshold that separates the background pixels from foreground pixels. The corresponding intra-class intensity variance will be minimum. This method was used if the histogram of the images has bimodal distribution and poses a deep and sharp valley between two peaks, as shown in

Figure 18. Manual thresholding was adopted in other situations. An interactive ImageSegmenter App in Matlab was used for manual segmentation with the aid of

graph cut, flood fill, and morphological operators. The segmentation of different phases in this study is detailed below.

The solids in the micromodel images are segmented from the red-dye image and are used as the two-phase segmented image. The image of the water-saturated micromodel (termed hereafter as a two-phase mask) was used to identify the gas-phase and colloids in the micromodel. The images were captured at different stages of the experiment, including the images of the micromodel after saturated with colloids, drainage and imbibition.

The colloids in the sat-colloids image were detected by automatic thresholding after subtracting the image from a two-phase mask. The area associated with the colloids was calculated by pixel counting. It was divided with the area of pore space from the two-phase segmented image to calculate the percentage colloids retained in the pore space in the saturated flow experiments.

As the bimodality in the histogram is absent, manual segmentation was adopted to separate the gas phase in the drain and imbibe images. Flood fill algorithm followed by morphological closing and dilation can be utilized to segment the gas phase (gas-segmented). The pixels corresponding to the gas phase was counted and was divided with the area of pore space to obtain the gas saturation. The dark pixels in the drain image and solid phase in the two-phase segmented image were projected to the gas-segmented image to extract a four-phase segmented image (Figure 19). The percentage of colloids in the four-phase segmented can be calculated by pixel counting.

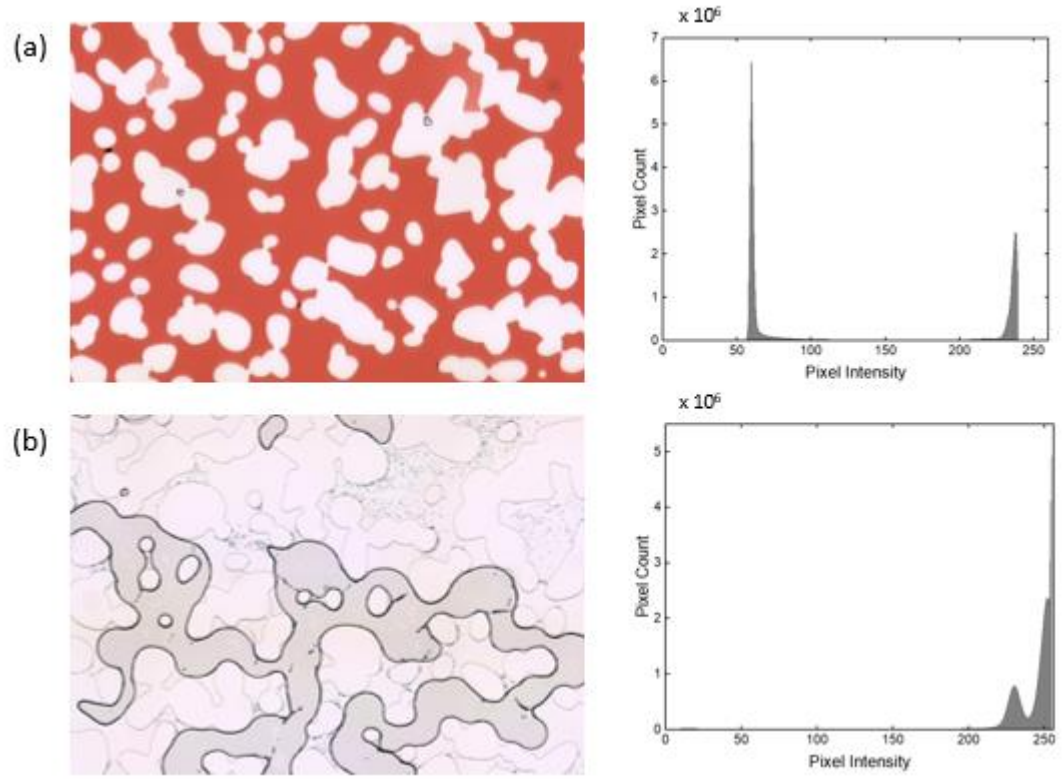

Figure 18. The images and corresponding histograms are shown for (a) Automatic and (b) Manual thresholding

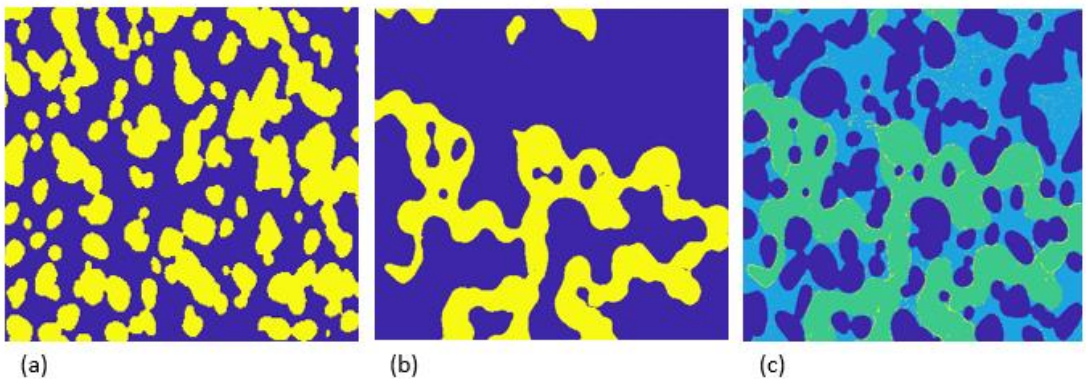

Figure 19. The segmented images: (a) two-phase segmented, (b) gas-segmented and (c) four-phase segmented

CHAPTER 4: COLLOID RETENTION MECHANISMS UNDER DIFFERENT GEOCHEMICAL CONDITIONS DURING SINGLE AND TWO-PHASE FLOW

4.1. Introduction

Colloids promote the transport of pathogens, pesticides, and radionuclides through subsurface environments. Immobilization of the colloids in the porous media limits the transport of colloids and potential contaminants into subsurface water bodies. The configuration of solid-fluid and fluid-fluid interfaces and the geometry of the pore throats controls the retention of colloids in single-and two-phase porous media systems [9,74,228]. The re-mobilization and transport of retained colloids due to changes in flow rate or fluid chemistry during drainage or infiltration might present a potential health hazard due to the outreach of contaminants in subsurface water bodies [87,229]. Therefore, to better design an efficient cleanup and remediation method, there is a need to understand the behavior of colloid retention and mobilization mechanisms and factors that influence them in a microscale single and two-phase porous media systems. Many studies have been conducted on colloid transport and retention through porous media in single and two-phase flow systems [7,9,218,34,57,59,68,101,102,147,179]. However, only a few have focused on pore-scale visualization studies to understand the mechanisms associated with colloid retention and mobilization on various interfaces [2,13,141,14,17,18,24,26,30,31,34]. Moreover, previous studies investigated the retention mechanisms considering the underlying factors individually, which in turn led to contradicting predictions of the behavior of hydrophilic or hydrophobic colloids on various interfaces at different conditions [2,18,25,42]. Therefore, the need to investigate the combined effects of factors such as solution chemistry and colloid

hydrophobicity is critical to better understand colloid retention mechanisms at various conditions and their relations to fluid-fluid and fluid-solid interfaces.

The objective of this work was to investigate the impact of hydrophobicity, solution ionic strength, and pH on colloid retention mechanisms in single-phase and two-phase flow in porous media systems. A physically representative micromodel was used to obtain direct pore-scale visualizations at different experimental conditions. Visual findings were then compared and discussed within the context of the Derjaguin Landau Verwey Overbeek (DLVO) theory.

4.2. Materials and Methods

4.2.1. Materials

A microfluidic chip etched on a borosilicate glass (Micronit Micro Technologies B.V., Netherlands) with an area of 20 mm x 10 mm, and a depth of 20 μm represented the porous medium. The surface of the microfluidic channel was hydrophilic, with an average contact angle 15^0 - 25^0 (Manufacturer's data). The pore volume, porosity, and permeability of the micromodel were 2.3 μL, 0.58, and 2.5 Darcy, respectively. The microfluidic chip, holder, and the tube connections are shown in Figure 20-a and the segmented image of the entire chip in Figure 20-b.

The colloids used in this study were Polystyrene (Hydrophobic PS) and Carboxylate Modified PolyStyrene (Hydrophilic CMPS) (Magsphere Inc., Pasadena, CA) with a mean diameter of 5 μm and a density of 1.05 g/cc. Colloid suspensions of 0.5% concentration were prepared in brine with approximately 7.3×10^7 colloids/mL. The diluted suspensions were sonicated in a water bath for 30 minutes prior to each experiment using an ultrasonic processor (SONICS, Vibra cell) to obtain a monodispersed colloidal suspension. Zeta potential values of the colloids with different

solution chemistry used in this study were measured with Zetasizer (Nano ZSP, Malvern Panalytical, Southborough, MA) at 21^0C. The experimental conditions used in this study are given in Table 2.

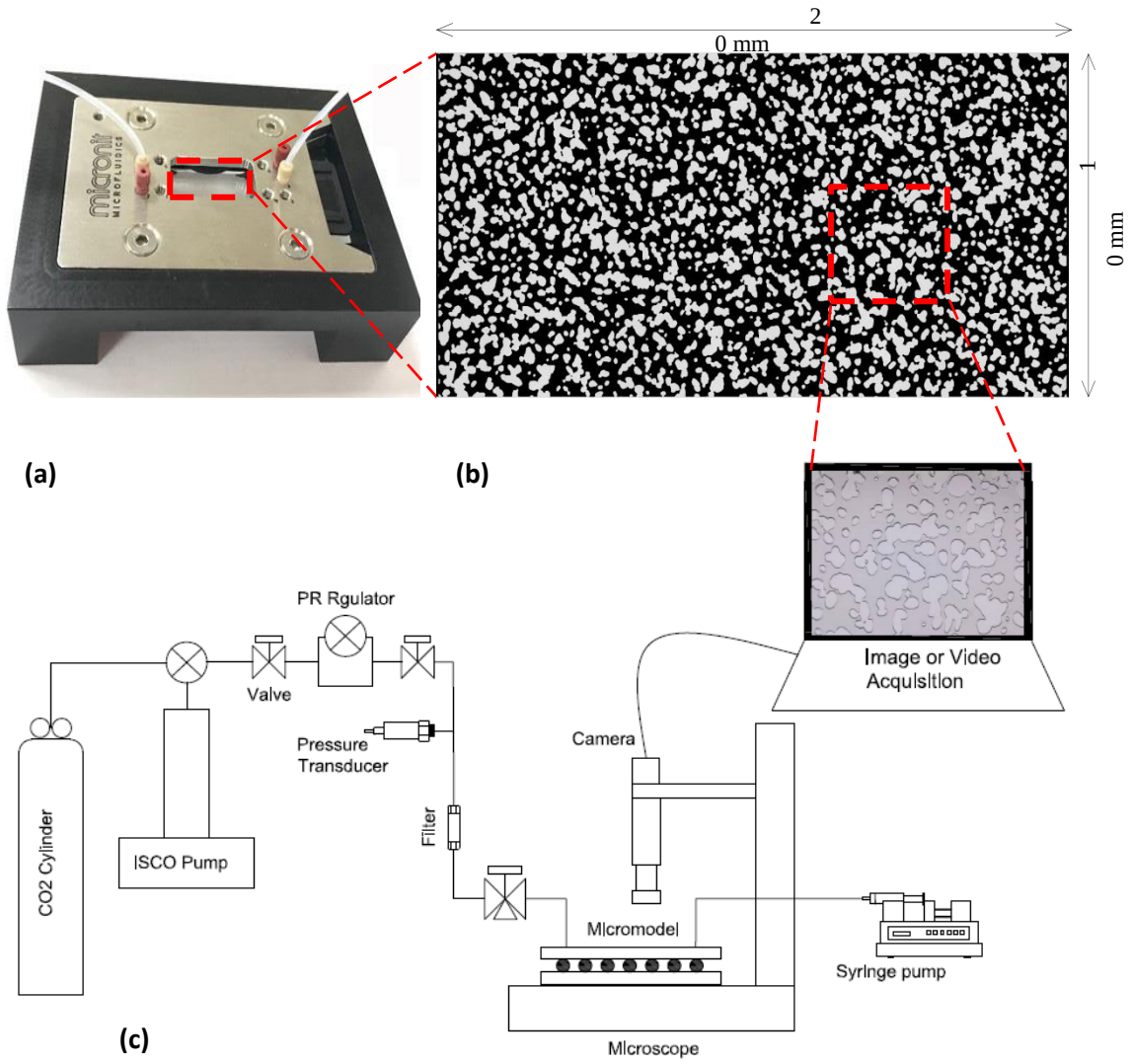

Figure 20. (a) The microfluidic chip, holder and connections used in this study; (b) Segmented image of the entire chip used in this study (black color represents the pore space, and white color represents the solid phase) (c) Schematic diagram of the experimental set up (Note: Figure not drawn to scale).

Brine and Carbon dioxide (CO_2) gas were the two immiscible fluids used in this study. The gas-phase is termed as air-phase in this study. The ionic strength of the brine was changed by adding NaCl, and the pH was adjusted by adding 0.1M HCl or 0.1 M NaOH.

Table 2. List of Experimental Conditions used in this Study

Experiment No.	**Colloid**	**Solution Ionic Strength (mM)**	**Solution pH**	**Zeta Potential (mV)**
PS1	Hydrophobic PS	0	7	-35.00
PS2	Hydrophobic PS	1	4	-31.40
PS3	Hydrophobic PS	1	10	-38.00
PS4	Hydrophobic PS	100	4	-12.74
PS5	Hydrophobic PS	100	10	-29.90
CMPS1	Hydrophilic CMPS	0	7	-15.20
CMPS2	Hydrophilic CMPS	1	4	-3.60
CMPS3	Hydrophilic CMPS	1	10	-10.40
CMPS4	Hydrophilic CMPS	100	4	-3.47
CMPS5	Hydrophilic CMPS	100	10	-5.28

4.2.2. Experimental Setup

Figure 20-c shows a schematic of the experimental setup. The micromodel was placed on a microscope stage (Leica Z6 APO), and the inlet port of the micromodel was connected to a precision syringe pump (Kats Scientific, NE-1010) to inject brine along with colloids. Another port of the micromodel was connected to a Teledyne ISCO pump (500 HP) for CO_2 injection at constant pressure (10 ± 1 kPa) and room temperature (21 ± 1 ^{0}C). The injection pressure was achieved using a high-sensitivity diaphragm-sensing pressure-reducing regulator (Swagelok co), and the pressure was monitored with a pressure transducer (OMEGA PX309-100GV). A commercial CO_2 cylinder (Buzwairgas, 99.99%) supplied the CO_2 gas to the ISCO pump. An inline filter was connected to the micromodel to prevent the flow of colloids to the pressure regulator.

The flow processes in the micromodel were observed using a high-resolution camera (Leica MC170 with a resolution of 5 Mpixels) attached to the microscope with image and video capturing function controlled by a computer. The resolution of the acquired images of the experiments was 0.94 µm/pixel.

The experimental system, including micromodel, tubing, and other components, was cleaned before each test by injecting 100 Pore Volumes (PV) of ethanol followed by 500 PVs of deionized water. The micromodel was dried at 80 ^{0}C for 48 hours and was assembled with all components (Figure 20-c) at room temperature (21 ± 1 ^{0}C). The trapped air and ions inside the micromodel were displaced by injecting several PVs of deionized water. For each experiment, the micromodel was initially saturated with a colloid-free brine solution that would carry the colloids at later steps in the experiments. The colloidal suspension was then injected into the micromodel carefully to avoid inlet clogging. Images of the micromodel saturated with colloids were captured at the end of this step. Then, the system was pressurized using the ISCO pump up to 10 kPa by injecting CO_2 at constant pressure to avoid the effect of change in pressure on colloid migration. While maintaining the pressure in the network, brine was drained at a rate of 10 µL/min (mean pore water velocity of 5.2 m/h, Capillary number, Ca =3.2 x 10^{-7}). The images and videos of colloid mobilization during two-phase flow and their retention on different interfaces were captured. The interfaces of interest include Solid-Water interfaces (SWI), Air-Water Interfaces (AWI), Air-Water-Solid Interfaces (AWSI), and thin films.

4.2.3. Image processing

The number of colloids retained in the micromodel at each stage of the experiments was computed from the captured images and was represented as a

percentage of the pore space. Images were captured at the Representative Elementary Area (REA) of the microchip. REA was determined by calculating the porosities of an expanded rectangular area as shown in Figure 17-a. The minimum REA represents an area of 20 mm^2 with a porosity of 0.58, which matches that of the entire microchip (Figure 17-b). The images were captured at 2.5x magnification with a 2x plan apochromatic objective (0.234 numerical aperture, 0.94 µm/pixel resolution, 2.4 x 1.8 mm^2) to obtain images at a higher resolution. Nine adjacent images were combined using image registration to obtain a large image of an area of 29.6 mm^2 (6.3x 4.7 mm^2) at a resolution of 0.94 µm/pixel, which is REA. A moving stage was used to move the sample holder at a spatial movement in the x and y direction (2 mm and 1.5 mm, respectively), which in turn provides sufficient overlap for image registration to allow imaging at different locations to assemble a large image.

Pore space in the micromodel was identified by segmentation of image captured with dye-mixed water using a threshold value determined by Otsu's method [242]. Air-phase and colloids in the pore space were segmented using a flood fill algorithm and Otsu's method, respectively [242,243]. Each segmentation process was preceded by the application of an edge-preserving Gaussian bilateral filter followed by a median filter to enhance the contrast of the phases and remove any possible noise in the image. Pixel counting was adopted to obtain the percentage of particles retained after single and two-phase flow experiments. Colloids on AWI were quantified by counting the pixels in the colloid phase that has Air-phase in the neighboring pixel.

4.3. Theoretical Considerations

4.3.1. DLVO forces

The theoretical DLVO profiles of the colloids interacting with other colloids or

interfaces were calculated as the sum of van der Waals (E_{vdW}), electrostatic (E_e), and hydrophobic (E_h) energies [2,80–82,94]. Surface potentials replaced the measured zeta potential values in electrostatic energy calculations. All parameters and equations used to compute the DLVO energy profiles are given in Section 2.2.2: and 2.2.3: In the DLVO energy profiles, negative interaction energies indicate an attraction while the positive energy represents a repulsion for colloid-colloid, colloid-SWI or colloid-AWI interactions.

4.3.2. Detachment forces

While fluid drag force is acting as the detachment force in single-phase flow, capillary forces are dominant in mobilizing attached colloids from SWI in two-phase flow. The drag forces generated on a partially submerged particle will be smaller in magnitude compared to the adhesive forces during two-phase flow [23,34,108]. The capillary forces acting on a colloid along the contact line between SWI and AWI (can be termed as AWSI, i.e., Air-Water-Solid Interface) can be calculated as a function of surface tension, the contact angle of the colloid (θ) and the angle determining the position of AWI on the colloid surface (φ) [34]. Two magnitude maxima can be obtained for capillary force; one for $\varphi < \theta$ (capillary forces directing towards Air-phase) and other for $\varphi > \theta$ (capillary forces directing away from Air-phase, 2.2.6:) [34]. The two components of capillary forces can be derived based on the contact angle of the solid surface (α). A friction force acts at the contact point that opposes the colloid movement on the solid surface.

Figure 21 provides a conceptual schematic of forces acting on a colloid as AWI advances along the colloid surface. While AWI encounters a deposited particle, a small initial value of φ ($\varphi < \theta$) can result in colloid lifting by AWI, assuming the capillary

force exceeds the magnitude of adhesion force on SWI (Figure 21-a). The capillary force acting on a colloid at AWSI was reported to be two orders of magnitude higher than DLVO forces [21,141]. Further wetting of colloid ($\varphi > \theta$) can change the direction of the capillary force, as shown in Figure 21-b. The frictional force can balance the horizontal component of the capillary force that pushes the colloid back into bulk fluid. The retained colloids remain attached to AWSI and later on thin films while AWI advances further on the solid surface, as shown in Figure 21-c. Thick water films, as shown in Figure 21-d, prevent colloid pinning on AWSI; instead, the interaction is similar to the case in Figure 21-a, where the colloid remains attached to AWI. Thick water films formed around the solid surfaces due to the etched shape of the channel, as shown in Figure 21-e.

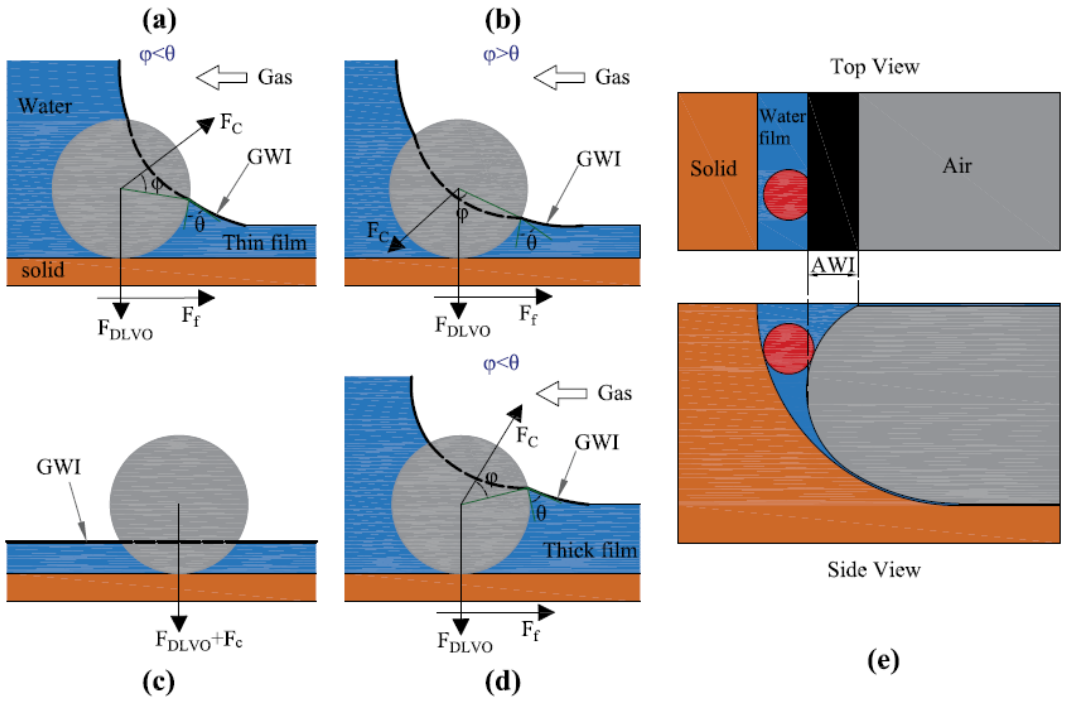

Figure 21. Colloids are interacting with the drainage front. Capillary forces and DLVO forces are considered. Interface position on colloid (a) for AWI interaction; (b) for AWSI capillary retention; (c) thin-film attachment; (d) for AWSI straining; (e) thick water film formed around the solid surface due to the channel shape. φ is the angle

determining the interface position on the colloid surface, and θ is the colloid contact angle.

4.4. Results and Discussion

Ten sets of experiments were conducted at the experimental conditions given in Table 2. Each experiment was conducted under single and two-phase flow. Colloid mass retained in the pore space after single and two-phase flow was determined from the captured images by image processing and are shown in Table 3. The computed DLVO energy profiles for each experimental condition used in this work are presented in Figure 22 for all possible interactions: colloid-colloid, colloid-SWI, and colloid-AWI interactions. The computed primary energy minimum (ϕmin1), the energy barrier (ϕmax1), and secondary energy minimum (ϕmin2) are given in Table 4.

Table 3. Colloid Mass Retained in the Micromodel

Colloid type	**Exp. Condition**	**Initial colloid content (% of pore space)**	**The ratio of retained mass after drainage to the initial colloid content (%)**	**The ratio of retained mass on AWI to the initial colloid content (%)**	**The ratio of retained mass on AWI to the total mass retained after drainage (%)**
Hydrophobic Colloids	PS1	2.47	5.9	3.4	57.7
	PS2	1.63	29.8	25.93	87.0
	PS3	3.00	7.7	5.52	71.7
	PS4	3.50	62.6	38.43	61.4
	PS5	1.23	35.7	28.92	81.0
Hydrophilic Colloids	CMPS1	4.41	76.9	34.5	45.1
	CMPS2	2.08	77.6	54.32	70.0
	CMPS3	1.92	47.8	28.3	59.2
	CMPS4	2.17	90.0	47.88	53.2
	CMPS5	2.38	56.9	38.4	67.5

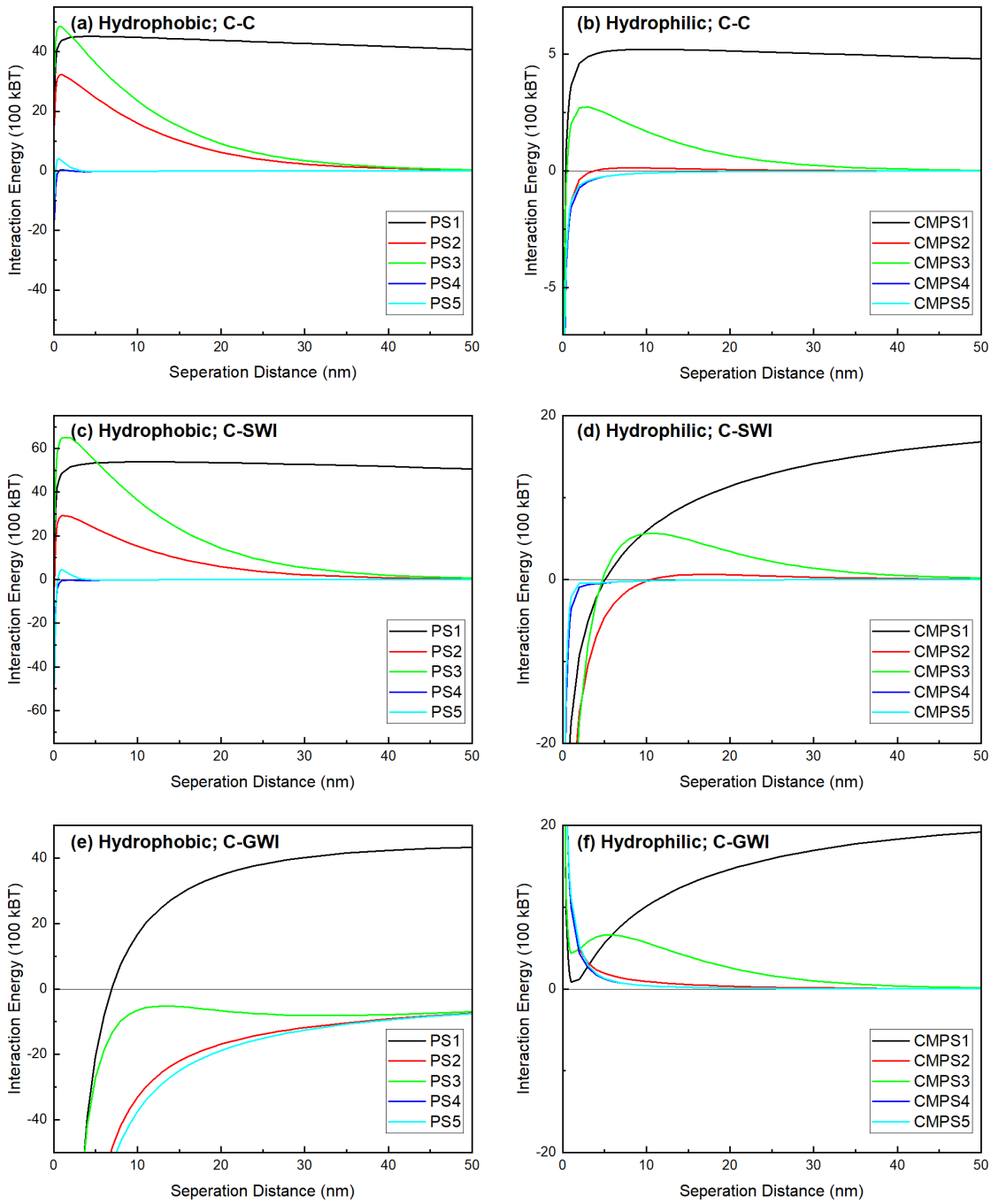

Figure 22. Computed DLVO interaction energies of colloids with other colloids (C-C), or SWI (C-SWI), or AWI (C-AWI) at different solution chemistry for hydrophobic and hydrophilic colloids.

Table 4. Estimated Values of φ_{min1}, φ_{max1} & φ_{min2} for Hydrophobic and Hydrophilic Colloids at various Interfaces

		Hydrophobic Colloids (PS)			**Hydrophilic Colloids (CMPS)**		
ID	Interaction	φ_{min1} (100 kBT)	φ_{max1} (100 kBT)	φ_{min2} (100 kBT)	φ_{min1} (100 kBT)	φ_{max1} (100 kBT)	φ_{min2} (100 kBT)
1	Colloid-Colloid	na	45.2	na	-12.8	4.6	na
2	Colloid-Colloid	na	31.7	na	-25.8	0.03	na
3	Colloid-Colloid	na	47.7	na	-22.3	2.6	na
4	Colloid-Colloid	-23.6	0.08	na	-25.9	na	na
5	Colloid-Colloid	-3.72	3	-0.3	-25.3	na	na
1	Colloid-SWI	na	53.8	na	-70.3	8.5	na
2	Colloid-SWI	-3.2	29.36	na	-71	0.63	na
3	Colloid-SWI	na	65	na	-55	5.6	na
4	Colloid-SWI	-31	0.02	-0.42	-63.6	na	na
5	Colloid-SWI	-4.8	10.4	-0.25	-58.2	na	na
1	Colloid-AWI	-361	43.3	na	na	78.3	na
2	Colloid-AWI	-922	na	na	na	109	na
3	Colloid-AWI	-853	na	na	na	79.8	na
4	Colloid-AWI	-917	na	na	na	110.9	na
5	Colloid-AWI	-903	na	na	na	96.8	na

4.4.1. Colloid Retention in Single-Phase Flow

Single-phase colloid transport experiments were conducted to examine the effects of solution chemistry and the type of colloid on colloid retention mechanisms. Figure 23 shows the pore-scale images of size, 2.0 mm x 1.5 mm (2127 x 1595 pixels) at different experimental conditions given in Table 2. The captured images confirm that there are two colloid interactions in single-phase flow; colloid–colloid and colloid-SWI interactions. The significance of these two mechanisms was greatly influenced by the ionic strength, pH, and type of colloid, as will be discussed in the following sections.

4.4.1.1. Colloid-Colloid Interaction

Pore-scale images shown in Figure 23 show three distinct mechanisms of

colloid-colloid interactions identified in single-phase flow, namely; (a) repulsive interaction (RI) that leads to the formation of dispersed colloids in the pore space (b) short-range interaction (SRI) that leads to the development of small flocs near the solid surface only and (c) long-range interaction (LRI) that leads to the formation of larger colloidal aggregates. Table 5 summarizes the observed interactions at different experimental conditions.

The repulsive interactions, RI, were observed for hydrophobic colloids at low ionic strength or high pH conditions (Figure 23-a, c, e, and i). In contrast, short-range interactions, SRI, was observed near the solid surfaces at high ionic strength and low pH case (Figure 23-g). Additionally, hydrophilic colloids at low ionic strength and high pH exhibited SRI (Figure 23-b and f). Long-range interaction, LRI, was detected only for hydrophilic colloids at high solution ionic strength or low pH (Figure 23-d, h, and j).

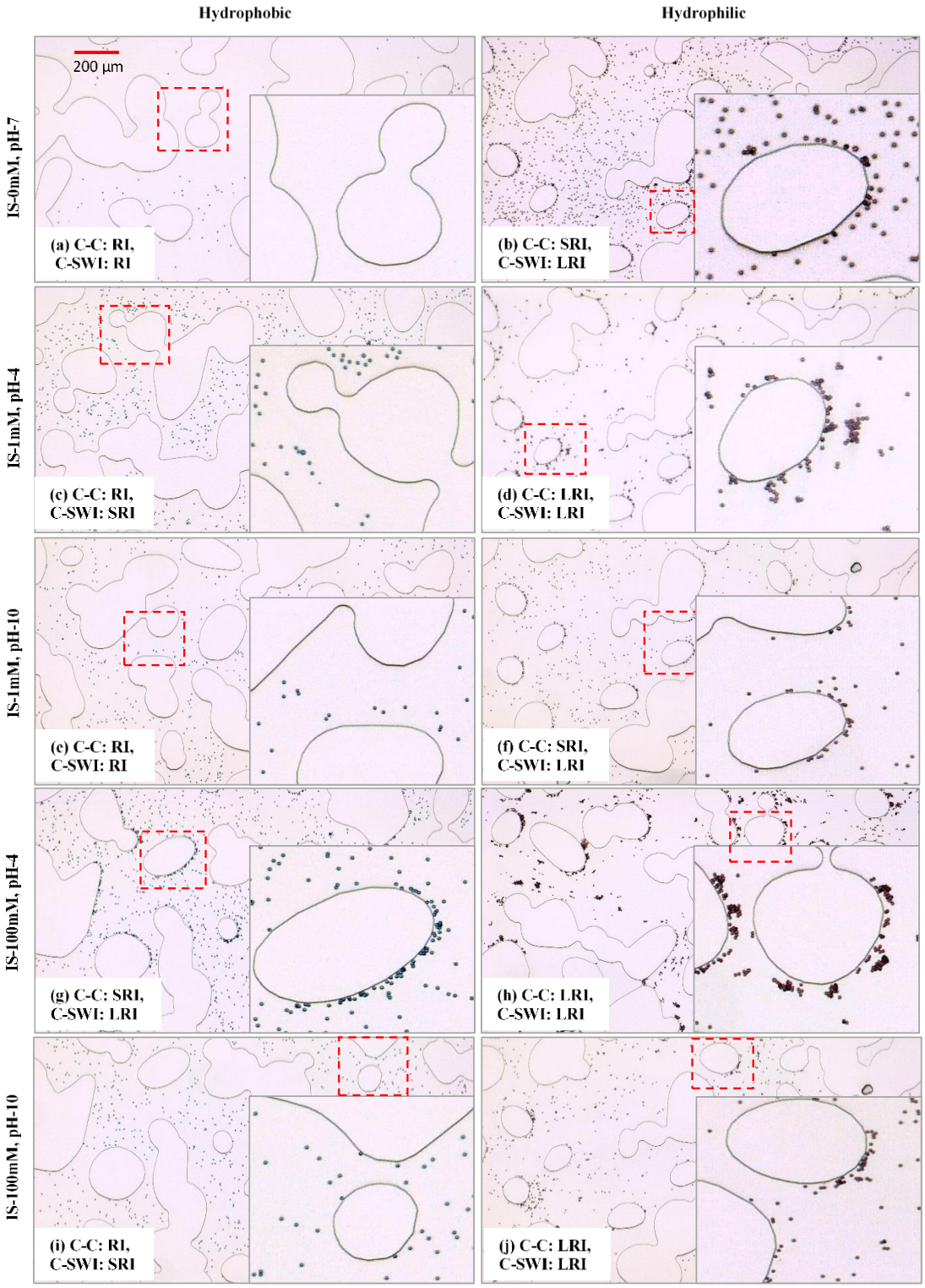

Figure 23: Colloid interactions in Single-Phase flow at different experimental conditions. RI: Repulsive Interaction, SRI: Short-Range Interaction, LRI: Long-Range Interaction

Table 5. Summary of Interactions for Colloids at Various Conditions

	Hydrophobic Colloids					Hydrophilic Colloids				
IS (mM)	0	1		100		0	1		100	
PH	7 (PS1) (a)	4 (PS2) (c)	10 (PS3) (e)	4 (PS4) (g)	10 (PS5) (i)	7 (CMPS1) (b)	4 (CMPS2) (d)	10 (CMPS3) (f)	4 (CMPS4) (h)	10 (CMPS5) (j)
C-C (Figure 23)	RI	RI	RI	SRI	RI	SRI	LRI	SRI	LRI	LRI
C-SWI (Figure 23)	RI	SRI	RI	LRI	SRI	LRI	LRI	LRI	LRI	LRI
C-AWI (Figure 24)	CR/HI	CR	CR/HI	CR	CR	CR	CR	CR	CR	CR
C-AWSI/Thin film (Figure 25)	S	S	S	CR	CR	CR	CR	CR	CR	CR

RI: Repulsive Interaction; **SRI:** Short-Range Interaction; **LRI:** Long-Range Interaction;

CR: Capillary Retention; **CR/HI:** Capillary Retention/Hydrophobic Interaction; **S:** Straining only.

Figure 23 indicates that hydrophilic colloids show a higher tendency to aggregate as compared to hydrophobic colloids. These visual findings contradict previous studies where it was suggested that the aggregation of hydrophobic colloids was caused by hydrophobic interaction [12,18]. However, pore-scale observations from Figure 23 confirm the independence of hydrophobic interaction on colloid aggregation, as hydrophobic particles were more stable at different conditions. Conversely, the magnitude of zeta potential plays a significant role in the observed stability trend in our study, as suggested in previous studies [244,245]. The measured zeta potentials were higher for hydrophobic colloids, which explains its greater stability compared to hydrophilic colloids. Moreover, the types of interaction can be effectively interpreted using the measured zeta potential values of colloids that are strongly affected by the solution chemistry for both types of colloids (Table 2). Zeta potential values given in Table 2 at different conditions ranged from -3.47 mV to -38 mV. These values are in agreement with the general trend that magnitude of zeta potentials decrease as the ionic strength increases or pH decreases. The type of interactions revealed from the pore scale images at different conditions (Figure 23) can be linked to their zeta potential values in Table 2. Accordingly, from pore-scale images, RI interactions were observed for zeta potential values greater than 30 mV. Whereas LRI were observed when the magnitude of zeta potential is less than 6 mV. For zeta potential values between 6 mV and 30 mV, SRI was the observed interaction in our study.

In addition to zeta potentials, the calculated DLVO energy profiles, as shown in Figure 22-a, b, and Table 4 also can explain the observed colloid behavior. In other words, the occurrence of repulsive peak (ϕ_{max1} in Table 4) on the energy profile without the energy minima (ϕ_{min1}) caused RI and thereby prevented particles from interacting to form aggregates (for systems PS1, PS2, and PS3). Similarly, when the energy barrier

between the colloids was negligible, significant colloid aggregation was observed due to LRI (as observed in the pore-scale images of systems CMPS2, CMPS4, and CMPS5). The aggregation was distributed primarily during diffusion among colloids. Therefore, the small energy barrier (less than 5 kBT) can be overcome by the diffusion kinetic energy, as observed in the CMPS2 system [130,131].

Moreover, the coexistence of the energy barrier and primary minima on the energy profile indicates that SRI dominates where the colloids overcome the repulsive barrier to interact with other colloids in the strong primary minimum. For instance, a greater repulsive peak for CMPS1 and CMPS3 (460 and 260 kBT, respectively) was defeated by the collision of dispersed colloids in bulk water with the deposited colloids on SWI (Figure 23-b and f). In contrast, SRI for PS5 (Figure 23-i) was not observed in the images (although the primary minimum exists and the energy barrier is 200 kBT) as the colloid interaction with SWI is unfavorable (with greater energy barrier) for that case.

Findings indicate that, in single-phase flow, the general colloid-colloid interaction behavior predicted by colloid zeta potential and DLVO energy profiles are in agreement with the trends observed in pore-scale images. In general, the interaction became favorable with the increase in ionic strength and the decrease in pH. However, pore-scale images obtained in this study reveals that the coupled impact of ionic strength and pH must be considered to understand colloid-colloid interaction mechanisms better.

More interestingly, the understanding of colloid interaction mechanisms is significant to predict their retention in porous media. Colloids that exhibits RI remain dispersed in the pore space, and therefore their potential to be transported along with the flowing fluid and release the contaminants into the groundwater sources is high. On

the other hand, in systems where colloids exhibit SRI, ripening or bridging in the porous media occurs, and larger aggregates formed as the interactions develop to LRI, which eventually causes clogging of small pore throats. The progressive clogging of the porous media by the SRI or LRI may lead to permeability decrease and potential formation damage. Conversely, the retention of colloids under those conditions prevent the outbreak of contaminant into the subsurface water bodies.

4.4.1.2. Colloid-SWI interactions

Three distinct colloid-SWI interaction mechanisms were observed as shown in Figure 23, namely, (a) repulsive interaction (RI) that leads to suspension of colloids in bulk water (b) short-range interaction (SRI) that leads to attachment only at the bottom of the micromodel and (c) long-range interaction (LRI) that leads to the colloid attachment on solid surfaces. RI was observed for hydrophobic colloids at low ionic strength and high pH conditions (Figure 23-a and e), whereas SRI was observed at low pH or high ionic strength case (Figure 23-c and i). Hydrophobic colloids exhibited LRI at high ionic strength and low pH (Fig. 5-g) as well as hydrophilic colloids at all solution chemistry in this study (Fig. 5-b, d, f, h, and j).

Pore-scale images obtained at different experimental conditions shown in Figure 23 clearly show that hydrophilic colloids were attached to the solid surfaces regardless of the solution chemistry. In contrast, hydrophobic colloids show a clear trend of the dependence of colloid attachment on solution chemistry (both ionic strength and pH). Previous studies suggested that colloid interactions on SWI are independent of solution chemistry under favorable attachment conditions (i.e., the colloid and solid surface have opposite surface charges [147,155,188]).

Pore-scale images show that although hydrophilic colloids and solid surfaces used in this study were negatively charged, favorable attachment conditions were

observed when the surface charge of the colloid was close to zero, as seen in Table 2 (i.e., less than 15 mV).

As shown on the DLVO energy profiles in Figure 22-d, although significant energy barrier existed at low ionic strength for hydrophilic colloids (i.e., systems CMPS1, CMPS2, and CMPS3), substantial attachment to the solid surfaces were observed under these conditions. This is because, as the colloids move, their kinetic energy increase and overcome the energy barrier and eventually transferred from the bulk fluid domain to the near-surface domain. Consequently, attachment occurs at SWI due to the occurrence of a considerable primary minimum at the near-surface domain (up to 5 nm, because of LRI), as shown in Figure 22-d. Also, for hydrophobic colloids, the coupled effects of high ionic strength and low pH (for PS4) resulted in LRI where the magnitude of zeta potential was less than 15 mV, and the interaction curve shows a negligible energy barrier (Figure 22-c).

As mentioned, the interaction of hydrophobic colloids with SWI follows a strong dependence on solution ionic strength as well as pH. This observation is consistent with previous studies where the colloids under unfavorable attachment conditions (like surface charges for colloid and solid surface) can retain at secondary energy minima at high ionic strength [147,188]. However, in our experiments, we confirm primary minimum attachment rather than secondary minimum attachment by observing colloid detachment by ionic strength perturbations (colloids attached to secondary minima release when the ionic strength reduced). Nevertheless, findings indicate negligible detachment with the ionic strength reduction from 100 mM to 0 mM (for PS5), and that predicts the occurrence of primary minimum interaction of those colloids at higher ionic strength. Additionally, the colloid attachment was observed for PS2 (low pH and ionic strength), although the secondary minimum was absent on the

DLVO profile. For those cases, the repulsive energy barrier prevents the near-surface interaction on the solid surfaces while the suspension flows through the porous media. However, during our experiments, single-phase flow ceases before beginning two-phase flow, and therefore, the colloids settle down the bottom of the micromodel (as the pore depth is 20 μm and the settling time calculated based on Stoke's law was less than 1 minute). Consequently, the colloids come closer to SWI and interact at shorter separation distance to attach at the micromodel bottom because of SRI. Conversely, the absence of energy minima at lower ionic strength and higher pH (for systems PS1 and PS3) prevent the attachment of those colloids settled down the porous media (due to RI). They remain suspended in bulk water and transported along with the moving fluid. However, very few colloids interact with SWI due to the charge variability or nanoscale surface roughness of the micromodel, as reported in previous studies [204,212,246,247].

Pore-scale images reveal that hydrophilic colloids exhibited favorable attachment condition, whereas hydrophobic colloids show unfavorable conditions. Therefore, hydrophilic colloids extensively retained on SWI in porous media irrespective of the solution chemistry. However, for hydrophobic colloids, with the increase in ionic strength, the retention mechanism varies from RI to SRI at higher pH (PS3 and PS5) and from SRI to LRI at lower pH (PS2 and PS4). This observation was consistent with the decrease in the magnitude of the zeta potential of the colloids (Table 2) as well as the solid surface, which is glass. Zeta potential of glass surface increased from -60 mV to -18 mV with an increase of ionic strength from 0 mM to 600 mM. and from -85 mV to -45 mV for a decrease in pH from 10 to 2.5 [84,85,248].

4.4.2. Colloid Mobilization and Retention in Two-Phase Flow

As mentioned earlier, single-phase experiments were followed by drainage with

CO_2 at a constant flow rate of 10 µL/min. Consequently, water saturations were reduced to the residual values in all experiments, which was determined from image processing as 54.8 % (± 4.6). Table 3 shows the masses of colloids retained after two-phase flow, as estimated by processing the images for an REA. Figure 24 shows pore-scale images of size, 2.0 mm x 1.5 mm (i.e., 2127 x 1595 pixels) after drainage at different experimental conditions in this study. As observed from the pore-scale images, the deposited colloids were mobilized by moving AWI during two-phase flow. The mobilized colloids remain attached on AWI and transported along with moving AWI or retained on stationary AWI in the pore space, besides a small number of colloids observed in the Gas-phase (retained in thin films, will be explained later). Generally, there was no detachment of colloids observed from AWI during drainage experiments. Nevertheless, colloids on AWI freely move along the interface and immobilize on other retention sites, including Gas-Water–Solid Interface (AWSI) and thin water films. The random movement of colloids on AWI occurs due to Brownian motion or hydrodynamic forces, as reported in previous studies [14,23,237].

The ratio of the retained mass of colloids after drainage to the initial colloid content (given in Table 3) indicates the effect of hydrophobicity, ionic strength, and pH on colloid mobilization. There was a significant difference in the number of colloids retained after drainage for the hydrophobic (ranged from 5.9% to 62.6%) and hydrophilic colloids (ranged from 47.8% to 90%) at similar experimental conditions. This data shows that a substantial mass of colloids was detached and removed from the porous media for hydrophobic colloids compared to hydrophilic colloids during drainage. Moreover, the percentage of retained hydrophobic colloids on AWI after drainage approximately 20-30% higher than hydrophilic colloids. This observation indicates a strong colloid-SWI interaction for hydrophilic colloids (Table 3, column 6).

Data in Table 3 shows a clear trend of increasing colloid retention as ionic strength increases or as pH decreases upon the invading of the AWI. Colloid retention ranged from 5.9% to 62.6% for hydrophobic colloids, whereas it ranged from 47.8% to 90% for hydrophilic colloids. However, unlike the expected reduced colloid retention of CMPS1 (due to low ionic strength and high pH), greater retention was observed (76.9%), as indicated in Table 3. A possible reason for this observation could be a higher initial colloid concentration in the porous media, and this result shows the effect of in situ colloid concentration on colloid mobilization. Furthermore, the smaller colloid retention on AWI for higher ionic strength and lower pH cases (for PS4 61.4% and CMPS4 53.2%) indicates enhanced colloid affinity to SWI with the increase in ionic strength. The greater affinity of those colloids to SWI was reported in the previous literature due to the ionic strength and pH effect [26,34].

4.4.2.1. Colloid-AWI interaction

Retention of colloids on AWI was observed in all the experimental conditions irrespective of the type of colloids and solution chemistry, as shown in Figure 24. Colloid retention occurs due to two types of interactions, namely hydrophobic interaction, HI, of mobile colloids on stationary AWI, and capillary retention, CR, of colloids attached to the SWI by moving AWIs. HI was observed only for hydrophobic colloids at low ionic strength and high pH conditions (Figure 24-a, and e), whereas CR was the dominant mechanism for colloid attachment on AWI and was observed in all experimental conditions including those cases where HI was observed (Table 5).

DLVO forces calculated incorporating hydrophobic forces shows attractive interaction of hydrophobic colloids on AWI (Figure 22-e), whereas repulsive forces were observed for hydrophilic colloids as hydrophobic forces are negligible (Figure 22-f). As the hydrophobic force is attractive between two hydrophobic surfaces, the

superhydrophobic AWI should be a favorable site for retaining hydrophobic colloids [92,93,249,250] when a mobile hydrophobic colloid approach a stationary AWI, hydrophobic forces prevail after thinning and rupture of the hydration layer around the colloid. Previous studies reported that the hydration layer of hydrophobic colloids was less stable compared to hydrophilic colloids and can be ruptured easily to form a three-phase contact line with AWI [251–253]. Additionally, it is unlikely that hydrophilic colloids transport to stationary AWI as the strong adhesion forces eradicate the existence of mobile colloids at all experimental conditions.

Repulsive colloid-SWI interaction for PS1 and PS3 induced colloids to move in the bulk water. The absence of mobile colloids in the rest of the conditions eliminated the chance of hydrophobic interaction. Comparatively less retention was observed for these colloids as the mobile colloids transported through the connected flow path, and only a few colloids trapped in immobile water zones were available to interact with AWI as observed from Figure 24-a and e. The hydrodynamic forces in the stagnant water zones bring the colloids close to AWI and slide along the interface, as seen in Movie 1. During its movement closer to AWI, the attachment occur when the contact time is greater than the time required for thinning and rupture of the hydration layer and formation of a three-phase contact line [252,254,255]. The reversal of the flow field (through the water film) near the solid surface distracts the moving colloids near AWI and prevents further interaction, as observed from Movie 1 (Supporting Material). However, very few colloids were attached to AWI by film rupture and hydrophobic interaction.

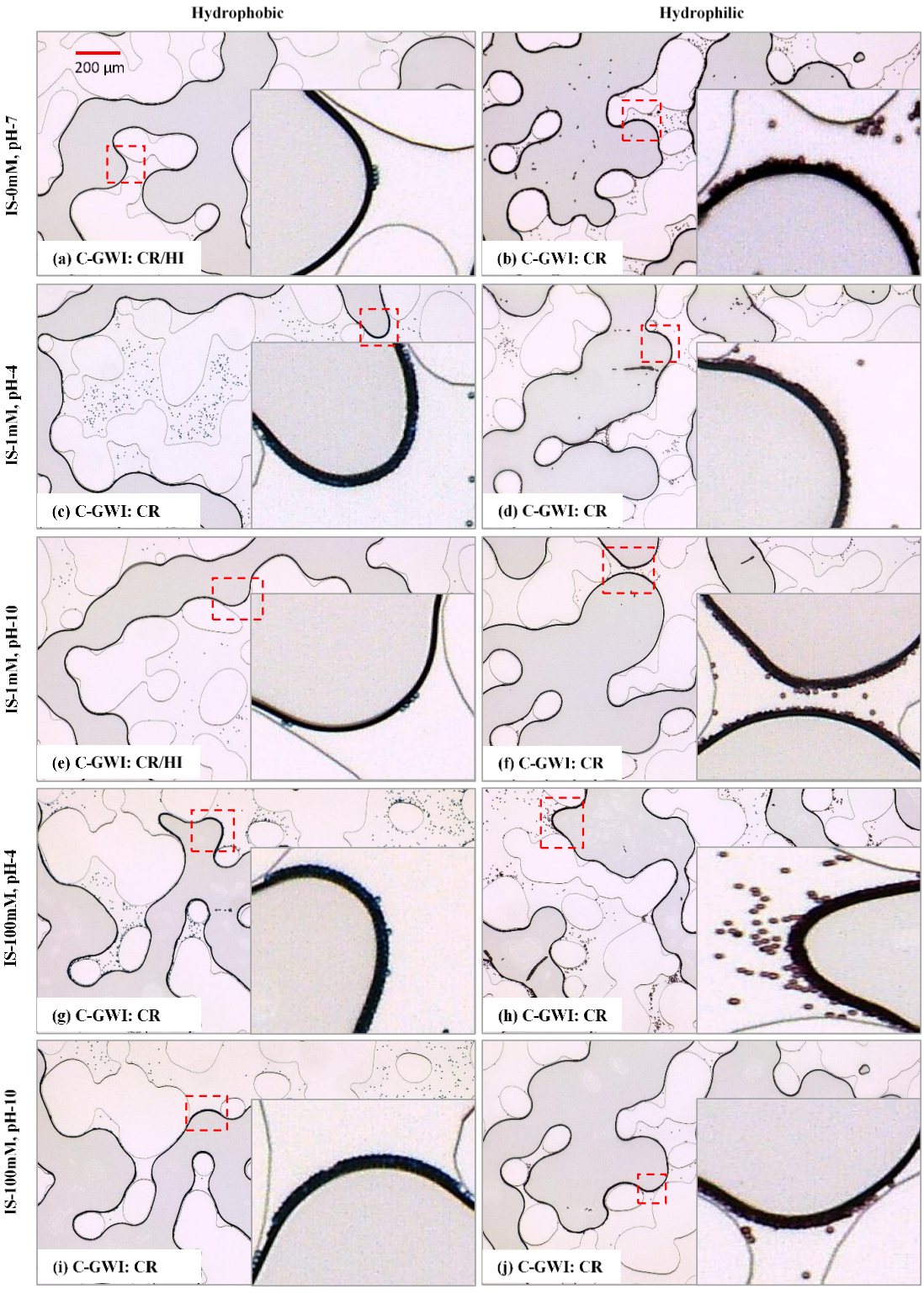

Figure 24: Colloid interactions in Two-Phase flow at different experimental conditions; colloids interacting with GWI. CR: Capillary Retention, HI: Hydrophobic Interaction

Initially, deposited colloids (during single-phase flow) were detached by the

passage of AWI during drainage, as observed in Movie 2. When the moving GWI encounters deposited colloids, the interface deforms to form a three-phase contact line. Considering the force balance (Fig. 3), the vertical component of the capillary force exerted on the colloid lifted the colloids from SWI as it dominates over the adhesion force resulting in Capillary Retention (CR) on GWI.

The findings from our study conclude that the mobile colloids in the porous media (due to repulsive SWI interactions) can interact with stationary AWI, and the attachment occurs if the contact time is enough to establish hydrophobic interaction. This interaction was not observed for hydrophilic colloids as they are strongly attached to SWI. CR was the major retention mechanism (on AWI) observed under this study irrespective of the type of colloid. As the number of colloids available to interact with the moving AWI increases (with an increase in ionic strength or decrease in pH), the number of colloids interacting with AWI also increases as indicated by the higher percentage of initial colloids retained on AWI (38.43% for hydrophobic and 47.88% for hydrophilic colloids, Table 3, column 5). However, greater colloid affinity to SWI under these conditions can explain the reduced colloid mass on AWI as a percentage of colloids retained after drainage (61.4% for hydrophobic and 53.2% for hydrophilic colloids, Table 3, column 6).

4.4.2.2. Colloid-AWSI interaction and thin film attachment

Figure 25 shows pore-scale images of colloid retention on AWSI and thin films after drainage. AWSI and thin films around the solid surfaces (formed due to the channel shape, Figure 21-e) were visualized in these experiments. Two distinct types of colloid retention mechanisms were observed on AWSI in this study, namely straining, S, around the solid surfaces and Capillary Retention, CR, on AWSI, and thin films at the top and bottom of the micromodel. Straining was observed in all

experimental conditions conducted in this study, whereas capillary retention was observed for hydrophilic colloids and hydrophobic colloids only at higher ionic strength conditions (Figure 25).

Colloids that are freely moving on AWI are trapped and immobilized near the solid phase, as seen in Movie 2 (Supporting Material). This observation was consistent with previous studies that reported that the hydrodynamic drag was influenced by the film thickness on the solid boundary; colloids were trapped on thin films around the solid phase when the film thickness became less than the colloid diameter. [256–258]. As measured from the captured images, film thickness approximately equals the colloid diameter (i.e., 5 μm). In such a case, colloids were trapped by a straining mechanism on the AWSI. Further invasion of AWI in the pore space led to more straining on water films around the solid phase (e.g., Figure 25-a, c, and e). Straining of colloids on AWSI and water films were observed for all the experimental conditions in this study due to the rearrangement or alignment of colloids retained on AWI towards the solid surfaces. However, Capillary Retention was feasible only when DLVO and capillary forces are strong enough to pin the colloids on SWI at AWSI. Therefore, all hydrophilic colloids and hydrophobic colloids only at higher ionic strength were experienced CR at AWSI and thin films near the top and bottom of the micromodel. On the other hand, hydrophobic colloids at low ionic strength experience retention on AWSI and thin films by straining only, as shown in Figure 25-a, c, and e.

Unlike DLVO forces, capillary forces are independent of electrostatic characteristics and affected solely by the size and contact angle of the particle and surface tension between two fluids. Although the size of the particles and surface tension remained the same, the contact angle was smaller for hydrophilic colloids compared to hydrophobic colloids. It is, therefore, likely that higher capillary retention

occurs for hydrophilic colloids due to its greater capillary potential (Figure 25, Table 5).

Colloids on AWSI would experience capillary forces directing towards the water phase, as shown in Figure 21-b. The vertical component of this capillary force, along with the DLVO forces, can cause colloid pinning on AWSI. The frictional force on solid surface opposes the horizontal component of the capillary force, which tends to release the colloid back into bulk solution and thereby retain the colloid on AWSI. A solid-water contact angle greater than 45^0 was not expected to retain the colloid on AWSI [21,141]. Nevertheless, the pinning of AWI, as seen in Figure 25-b, d, f, g, h, i, and j confirm the AWSI attachment in our study where the average contact angle of the micromodel was 20^0. For hydrophobic colloids at lower ionic strength, smaller or absence of adhesive forces (i.e., ϕ_{min1}) with SWI prevent capillary pinning on AWSI or thin films.

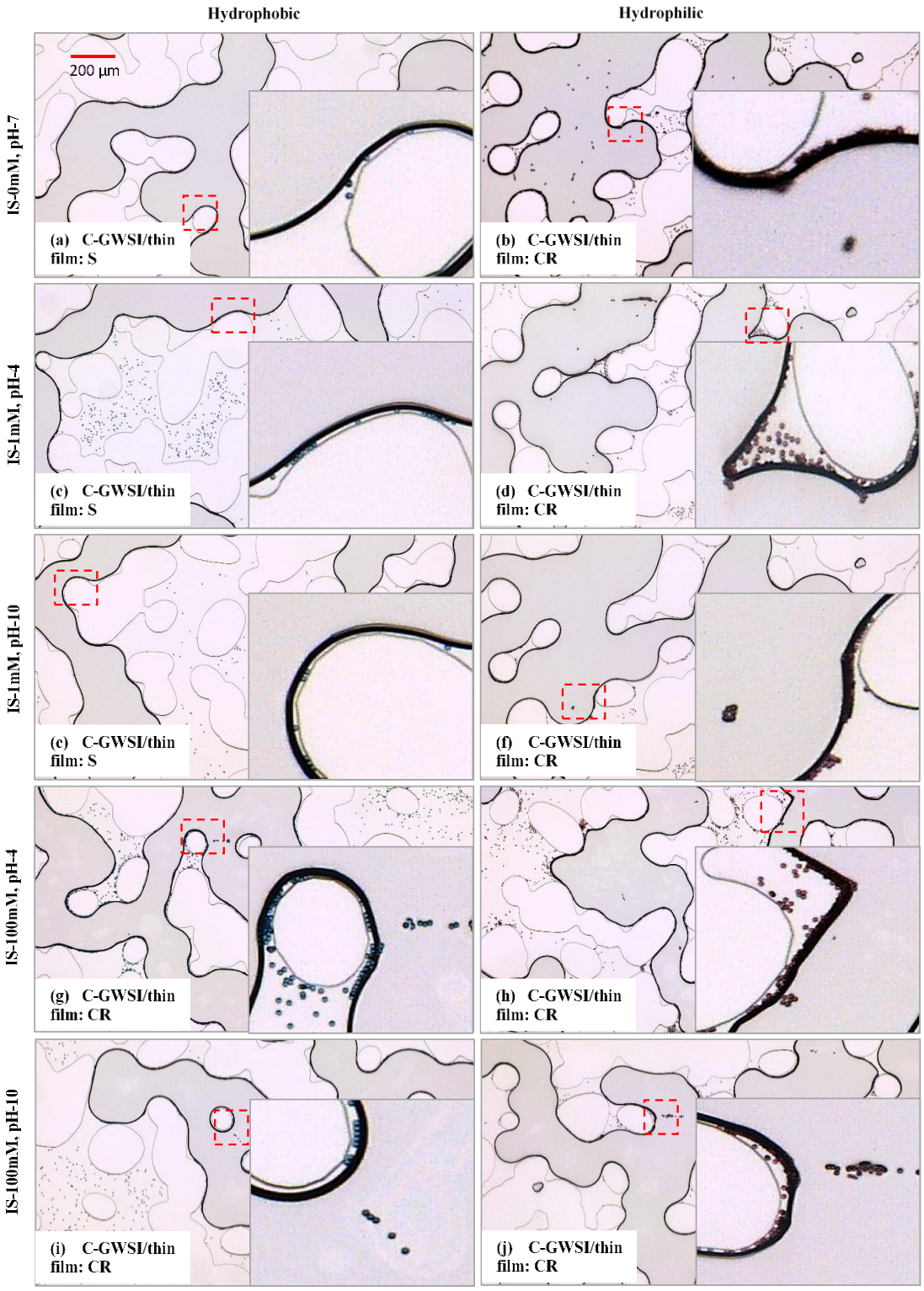

Figure 25: Colloid interactions in Two-Phase flow at different experimental conditions; colloids interacting with GWSI/thin films. CR: Capillary Retention, S: Straining only

Furthermore, larger film thickness at AWSI alters the capillary interaction as

seen in Figure 21-d, resulting in straining rather than capillary pinning at AWSI. Therefore, capillary retention was not observed near the thick films formed around solid surfaces due to the micromodel channel shape. As the water film thickness was very small (less than 500 nm) at the top or bottom of the micromodel, capillary retention was observed mostly between AWI and the micromodel top or bottom. The possible conditions to occur thin-film CR were identified in this study based on the pore-scale observations. They are; (1) presence of excess colloids on AWI, (2) rapid invasion of the interface in the pore space, and (3) coalescence of 2 AWIs containing colloids. The excess colloids on AWI rearrange to AWSI under conditions (2) and (3) leaving them on thin films while the receding interface changes its position on colloid, as shown in Figure 21-c. Consequently, the capillary forces act together with adhesion forces to retain colloids in thin water films. The horizontal forces acting on the colloid at thin films were balanced in all directions and were permanently attached as long as the film exists.

Capillary retention was observed more for hydrophilic colloids compared to hydrophobic colloids in our experiments. A possible reason for this observation could be (1) the higher capillary potential of hydrophilic colloids due to the smaller contact angle together with the strong adhesive forces on SWI, and (2) increased availability of colloids on AWI leads to the rearrangement towards AWSI and further to thin films while AWI invade the pore space. To the best of our knowledge, this study is the first to explain the possible conditions for thin-film attachment.

4.5. Conclusions

In this study, pore-scale experiments were conducted to investigate the coupled effects of solution ionic strength, pH, and colloid hydrophobicity on colloid retention and mobilization mechanisms in porous media. Microfluidic systems were used to

conduct single and two-phase flow experiments at different conditions. Main findings of this study are:

1. Pore-scale visualizations indicate that colloid interaction mechanisms in single-phase flow can be predicted and interpreted by the DLVO theory. However, in two-phase flow, the DLVO theory fails to predict colloid retention mechanisms as revealed from pore-scale experiments and images at different conditions.
2. In single-phase flow conditions, significant colloid retention was observed for hydrophilic colloids due to long-range interaction with solid-water-interfaces and long-range/short-range interaction with other colloids. However, repulsive interactions were dominant for hydrophobic colloids, which facilitated effective transport of colloids through the porous media.
3. For hydrophobic colloids, changes in solution chemistry (i.e., an increase in ionic strength or decrease in pH) significantly increase colloid interactions with other colloids or solid-water-interface. At these conditions (i.e., high ionic strength or low pH), it was observed that short-range interaction and long-range interaction were the dominant retention mechanisms. However, the impact of solution chemistry is insignificant for hydrophilic colloids.
4. In two-phase flow conditions, mobile colloids attach to the gas-water interface by hydrophobic interaction. The colloids deposited on solid-water interface mobilize by the moving gas-water interface and attach there due to capillary retention. Capillary retention was the dominant mechanism for colloid attachment on the gas-water interface for both types of colloids.
5. Colloids on gas-water interface redeposit on the gas-water-solid interface or thin water films for hydrophilic colloids due to their greater capillary potential. In

contrast, hydrophobic colloids mobilize easily by the gas-water interface and can be effectively removed from the porous media.

6. As the ionic strength increases or the pH of the solution decreases, colloid interaction with solid-water interface strengthen, which in turn reduces colloid mobilization by gas-water interfaces for hydrophobic and hydrophilic colloids.
7. Findings indicate that the coupled effects of solution chemistry and colloid hydrophobicity must be investigated to understand colloid retention mechanisms better.

CHAPTER 5: MOBILIZATION OF COLLOIDS FROM AIR-WATER INTERFACE DURING IMBIBITION

5.1. Introduction

Colloids can enhance pollutant mobility, including heavy metals, pesticides, and radionuclides in the subsurface porous media. Also, colloids themselves could be pathogenic such as viruses, bacteria, and protozoa [38,67,68,94]. Colloid mechanisms in the subsurface media control the transport and spread of these contaminants into the groundwater. Vadose zone plays a significant role in colloid immobilization on various interfaces including, Solid-Water Interfaces (SWI), Air-Water Interfaces (AWI), Air-Water-Solid Interfaces (AWSI) and thin water films [2,9,22,83,89,253]. Moving AWI generated during capillary fringe fluctuations in the vadose zone plays a major role in mobilization and transport of initially deposited colloids [23,29,110,111]. Additionally, alternate drying and infiltration events (i.e., rainwater or snowmelt infiltration) in the subsurface can also create moving AWI [44,71]. The detachment of colloids from SWI by the moving AWI has been reported in previous studies due to the strong capillary force exceeding the adhesion force on SWI [34,114,118,231]. However, the detachment or mobilization of colloids retained on AWI has not understood well.

Previous studies reported the mobilization of colloids deposited in water-saturated or dry porous media [29]. The colloid detachment was found to be affected by the capillary force exerted on the colloids, interface velocity, colloid size, shape and surface properties, numbers of AWIs and advancing and receding AWI, etc [111,114,126,259,260]. Several researchers indicated that colloids were mobilized on AWSI (where AWI contacts the solid phase) when the applied forces or torques (i.e., capillary and drag forces) exceeds the resisting forces and torques (i.e., adhesion forces) [18,21,26,34,141]. Theoretical conceptualization of the colloid mobilization

mechanisms with advancing and receding interfaces (corresponding to drainage and imbibition, respectively) was developed based on the forces acting on a colloid at AWSI and studied for different colloids (i.e., hydrophilic and hydrophobic) on different substrates (i.e., hydrophilic and hydrophobic) [34]. Colloids can be mobilized via lifting, sliding, or rolling depending on the direction and magnitude of the forces acting at AWSI and were relocated to AWI. The detached colloids remain attached to AWI irreversibly, and further mobilization from the AWI was reported only when the air bubbles dissolved or flushed out [29]. The formation of colloid clusters near the end of the air bubble dissolution was reported by Sirivithayapakorn and Keller [1]. The effect of interface capacity on colloid mobilization from AWI and the possible mechanisms has not been previously addressed.

In this work, the colloid mobilization from SWI (deposited in a saturated porous media) or AWI (retained during drainage) by the moving AWI during drainage or imbibition was investigated using a micromodel. The specific objectives were to (1) examine the impact of colloid hydrophobicity on colloid mobilization from different interfaces, including SWI and AWI, and (2) theoretically explain the possible mechanisms for the visual findings.

5.2. Theoretical Considerations

5.2.1. Forces acting on colloids at AWSI

Figure 26 provides a schematic of forces acting on a colloid at the point of three-phase contact line (AWSI) with the receding (during drainage) and advancing (during imbibition) AWI interfaces on a hydrophilic SWI. Colloid adhesion forces on the solid surface and capillary forces on AWI can be calculated as per Section 2.2.2:and 2.2.6:, respectively. The hydrodynamic forces described in Section 2.2.5: was neglected as the drag force acting on a partially submerged particle will be smaller compared to adhesion

and capillary forces [34,114].

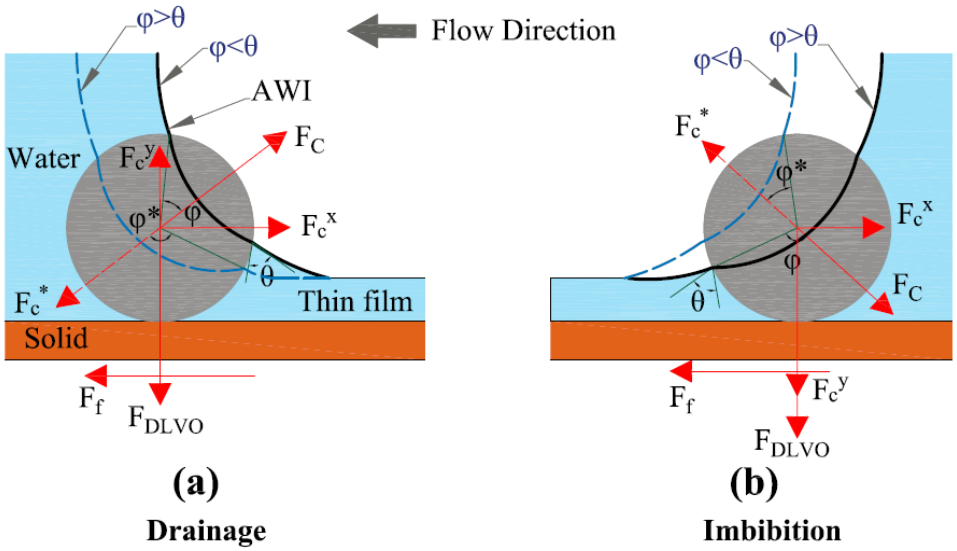

Figure 26: Colloids interacting with drainage and imbibition fronts on a hydrophilic channel. The dashed line shows the later position of the interface if the colloid not mobilized at the initial interface position (solid black line). The components and direction of forces are shown for the initial interface position (modified after Lazouskaya et al. (2013) [34].

As indicated in Figure 26, a colloid on AWSI will first experience the maximum capillary force, according to Eqs. 22 and 23 during drainage, and if not mobilized, it will experience the maximum force according to Eqs. 24 and 25. The detachment of colloid from AWI was considered to be irreversible, as the capillary forces are strong enough to retain them on AWI [21,141]. However, the reduced interface capacity during imbibition (advancing interface or dissolution of air-bubble) plays a vital role in the detachment of attached colloids on AWI. The excess colloids on AWI relocate to AWSI and experience maximum capillary force according to Eqs. 24 and 25, considering the dynamic (advancing) contact angle. With further movement of AWI

during imbibition, the colloids that are not mobilized in the previous interface position will experience a maximum capillary force, according to Eqs. 22 and 23 resulting in detachment from AWSI.

The force and torque balances at the contact point can be considered according to Section 2.2.7: to determine the colloid displacement mechanisms including, lifting, sliding, and rolling by the moving AWI at AWSI.

5.2.2. Water film thickness

Thin water films form around the hydrophilic solid-phase when the non-wetting phase advance or recede corresponding to imbibition and drainage, respectively. Film thickness generally depends on the fluid displacement velocity at higher velocities (Capillary number, Ca ranging from 5 x 10^{-3} to 10^{-5}). At smaller velocities (Ca < 10^{-5}), the film thickness is affected by capillary forces and can be found from [235]

$$h = (-Ar/6\pi\sigma)^{1/3} \quad 37$$

where h is the film thickness, A is the Hamaker constant for the three-phases near the film, r is the radius of the capillary, and σ is the surface tension.

5.2.3. Contact angle

Contact angle in a capillary tube can be obtained from [261–263]:

$$\theta = tan^{-1}\left(\frac{r^2+d^2}{2dr}\right) \quad 38$$

where θ is the contact angle, and d is the height of the meniscus, as shown in Figure 27. The thickness of AWI measured from the images can be used as d.

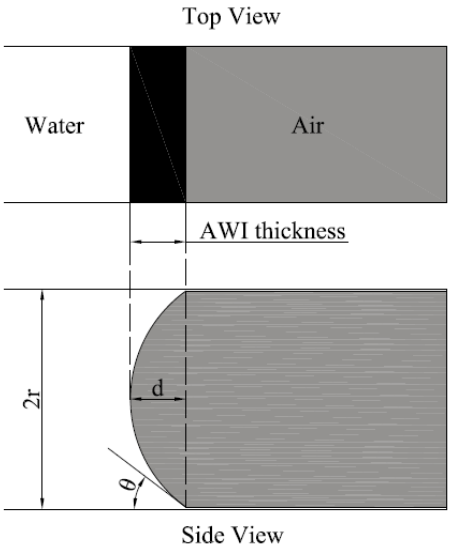

Figure 27: Contact angle measurement from the micromodel

5.3. Materials and Methods

5.3.1. Materials

A micromodel with representative geometry etched on a borosilicate glass for an area of 20 mm x 10 mm and a depth of 20 μm (Micronit Micro Technologies B.V., Enschede, Netherlands) was used as the porous medium (porosity, 0.58, pore-volume, 2.3 μL). Two colloids were used: polystyrene (i.e., hydrophobic) carboxylate modified polystyrene (i.e., hydrophilic) microspheres (Magsphere Inc., Pasadena, CA). Both colloids had diameters of 5 μm and a density of 1.05 g/cc. Colloids were suspended in background solution to final concentrations of 7.3x 10^7 colloids/mL.

Solution chemistry (i.e., ionic strength and pH) of the background solution was determined from the DLVO profiles (obtained from the measured zeta potentials at different ionic strength and pH) to achieve favorable colloid interaction with the micromodel. Accordingly, we chose those solutions in which colloids deposit on the micromodel without forming colloid aggregates. Therefore, hydrophilic colloids dispersed in deionized water and hydrophobic colloids suspended in a background

solution prepared by dissolving NaCl in deionized water to an ionic strength of 100 mM (pH for both solutions were 6.3). The contact angles of the colloids were measured on a uniform thin layer deposited on a glass slide using a sessile drop method. Measured equilibrium contact angles of hydrophobic and hydrophilic colloids were 86 ± 0.5^0 and 23 ± 0.5^0, respectively. Colloid zeta potential values measured using Zetasizer (Nano ZSP, Malvern Panalytical, Southborough, MA) at 21^0C and are -12.74 mV for hydrophobic and -15.4 mV for hydrophilic colloids.

5.3.2. Contact angle measurement

The contact angle can be measured manually on the captured images by tracing two vectors tangential to the gas phase and the solid phase at the three-phase contact point. The angle measured between these lines through the water phase will be the contact angle. However, a three-phase contact point was not visible in the captured images due to the presence of water film around the solid phase as a result of the etched channel shape of the micromodel (Figure 28). Therefore, the contact angle was measured from the projected thickness of AWI at different locations using the Eq. 38. The pore depth was 20 µm, which is the radius of the capillary (r), and the thickness of AWI was taken as the height of meniscus (d). The thickness of AWI was determined from the number of dark pixels at the interface and the corresponding resolution of the image.

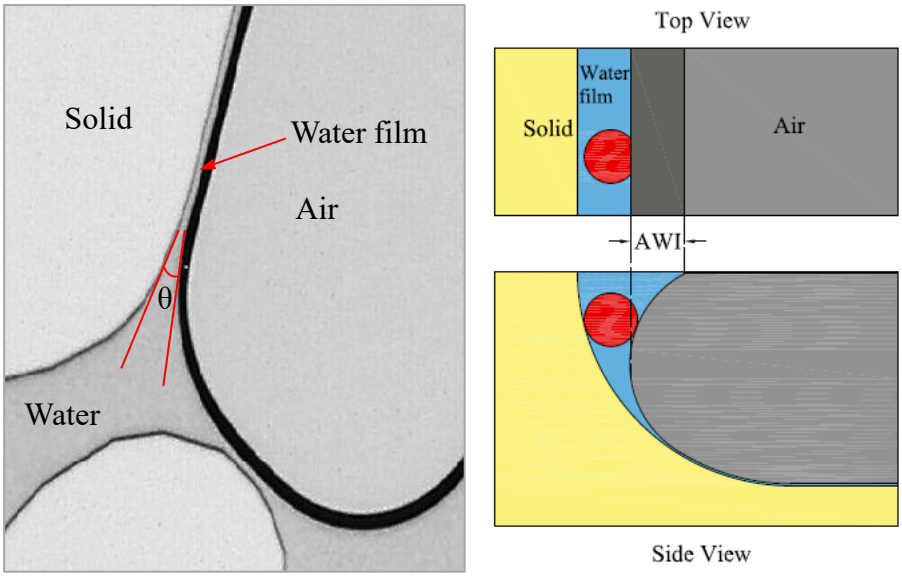

Figure 28: Micromodel image showing the absence of three-phase contact point due to the specific shape of the etched geometry

5.3.3. Experimental procedure

The micromodel was cleaned by injecting 100 pore volumes (PVs) of ethanol, followed by 500 PVs of deionized water. The dried micromodel was then placed on a microscope stage (Leica Z6 APO) and was connected to a precision syringe pump (Kats Scientific, NE-1010) using an inlet tubing. The air-bubbles in the micromodel were displaced or dissolved by injecting several PVs of deionized water. Colloid-free background solution was pumped through the micromodel for about 100 pore volumes (PVs) followed by injection of colloid suspension at 10 µL/min for 30 PVs. Finally, a colloid free background solution was flushed to remove the unattached colloids from the micromodel. Figure 29 shows the experimental set-up used in this study.

Figure 29. Experimental setup for the drainage and imbibition experiments in the micromodel. Drainage and imbibition were replicated by injecting trapped air bubbles and background solutions, respectively, to the micromodel.

For the drainage of the saturated micromodel, the inflow tube was air-filled before connecting to the background solution in the syringe pump. The air-bubble trapped in the inflow tubing was injected at a flow rate of 1 µL/min (mean pore water velocity of 52 cm/h, Capillary number, Ca =3.2 x 10^{-8}) to initiate drainage. The complete injection of air in the inflow tube was taken around one hour, and the images were recorded at different locations in the micromodel. Background solution was injected at the same flow rate (i.e., 1 µL/min) followed by the air-bubble injection to replicate imbibition. The images and videos were taken using a high-resolution camera (Leica MC170 with a resolution of 5 Mpixels) attached to the microscope.

5.4. Results and Discussion

The air was the non-wetting phase in our system with a mean contact angle (measured through water) of 23^0 with a standard deviation of 3.2^0. The distribution of the determined contact angles from the images is shown in Figure 30. This distribution can be explained with the contact angle hysteresis between advancing and receding contact angles during imbibition and drainage, respectively. The mean contact angle

was taken as the equilibrium or static contact angle (which is 23^0), the largest angle (which is 43^0) was the maximum possible advancing contact angle, and the smallest angle (which is 9^0) was the minimum possible receding contact angle.

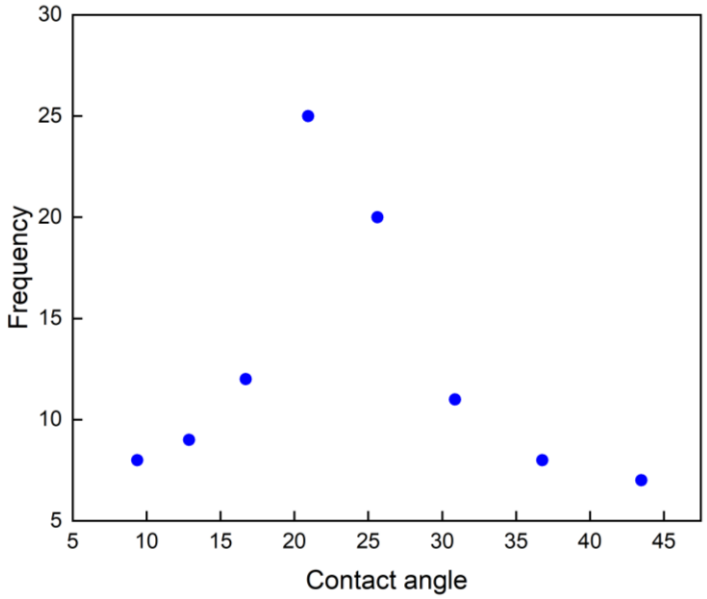

Figure 30. A histogram of the distribution of measured contact angles

Figure 31 shows the micromodel images before and after drainage for both types of colloids. The calculated DLVO profiles for colloids interacting with other colloids and SWI are given in Figure 32. The initial colloid deposition profile in the micromodel confirms the favorable colloid interaction with the SWI and unfavorable interaction with other colloids (Figure 31-a). However, a few of them interact with the deposited colloids on SWI to form small flocs as they overcome the energy barrier during the collision. Moreover, the presence of an energy barrier for hydrophilic colloids interacting with SWI was not observed in the micromodel images as the interaction was attractive at a separation distance less than 20 nm (Figure 32). The measure zeta potentials (-15.4 mV and -12.74 mV for hydrophilic and hydrophobic colloids, respectively) and the calculated maximum DLVO forces, as shown in Table 6 indicate

comparable values for both types of colloids.

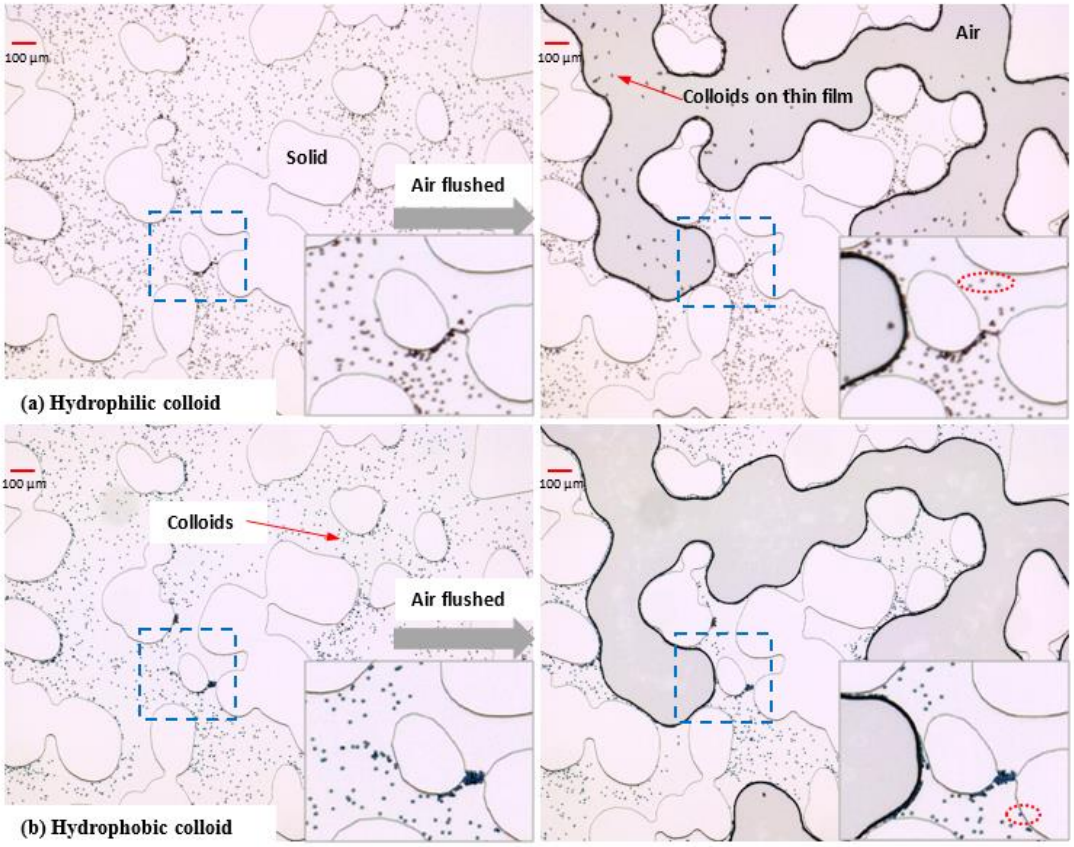

Figure 31. Snapshots of the air phase before and after injecting into the background solution for two types of colloids (i.e., hydrophobic and hydrophilic). AWI mobilized colloids. Red circles show the translocated colloids during drainage.

As reported in previous studies, colloid detachment and translocation by the receding interface (during drainage) were observed from the pore-scale images, as shown in red circles in Figure 31 [23,34,108]. However, attachment on AWI was the dominant mechanism for the detached colloids. While a moving AWI encounters a colloid in its path, a three-phase contact line forms and exerts a capillary force on the colloid. Likely, a smaller water film thickness (calculated as 0.44 µm from Eq. 37) compared to colloid diameter on a smooth micromodel can lead to colloid mobilization

by capillary retention on AWI. Conversely, the drag force generated by the flow itself has not mobilized the deposited colloids, as no colloids were detached during the flow in the absence of AWI, indicating the dominance of capillary force over hydrodynamic forces in colloid detachment.

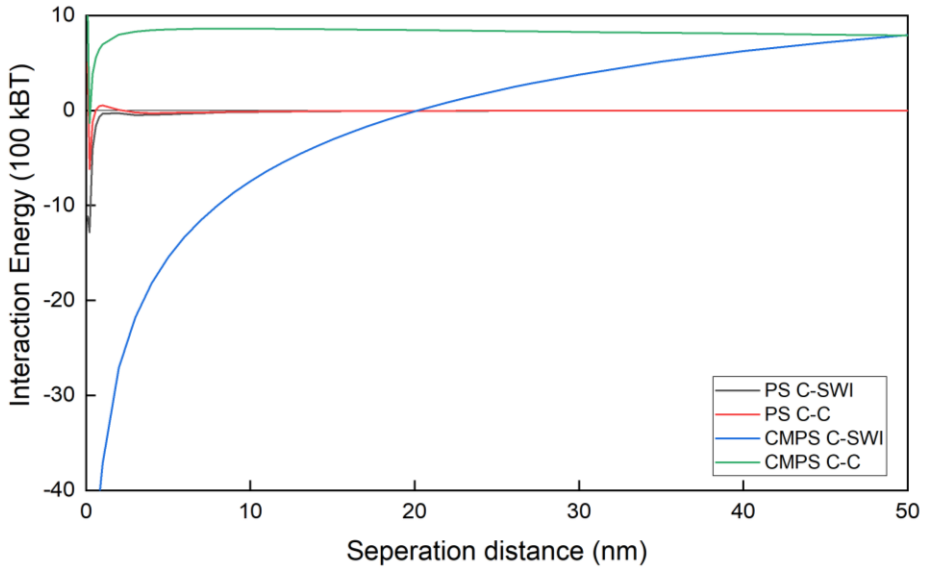

Figure 32. DLVO energy profiles for hydrophilic (CMPS) and hydrophobic (PS) colloids interacting with other colloids (C-C) or SWI (C-SWI)

Table 6 summarizes the forces exerted on hydrophilic and hydrophobic colloids during the passage of advancing and receding AWI. The attractive forces on SWI are negative, and repulsive forces are shown as positive in the table. Hydrodynamic forces were ignored in the force balance considerations due to its negligible magnitude comparing to adhesion and capillary forces. Mobilization of both types of colloids was observed in our experiment as expected from the greater magnitude of upward vertical capillary force compared to downward adhesion force (mobilization due to lifting, at $\phi < \theta$). The comparatively greater magnitude of mobilizing vertical force (i.e., F_{cymax}) was found for hydrophobic colloid (an order of magnitude), resulting in their enhanced

detachment. However, a lower magnitude of lifting force for hydrophilic colloids can change to an adhesive capillary force of two orders of greater magnitude for $\phi > \theta$ (where $\theta=23^0$). Therefore, a small increase in the colloid wetting profile can result in the capillary pinning of hydrophilic colloids on AWSI and later on thin films. Our visual observations confirm the thin film retention of hydrophilic colloids (Figure 31). This is in general agreement with the results of previous studies [12,17,22,141]. After drainage, some colloids removed from the micromodel along with the moving AWI, while others remain on stationary AWI, AWSI, or thin water films. In no case, detachment of colloid from receding AWI was observed during our study. Previous studies also reported the mobilization of deposited colloids by moving AWI even when the colloids attached in the primary minimum [44,110,114].

Table 6. Forces Acting on a Colloid at AWSI during Drainage and Imbibition

			Hydrophilic Colloid (μN)	Hydrophobic Colloid (μN)
F_{DLVO}, C-SWI			-3.6×10^{-2}	-2.0×10^{-2}
F_{DLVO}, C-C			-1.0×10^{-2}	-1.0×10^{-2}
Drainage (Receding AWI)	Initial Interface position ($\phi < \theta$)	$F_{cx}max$	7.0×10^{-3}	8.2×10^{-2}
		$F_{cy}max$	4.4×10^{-2}	5.2×10^{-1}
	Later Interface position ($\phi > \theta$)	$F_{cx}max$	1.7×10^{-1}	9.5×10^{-2}
		$F_{cy}max$	-1.07	-6.0×10^{-1}
Imbibition (Advancing AWI)	Initial Interface position ($\phi > \theta$)	$F_{cx}max$	7.4×10^{-1}	4.1×10^{-1}
		$F_{cy}max$	-7.9×10^{-1}	-4.4×10^{-1}
	Later Interface position ($\phi < \theta$)	Fcxmax	7.0×10^{-3}	8.2×10^{-2}
		$F_{cy}max$	3.3×10^{-2}	3.9×10^{-1}

Injection of background solution follows the passage of air-bubble, resulting in imbibition (i.e., advancing AWI). The porosity and pore geometry of our micromodel resulted in the faster displacement of air (during imbibition) than water (during drainage). Therefore, colloids retained on AWI during drainage were transported from the micromodel along with the displaced air phase. The mobilization mechanism of

colloids retained on receding AWI was similar to the process discussed for drainage (either transported along with the interface or retained on thin films, no detachment from AWI). However, detachment from AWI was noticed during the snap-off of the trapped air bubble during imbibition (Figure 33). In general, there was no desorption of colloids from AWI was reported in previous studies due to the strong capillary forces holding the particle on AWI [1,29,114]. While reorganizing the available colloids on AWI during rapid rearrangement of the air bubble at the time of snap-off, many colloids detached, and others remain attached to the interface of newly formed air-bubbles. The detached colloids either transported for a short distance and reattach on SWI or AWI downstream or carried along with the moving fluid. The lower contact angle of the micromodel, high pore body – pore throat aspect ratio, and lower flow rates promote significant snap-off in our porous medium system, as reported in previous studies [264,265]. As a result, the air-phase becomes disconnected and trapped in the pore space.

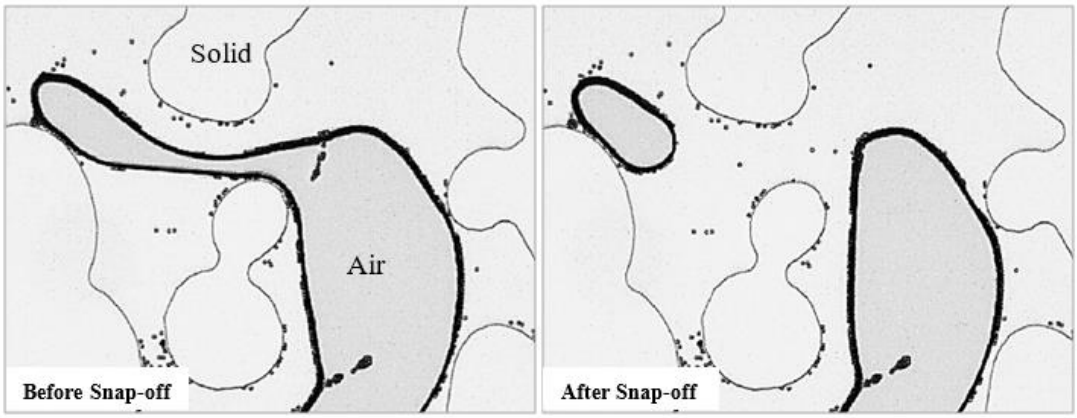

Figure 33. Rearrangement of colloids on AWI after snap-off

The dissolution of the air-bubble trapped in the pore space occurs during imbibition. Sirivithayapakorn and Keller [1] described the formation of the colloid

cluster after the complete dissolution of an air bubble. However, to the best of our knowledge, the effect of excess colloids on AWI (exceeding the interface capacity) during bubble dissolution was not explained elsewhere. We observed different behavior for hydrophobic and hydrophilic colloids with a reduction in the interface capacity at the time of dissolution, as seen in Figure 34. For hydrophobic colloids, colloids exceeding the interface capacity were transferred near to the adjacent colloids and were aggregated on the interface (Figure 34-a). However, excess hydrophilic colloids were shifted to AWSI and were not mobilized from the solid phase by further movement of the advancing interface. Therefore, reattachment on SWI was observed for hydrophilic colloids.

Considering the calculated capillary forces on the colloids shifted to AWSI (Table 6, imbibition), no lifting, sliding, or rolling was expected for both hydrophilic and hydrophobic colloids at the initial interface position. Nevertheless, later interface position lead to colloid lifting for hydrophobic colloids and no mobilization for hydrophilic colloids. The lifted hydrophobic colloids overcome the energy barrier for colloid-colloid interaction and form colloid aggregates on the interface. In the case of hydrophilic colloids, the smaller lifting capillary force failed to mobilize from the solid phase and was reattached on SWI, as observed in the micromodel images.

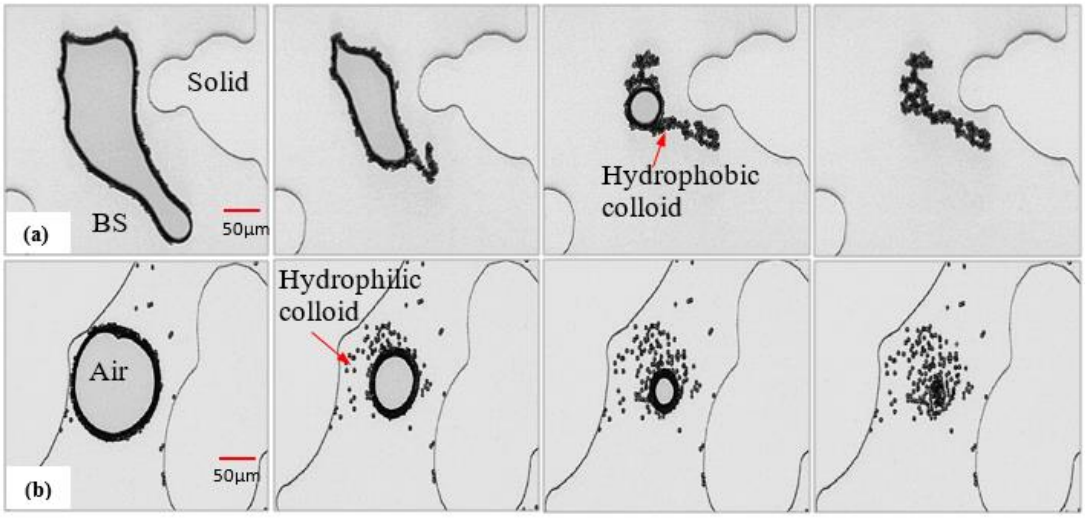

Figure 34. Snapshots of dissolution of air bubble during imbibition, (a) hydrophobic colloid, (b) hydrophilic colloid. BS – Background solution; brine solution (100 mM IS) for hydrophobic colloid and deionized water for hydrophilic colloid.

5.5. Conclusions

In subsurface porous media, moving air-water interfaces are common in continuous cycles of drainage and infiltration events or capillary fringe fluctuations. Such interfaces significantly influence the mobilization of deposited colloids. Enhanced colloid transport can be expected for the colloids attached to moving AWI whereas, colloids on stationary AWI remain in the porous media unless a transient flow occurs (high rate of drainage or imbibition). In general, colloid detachment from AWI was not observed unless the snap-off or dissolution of the air bubble occurs during imbibition. Moreover, this study provides the visual evidence on the impact of colloid hydrophobicity on various mobilization mechanisms. For instance, desorption of excess colloids from AWI during imbibition resulted in the formation of aggregates for hydrophobic colloids while hydrophilic colloids reattach on SWI. The observed difference in the mobilization mechanisms can be effectively interpreted using the changes in the capillary potential of two types of colloids. Theoretical force balance

considerations explain the observed behavior of colloid mobilization during drainage and imbibition, considering the dynamic contact angles of the solid phase.

CHAPTER 6: MOBILIZATION OF COLLOIDS IN SATURATED POROUS MEDIA UNDER TRANSIENT HYDRO-CHEMICAL CONDITIONS: A PORE-SCALE STUDY

6.1. Introduction

The outbreak of waterborne diseases followed by heavy rainfall events are common due to the rainwater infiltration into the groundwater sources and associated contaminant release [266,267]. The immobile colloids at native groundwater conditions are prone to release during perturbations in the flow velocity and solution ionic strength [147,148,187,198]. Consequently, the contaminants sorbed onto the deposited colloids (on the grain surfaces) are mobilized during an increase in flow velocity and a decrease in solution ionic strength during rainwater infiltration [268].

Previous studies have conclusively reported that the mobilization of colloids from the grain surface depends on the relative strength of resisting adhesive forces (and torques) and the applied hydrodynamic forces (and torques) [105,106,128,138,191]. The adhesive force is greatly influenced by the solution chemistry (i.e., ionic strength, pH, and ionic composition) whereas, the hydrodynamic force increase with an increase in flow velocity [65,115,147,191]. Many attempts have been made to elucidate the experimental observations on colloid release with the alterations in solution chemistry (i.e., decrease in ionic strength or increase in pH) within the framework of the DLVO theory. The theory calculates the adhesion forces as the sum of van der Waals and electrostatic forces [15,16,193,206].

Previous studies are mostly focused on indirect observations on the colloid deposition or release behavior based on the laboratory column breakthrough curve [59,115,147,148,152,225]. The mass of colloids retained was analyzed in response to the changes in colloid or collector size and surface properties (changed by varying

solution chemistry), and fluid flow rate. The pore-scale processes that influence colloid retention were inferred from the indirect observations based on the theoretical considerations [100,105,226]. However, the changes in the breakthrough or retention may often occur due to multiple mechanisms in the column including straining (grain-grain contacts, small pore throats), size exclusion, ripening, bridging, clogging, attachment on nanoscale surface heterogeneity, etc. which cannot be accurately predicted from these studies [100,147,193,227]. Moreover, colloid release and further re-deposition in the porous media were also interpreted indirectly in the previous studies. For instance, the negligible release of colloids with a decrease in ionic strength was explained by the solid phase colloid mass transfer to low-velocity regions (grain-grain contacts) where the hydrodynamic forces are insignificant to release them back to bulk water [105,115,228].

Direct visualization studies on colloid release with perturbations in solution chemistry and flow rate are very limited, and many of them are focused on the impinging jet experiments where the colloids attach on a flat surface only [203]. The real pore-scale processes cannot be directly compared with those studies as they do not show multiple mechanisms, as explained above. Also, the spatially distributed hydrodynamic forces (because of pore-scale velocity distributions) in the actual porous media were not recreated in the impinging jet experiments [115,193].

Systematic direct visualization studies are required to determine the coupled effects of various factors that influence the colloid retention and release in saturated porous media. Our goal was to characterize the mechanisms of colloid retention across a variety of colloid surface properties (favorable and unfavorable) in porous media with physically representative geometry (i.e., micromodel) that allows direct observation in real-time. The reversibility of colloid retention in response to the perturbations in

solution chemistry and flow rate was also examined to expand the knowledge of release mechanisms further. The image processing technique was adopted to quantify the colloid retention and mobilization in this study. From this research, the following questions were attempted to answer:

- How the colloid deposition profile vary in porous media under favorable as well as unfavorable attachment conditions?
- Do we observe significant retention of colloids in secondary energy minima (which are mobilized by the reduction in ionic strength)
- Do we find colloid release in response to perturbations in solution chemistry and flow rate under favorable as well as unfavorable conditions?
- How the release of colloids related to the colloid deposition profile in the porous media?

6.2. Materials and Methods

6.3.1. Materials

A micromodel etched on a borosilicate glass for an area of 20 mm x 10 mm and a depth of 20 μm (Micronit Micro Technologies B.V., Enschede, Netherlands) was used as the porous medium (porosity, 0.58, pore-volume, 2.3 μL). Three colloids were used: polystyrene (PS), carboxylate modified polystyrene (CMPS), and aminate modified polystyrene (AMPS) microspheres (Magsphere Inc., Pasadena, CA). All colloids had diameters of 5 μm and a density of 1.05 g/cc. Colloids were suspended in background solution to final concentrations of 2.9×10^7 colloids/mL.

The background solutions were prepared by dissolving NaCl in deionized water to obtain the required ionic strength, as shown in Table 1 for each experiment. The pH for all the solutions was maintained as 6.3 by adding drops of 0.1 M NaOH solution.

Colloid zeta potential values were measured using Zetasizer (Nano ZSP, Malvern Panalytical, Southborough, MA) at 21^0C for the colloids in their respective background solution, and is given in Table 7.

Table 7. Summary of Experimental Conditions used in this Study

Exp. ID	Colloids	Initial IS	Zeta Potential (mV)	Transient Conditions		
				Flow Perturbation (µL/min)	Solution chemistry	
					DI	pH 11
AMPS_DI_1	AMPS	0	20.2	10 and 100	-	✓
AMPS_DI_2		0	20.2	-	-	✓
CMPS_DI_1	CMPS	0	-15.2	10 and 100	-	✓
CMPS_DI_2		0	-15.2	-	-	✓
PS_DI	PS	0	-63.8	-	-	✓
PS_10mM_1		10	-51.8	10 and 100	✓	✓
PS_10mM_2		10	-51.8	-	-	✓
PS_100mM_1		100	-21.7	10 and 100	✓	✓
PS_100mM_2		100	-21.7	-	-	✓

6.3.2. Experimental procedure

Figure 35 shows the experimental set-up used in this study. The micromodel was cleaned by injecting 100 pore volumes (PVs) of ethanol, followed by 500 PVs of deionized water. The dried micromodel was then placed on a microscope stage (Leica Z6 APO) and was connected to a precision syringe pump (Kats Scientific, NE-1010) using an inlet tubing. The air-bubbles in the micromodel were displaced or were dissolved by injecting several PVs of deionized water. The micromodel was then equilibrated (100 PVs) by injecting a colloid-free background solution at the same flow rate used during the experiments. After equilibration, the colloid suspension was injected at 5 µL/min (mean pore water velocity of 36 m/d) for 30 PVs. This was followed by elution with the colloid-free background solution at the same flow rate of colloid injection to remove the unattached colloids from the micromodel.

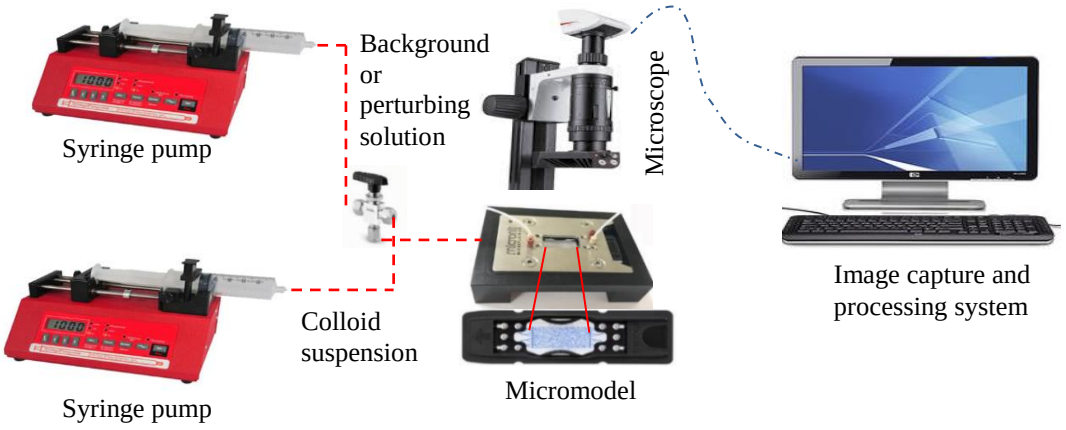

Figure 35. Experimental setup for colloid retention and release experiments in the micromodel.

After flushing the micromodel with colloid-free background solution, the images were captured to represent the initial condition (Phase 1). Colloid release and the reversibility of colloid retention was investigated during different elution phases: (1) background solution with sequential increases in flow rate by factors of 2 and 10; (2) reduction to 0 mM NaCl solution with no changes in flow rate; (3) solution with pH increase to 11 (1mM NaOH) with no changes in flow rate; (4) continuation of pH 11 solution with a sequential increase in flow rate by factors of 2 and 10. The selected series of phases are shown in Table 7.

6.3.3. Image Processing

We captured micromodel images at different stages of the experiment using an optical microscope and a high-resolution camera (Leica MC170 with a resolution of 5 Mpixels). We used 2.5x magnification with a 2x plan apochromatic objective (0.234 numerical aperture, 0.94 µm/pixel resolution) for visualization and image capturing, which was sufficient to resolve individual colloids. The horizontal and vertical

movement of the microscope stage allowed us to capture the central portion of the micromodel of an area 4.7 x 18.9 mm^2 (3 rows and 9 columns of images stitched together).

An image of the water-saturated micromodel (mask) was used to identify the colloids by removing other features in the image, such as solid-water interfaces and colloids, which were not removed from the previous experiments by the cleaning process. An image of micromodel after each stage of the experiment was subtracted from the mask to detect colloids in the images. In this way, the background pixels associated with the water and solid phase were removed to create an image containing only the colloids. Then the image was segmented to a binary image using the threshold value identified by Otsu's method [242]. A median filter was applied to remove the possible noise due to uneven contrast,. The pixels corresponding to the colloids were identified from the binary image by pixel counting. Similarly, the pixels corresponding to the pore space was evaluated from the total number of pixels of the image using the porosity of the micromodel (i.e., 0.58). The percentage of colloids retained (i.e., percentage of pore space) in the micromodel after each stage of the experiment was obtained by the above image processing technique.

6.3. Results and Discussion

6.3.1. DLVO calculations

Table 7 shows the measured zeta potentials for AMPS, CMPS, and PS colloids for various ionic strength conditions. The DLVO profiles calculated from the measured zeta potentials are shown in Figure 36 for the colloid-SWI and colloid-colloid interactions under the experimental conditions given in Table 7. It can be inferred from the profiles (Figure 36-a) that three types of favorability conditions exhibited by the AMPS, CMPS, and PS colloids as favorable, medium favorable, and unfavorable

interaction conditions, respectively. The experiments were repeated at two different ionic strengths for PS colloids (PS_10mM and PS_100mM) to study the impact of ionic strength on colloid retention and release. The DLVO profiles in Figure 36-a show the general trend of increase in secondary minima depth and decrease in energy barrier with the ionic strength increase for PS colloids-SWI interaction. Although the primary minimum exists for PS_10mM and PS_100mM, the higher energy barrier (greater than the diffusion kinetic energy) indicates lower chances of primary minimum interaction. Therefore, those colloids retained in the porous media possibly attached via weak secondary minimum interactions. Conversely, primary minimum interaction can be predicted for AMPS and CMPS colloids based on the computed DLVO energy profiles (Figure 36).

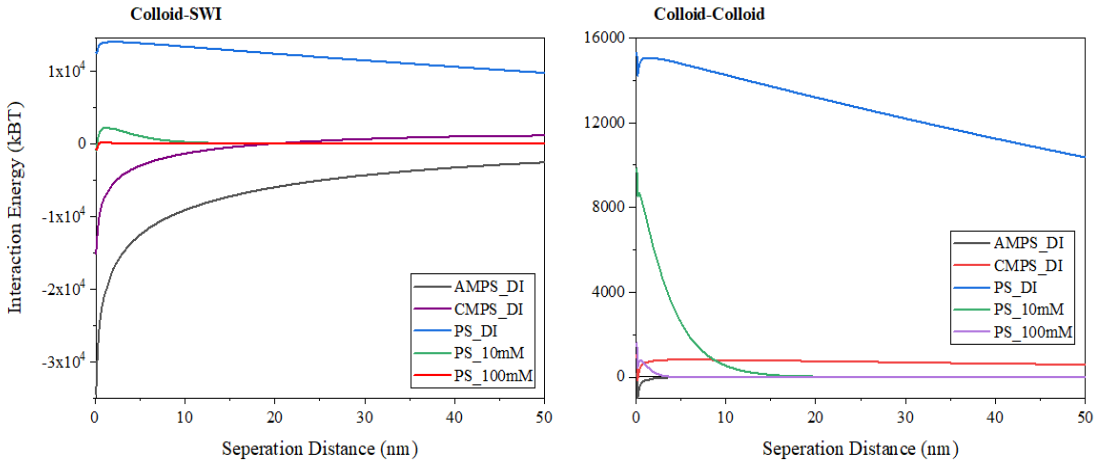

Figure 36. DLVO energy profiles for various colloids interacting with the SWI and other colloids

6.3.2. Colloid Deposition Profiles

Figure 37 shows the quantity of colloids retained (as a percentage of pore space) in the micromodel at different experimental conditions given in Table 7. Figure 38

shows the pore-scale images of size 1.5 mm x 1.0 mm at different conditions. The percentage of colloids retained in the pore space shows a clear trend of increase in a deposition with the favorability of interaction as well as an increase in ionic strength for unfavorable conditions (Figure 37). Thus enhanced deposition was observed for AMPS followed by CMPS colloids. As can be seen from Figure 38-a and Figure A1 (Appendix), 0.2% of the PS_DI colloids were retained in the micromodel. Even though the colloid interaction was repulsive, the presence of organic matter in the micromodel acted as retention sites. Those organic matters cannot be removed while cleaning the micromodel due to the strong adhesive nature on the glass surface and clogging of the pore throats. A 6-fold increase in the colloid deposition was observed for PS colloids when the ionic strength increased to 100mM, where secondary minimum interaction was predicted from the DLVO theory.

Figure 38 shows the deposition profiles of colloids in the porous media. Colloid attachment on Forward Flow Stagnation Zone (FFSZ) was observed for PS_10mM and PS_100mM colloids, as seen in Figure 38-b and c. These visual observations confirm previous theoretical force balance considerations where they suggest the secondary minimum attachment of colloids under unfavorable conditions occur on forward and rear-flow stagnation zones where the fluid drag forces are absent or negligible [105]. Also, Elimelech and O'Melia [269] suggest that the fluid drag and shear can translate the particles trapped in the secondary minimum until they reach rear-flow stagnation zones. In contrast, we never observed colloid attachment on rear-flow stagnation zones. This can be explained as the secondary minimum interaction occurs only on FFSZ, and those retained via interception (on collector center as shown in Figure 39) were either re-entrained back to the bulk solution (not translated to rear-flow stagnation zones as hypothesized in previous studies) or stay attached there. For instance, for PS_100mM

colloids, the secondary minimum depth was great enough (-36 kBT), several colloids were retained via interception at the secondary minimum. Therefore, the colloids attached at the micromodel top or bottom for PS_100 mM were retained via interception, as observed in the pore-scale images (Figure 38-c). Moreover, colloid attachment at the micromodel bottom was also found near the blocked pore throats, as seen in Figure A2 (Appendix), where the Stoke's velocity exceeds the flow velocity, and thus settlement and attachment occur.

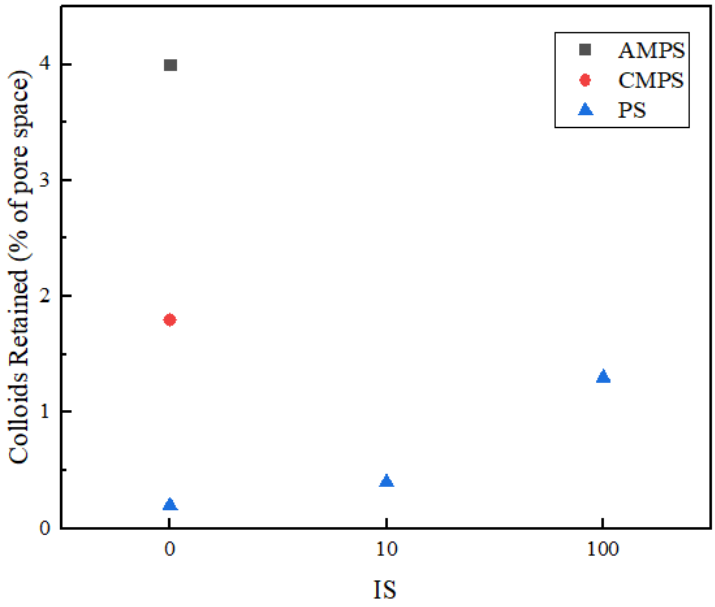

Figure 37. Colloids retained in the saturated micromodel as a percentage of pore space at different experimental conditions

AMPS colloids deposited mostly on micromodel top or bottom, as seen in Figure 38-e. The impact of colloid settlement at the bottom of the micromodel can be ignored as the flow velocity was much greater than the settling velocity of the colloid (as the colloid size and density are small). Therefore, the observed behavior can be explained with colloid filtration theory (CFT) that consider interception as the major transport mechanism for colloid retention under favorable conditions. As the AMPS

colloid interaction with the micromodel was highly favorable due to the unlike surface charges (i.e., positively charged colloid and negatively charged micromodel), those colloids come closer to the collector surface via interception were deposited. Also, the formation of clusters on the collector surface, micromodel bottom, or top was noticed for AMPS colloids. Under favorable colloid-colloid interaction conditions, a colloid in the bulk solution is attracted simultaneously by the SWI and by the colloid attached to SWI. Thus, the total attraction force deflects the colloid in bulk water towards the attached particle to form a cluster, as shown in Figure A3 (Appendix). This was frequently observed for AMPS colloids, whereas aggregation was less significant for other cases in our study due to the unfavorable colloid-colloid interaction conditions (Figure 36-b).

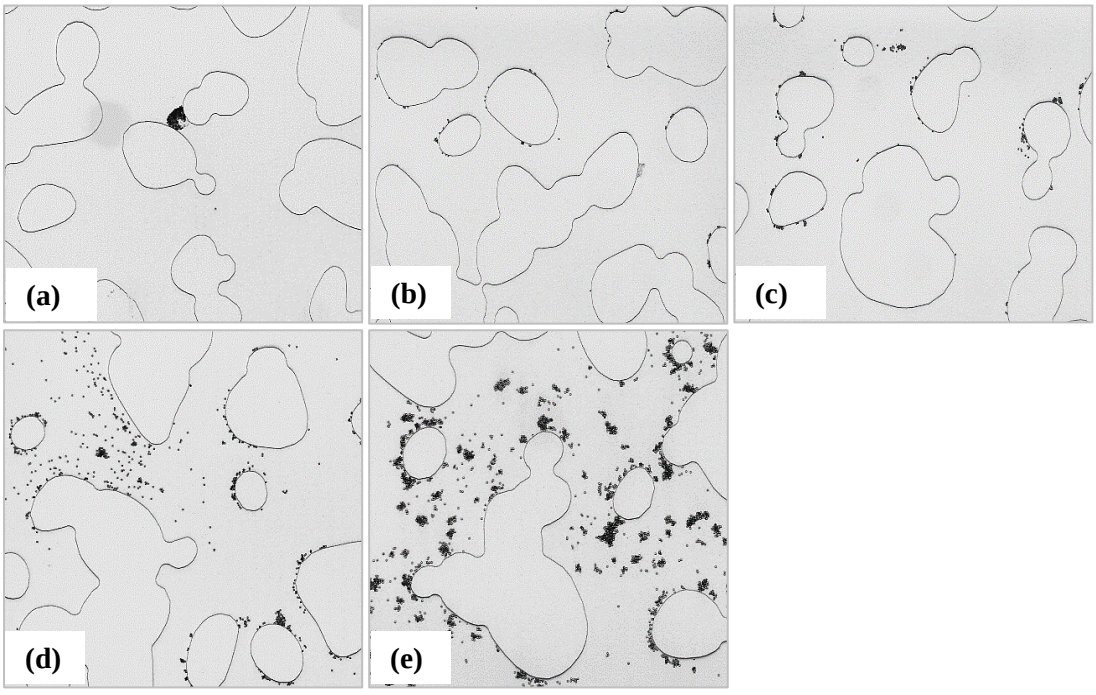

Figure 38. Colloid deposition profile for different type of colloids in the micromodel; (a) PS_DI, (b) PS_10mM, (c) PS_100mM, (d) CMPS, and (e) AMPS

Moreover, the attachment profile for the AMPS colloids significantly varies

compared to the other colloids in this study. For instance, greater colloid retention was observed on the collector center (Figure 39) via interception for AMPS colloids besides retention on flow stagnation zones for other cases (i.e., PS_10mM and PS_100mM). This is due to the greater availability of colloids to interact with the collector surface via interception, and their superior adhesion forces overcome the resisting hydrodynamic torque. However, theoretical calculations show that colloid retention on stagnation zones precedes the collector center due to the smaller resisting torque [105]. This was true for PS_10mM and PS_100mM colloids as the adhesive forces were smaller (compared to AMPS_DI and CMPS_DI in our study, where the adhesive forces are greater enough to overcome the resisting torque near collector center), and therefore, majority of the colloids attached on FFSZ. Nevertheless, few colloids attached at the collector center via secondary minimum were re-entrained back to the bulk water (when the hydrodynamic force exceed the adhesion forces) or remain attached (when adhesion forces exceed hydrodynamic forces) under static hydrodynamic conditions as observed from the pore-scale images (Figure 38-c).

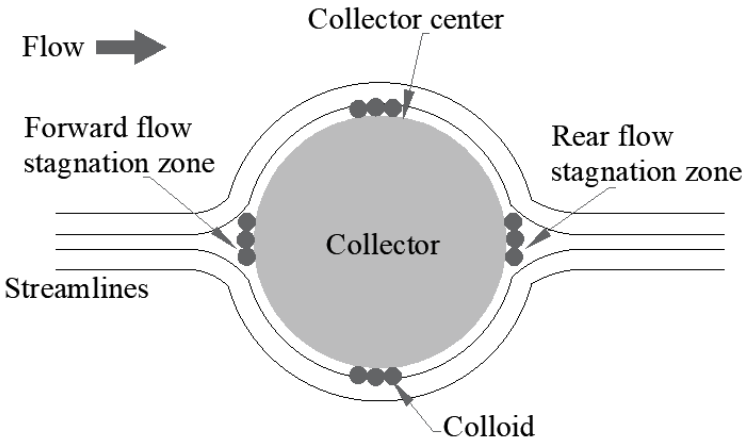

Figure 39. Colloid retention positions on the collector surface

The presence of a slight energy barrier for CMPS, unlike the AMPS colloids, as

shown in Figure 36-a, can explain the reduced colloid deposition for CMPS colloids (Figure 37 and Figure 38-d). As the colloid interaction was favorable up to 20 nm, colloid attachment via interception can occur for those colloids interacting at a separation less than this distance. Consequently, colloid attachment on the collector center occurs comparatively lesser than AMPS colloids. Also, the attachment of CMPS colloids occurs in FFSZ. Although ripening was perceived for CMPS colloids, it was less significant compared to AMPS, where substantial colloid aggregation occur because of ripening (Figure 38-e).

Under favorable attachment conditions, significant colloid attachment via interception occurs near smaller pores as visualized in our study (Figure 38-d and e). This is due to the greater availability of colloids to interact with the collectors near small pores as a large number of colloids follow the fastest route in the porous media. Colloid attachment and subsequent ripening at small pores near the inlet would block or clog the pore space. Consequently, enhanced colloid retention occurs near the inlet of the packed sand columns, as noticed by the dissection analysis in previous studies [10,160,270].

6.3.3. Colloid Detachment by Flow perturbations

Mobilization experiments followed colloid loading through perturbations in flow rate or solution chemistry. Figure 40 shows the amounts of colloids remaining at the micromodel after the perturbations in the flow rate. The negligible release was observed for all the colloid types in response to a factor of 2 increased fluid flow rate. However, the amount of colloids released after a 10x increase in flow rate was varied for different types of colloids. Approximately 80% and 90% of the initially deposited colloids remained in the micromodel after a factor of 10 increased fluid velocities for PS colloids at 100 mM and 10 mM ionic strength conditions, respectively. The greater

mobilization at higher ionic strength was contradicting the previous studies where colloids retained via secondary minimum under lower ionic strength were released to a greater extent than those under higher ionic strength (as they are retained permanently on deep energy well) [102,147,203]. Similarly, approximately 30% of the deposited CMPS colloids were mobilized with the flow velocity perturbations. In general, the trend for colloid mobilization was also followed a similar trend observed for colloid retention in our study.

The variations in the colloid deposition profile, as observed in the pore-scale images (Figure 38), can explain the release behavior of different colloids. The colloids deposited on collector centers (either solid surface or micromodel top or bottom) via interception were susceptible to release than the colloids deposited in forward flow stagnation zones. In other words, colloids deposited in the low-flow zones were irreversibly retained, and their mobilization was hindered even at high flow rates. Although forward flow stagnation zones are the major retention sites for PS colloids, retention via interception was increased with an increase in ionic strength, as explained before. Therefore, higher mobilization with the increase in flow rate was observed with an increase in ionic strength in contrast to the previous studies [102,147,203]. Additionally, very few colloids retained in the porous media under repulsive interactions (PS_DI) were irreversibly retained on low flow zones or surface impurities. The hydrodynamic forces imposed under our experimental conditions (even after tenfold increase in the flow rate) were not sufficient to release them back to bulk water.

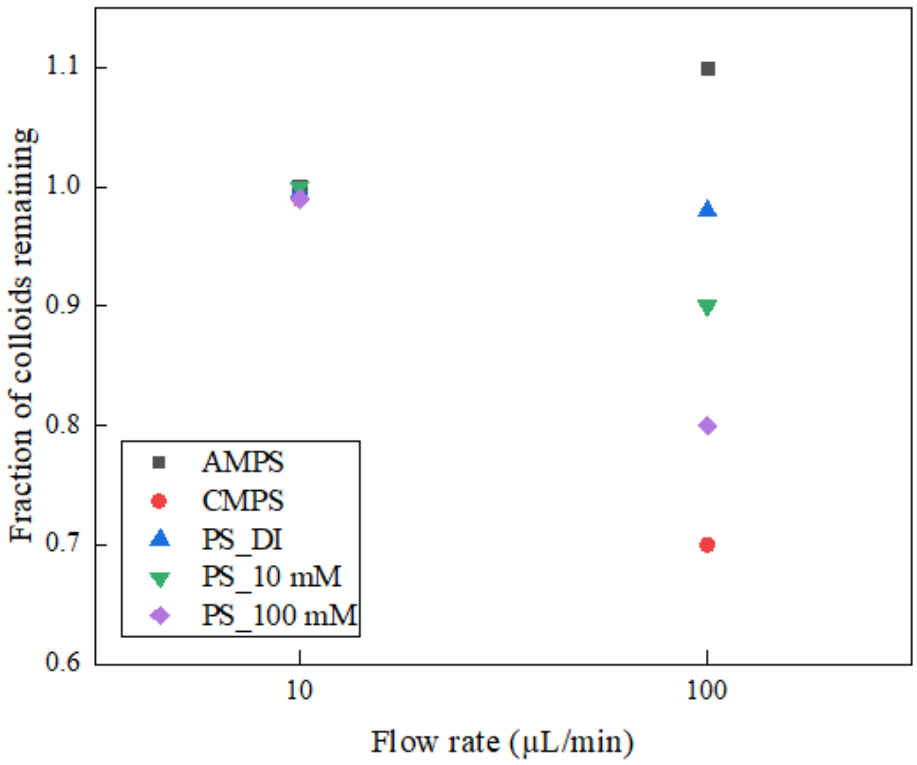

Figure 40. The fraction of colloids remaining in the micromodel after perturbations in flow rate from 5 µL/min to 10 and 100 µL/min

Conversely, the image analysis for AMPS colloids shows an increase in the number of colloids after the increase in flow velocity. This can be explained as the redistribution of the multi-layer colloid aggregates to mono-layered aggregates that are aligned along with the flow streamlines as observed from the images before and after flow perturbations (Figure 41). The drag forces acting on the colloid clusters were reduced by this redistribution, as shown in Figure A4 and A5 (Appendix). The multi-layered colloids will not be accounted for in the image processing technique, which underestimates the amount of initially deposited colloids in the micromodel for AMPS colloids. Therefore, after an increase in the flow rate, the restructured single-layered colloid aggregates exceeded the estimated percentage of initial colloid content. Consequently, the actual percentage of colloids retained after the flow perturbations

could not be estimated from our study.

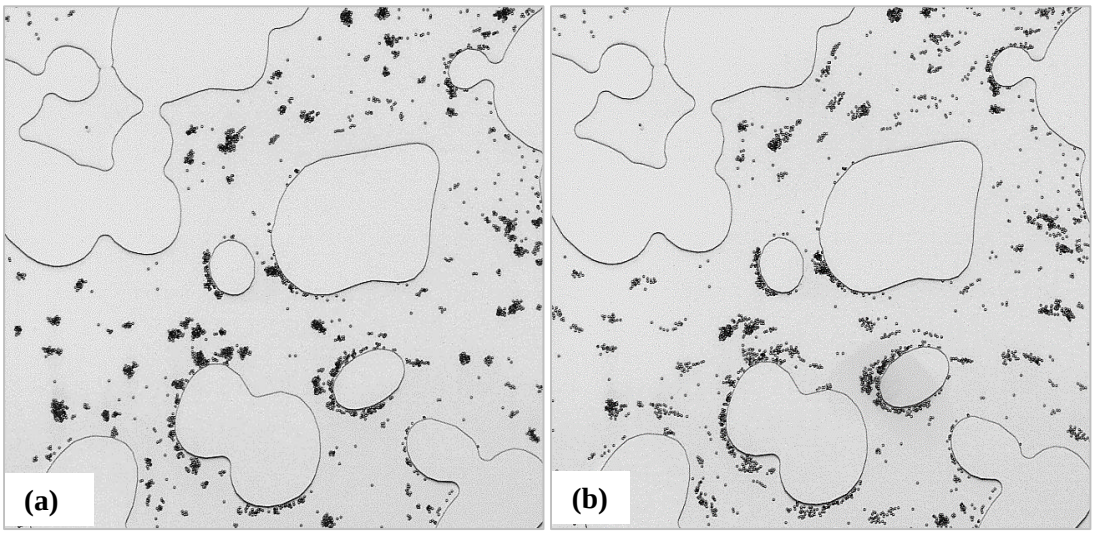

Figure 41. Redistribution of the multi-layered colloid aggregates of AMPS colloids to mono-layered aggregates that were aligned in the velocity streamlines after tenfold increase in the flow rate

6.3.4. Colloid Detachment by Perturbations in Solution Chemistry

Figure 42 shows the percentage of colloids retained after perturbations in solution chemistry for different experimental conditions in this study. Zeta potentials of AMPS, CMPS, and PS colloids at pH 11 were measured as -14, -25, and -72 mV, respectively. The corresponding DLVO curves are shown in Figure 43. In the release experiments, the solution ionic strength was reduced to DI for PS_10mM and PS_100mM colloids, where the release of the colloids was insignificant (approximately 3% and 8% respectively). An increase in pH from 6.3 to 11 was released a greater number of AMPS (70%) and CMPS (58%) colloids compared to PS colloids (0 – 15% for DI to 100mM cases).

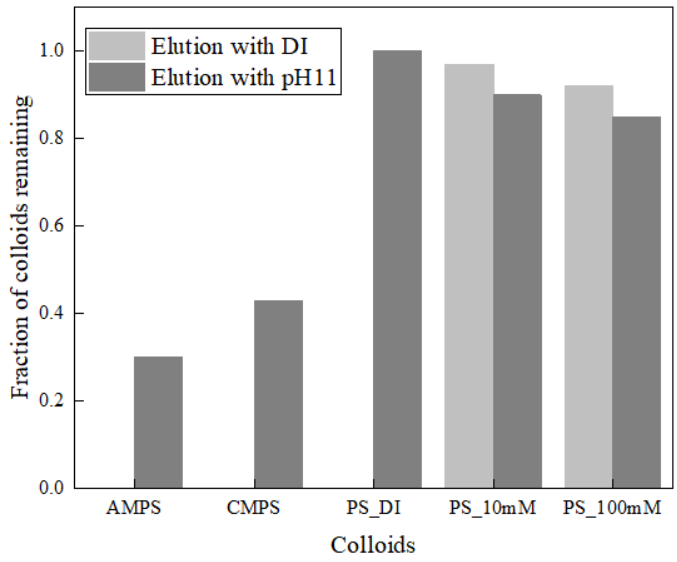

Figure 42. The fraction of colloids remaining in the micromodel after perturbations in solution chemistry.

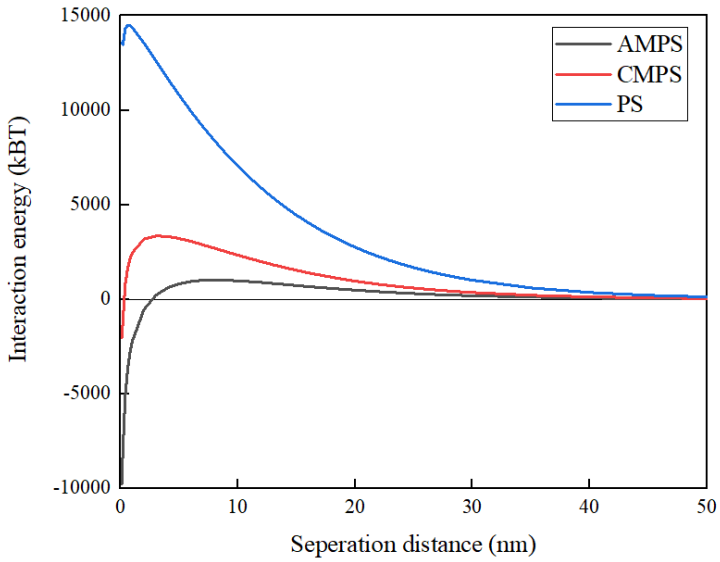

Figure 43. DLVO curves for different colloids interacting with SWI at pH 11.

During the elution step with DI water for PS colloids, the energy barrier became larger than the previous case (10mM and 100mM), and both the energy minima were almost eliminated. As reported in previous studies, the decrease in ionic strength may release the colloids adsorbed in the secondary minima [65,147,203]. Therefore, the

greater removal of colloids from the pore-space at higher ionic strength (100mM, 7%) compared to the one at lower ionic strength (10mM, 3%) can be explained with the depth of secondary minimum. The greater amount of colloids retained on deep secondary minima under higher ionic strength (PS_100mM) were released more compared to PS colloids at lower ionic strength (PS_10mM). Additionally, our visual observations suggest that colloids retained on FFSZ are unaffected by the changes in fluid chemistry (either ionic strength or pH). Besides, the colloids attached to the micromodel bottom via interception (maybe at a secondary minimum for PS_100mM) were translated or released by the perturbations, as seen in Figure 44. This can be explained with the hydrodynamic drag force that was greater on colloids attached at the micromodel top/bottom at the center of the pore space than at FFSZ. In other words, secondary minimum attachment via interception for PS_10mM colloids was negligible due to the shallow energy well (-2 k_BT) at larger separation distance (25 nm, greater tendency to re-entrained back to bulk water during initial deposition step itself).

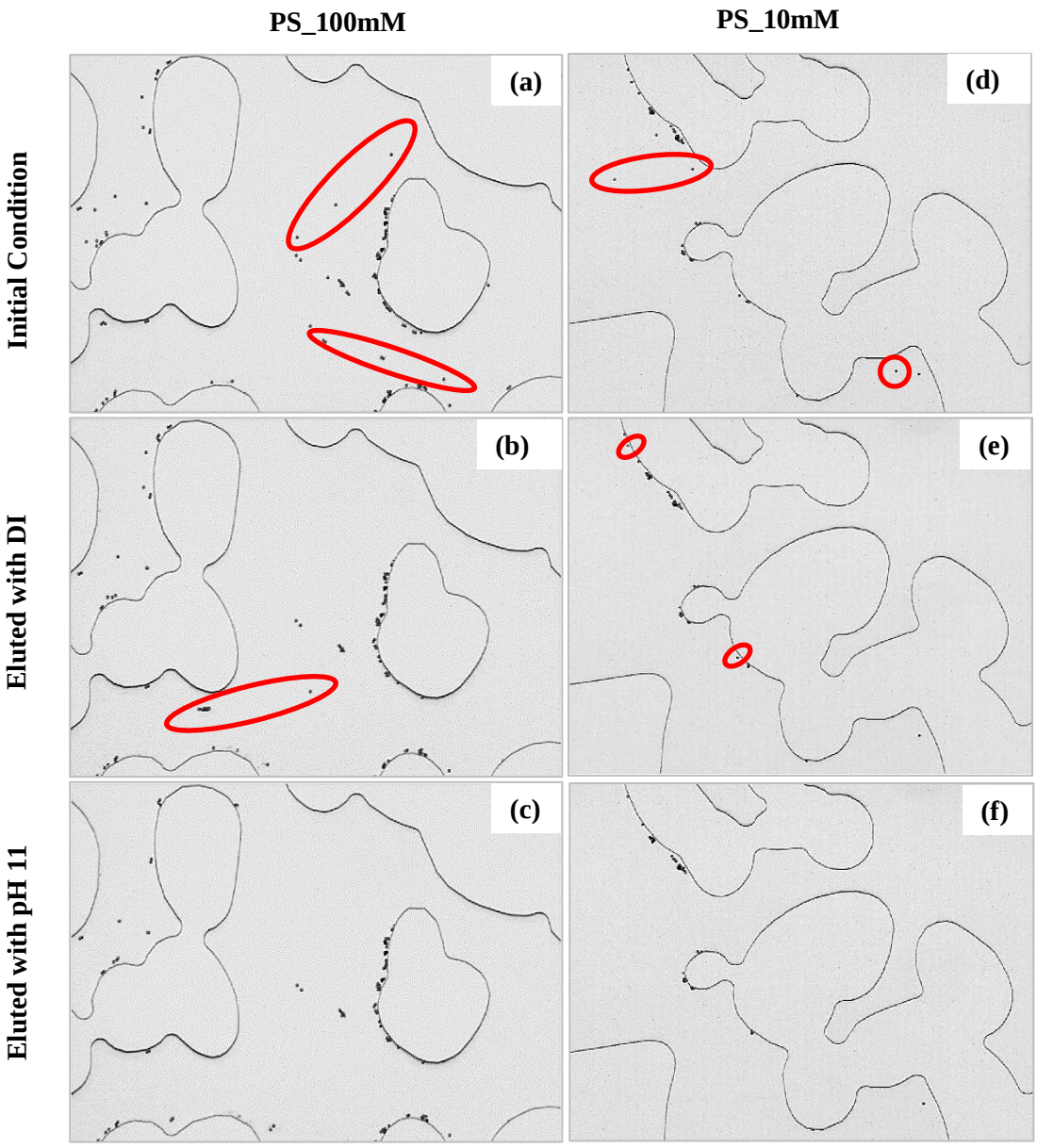

Figure 44. Pore-scale images at different stages of elution for PS_100mM and PS_10mM colloids

Although the interaction between AMPS colloids and SWI was attractive at all separation distances, the energy of interaction varies with separation distances (Figure 36). Also, the DLVO profiles at pH 11 (Figure 43) for AMPS colloids indicate that the interaction energy became repulsive after a separation distance of 3 nm. Therefore, those colloids attached at a separation distance beyond 3 nm are susceptible to release

during the elution stage for AMPS colloids. A similar observation can be made from Figure 43 that CMPS colloids interacting beyond 0.2 nm can release while eluting with a high pH solution. The pore-scale images show that the released colloids for both cases were attached via interception (either on collector centers or micromodel top/bottom) and those colloids left in the micromodel were attached on FFSZ (Figure 45).

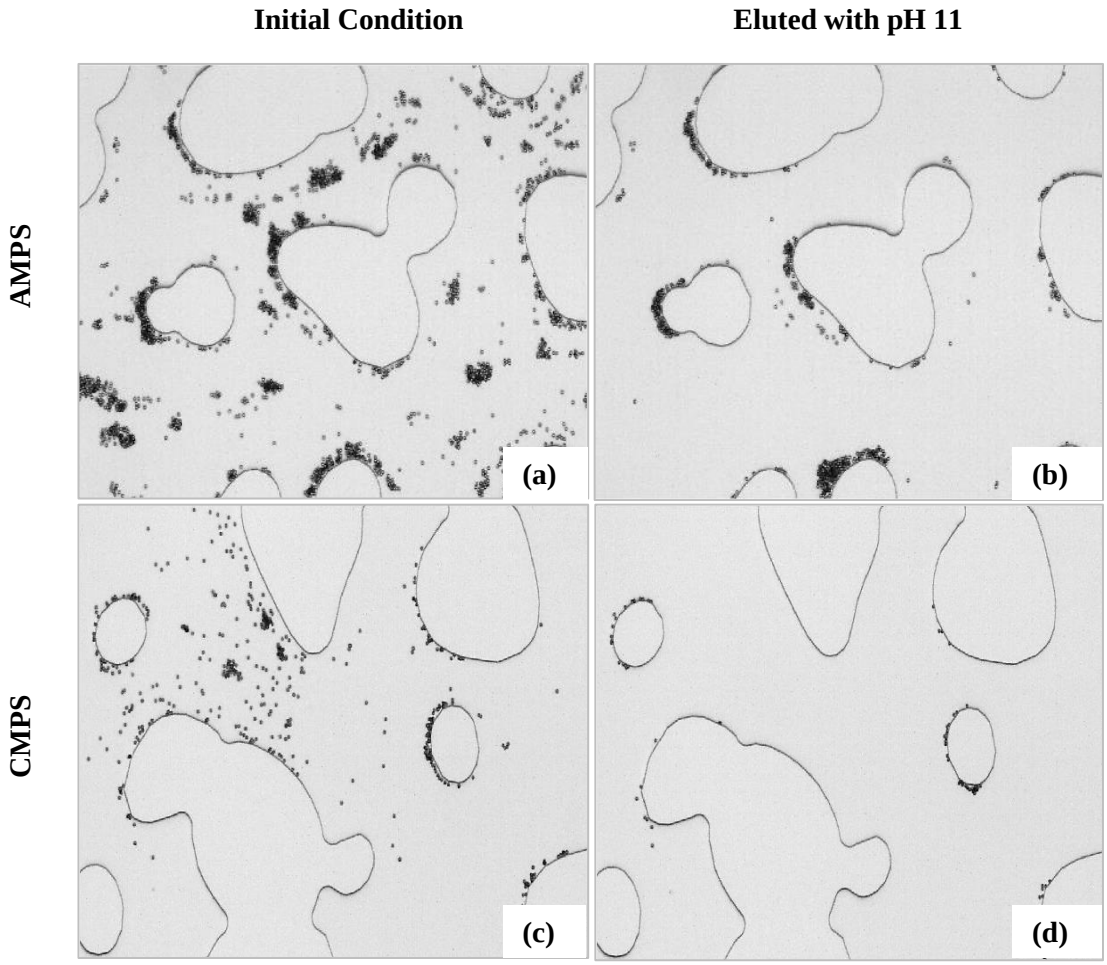

Figure 45. Pore-scale images at different stages of elution for AMPS and CMPS colloids

This observation was consistent for all types of colloids tested in this study. Therefore, we may conclude that the colloid interactions at FFSZ occur at a very short separation distance where primary minima exist for colloids even under unfavorable

conditions in this study (i.e., PS_10mM and PS_100mM). As reported in previous studies, colloids interacting at deep primary minima are unaffected by the changes in solution chemistry.

In general, the release of colloids attached at deep primary minima was negligible during perturbations in solution ionic strength or pH. However, some previous studies reported the release of colloids from primary minima with the increase in pH. Our pore-scale observations suggest that the colloids transferred to the FFSZ were translated to shorter separation distance where deep energy well exists even under unfavorable attachment conditions. Those colloids cannot be released even after an increase in flow velocity as the hydrodynamic drag forces are negligible compared to the adhesion forces. The greater release of colloids under favorable attachment conditions during perturbations in solution chemistry and flow rate can be explained with their long-range interaction (colloids interact with SWI at a long-range of separation distances). Only those colloids retained at short separation distances were remained after the perturbations with solution chemistry. In contrast, the short-range interactions of unfavorable conditions (primary and secondary minima are short-range) can release only those colloids retained via a secondary minimum. As the primary minima were deep enough and are very close to the surface (deposited in low flow zones), their mobilization was not observed in our visualization study.

6.4. Conclusions

It has been recognized in the literature that greater colloid release occurs for colloids under unfavorable attachment conditions than those under favorable conditions during perturbations in solution chemistry or flow rate. Our pore-scale observation, however, showed that the colloid release increase with an increase in flow rate, solution pH and decrease in solution ionic strength for favorably interacting colloids with SWI.

The real-time visualization of release behavior explained the significance of the colloid deposition profile in the porous media. Attachment on FFSZ dominates under unfavorable conditions, and deposition on collector centers via interception dominates under favorable conditions.

Additionally, primary minimum interaction at very short separation distance was perceived for those colloids attached to FFSZ as they are unaffected by the changes in fluid chemistry. Therefore, only those colloids attached to collector centers were released during the perturbations in fluid chemistry and flow rate as the hydrodynamic drag forces exceed the adhesion forces. Whereas those colloids attached to FFSZ remain attached due to the lower hydrodynamic drag forces (low-flow zones) compared to the adhesion forces (deep primary minimum). These results indicate that colloids attached via favorable conditions are more susceptible to release during the perturbations in solution chemistry or flow rate that can happen during massive rainfall events.

CHAPTER 7: SUMMARY AND CONCLUSIONS

Colloid transport in soil porous media involves complex processes. Therefore, laboratory studies often employ model experimental systems to investigate the pore-scale processes in porous media. This study utilized a geometrically representative micromodel, which served as a two-dimensional model of soil porous media. The use of optical microscopy allowed real-time visualization of the pore-scale mechanisms involved in colloid transport processes. Highly controllable physical and chemical environments in the micromodel enhance its applicability to focus on relevant and interested experimental conditions. Direct visualization of various retention mechanisms including straining, attachment on Soli-Water Interfaces, Air-Water Interfaces, Air-Water-Solid Interfaces, and thin films advanced the understanding of colloid transport in single and two-phase flow porous media systems. In addition to colloid deposition, mobilization of the deposited colloids in response to the perturbations in flow velocity or solution chemistry, which have been extensively studied using laboratory column experiments with significant ambiguity in explaining the pore-scale mechanisms.

The study of colloid retention during single and two-phase flow in the micromodel considered in Chapter 4, investigated the impact of colloid hydrophobicity, solution ionic strength and pH on various colloid retention mechanisms including Colloid-Colloid, Colloid-Solid Water Interface, Colloid-Air Water Interfaces, and Colloid-Air Water Solid Interfaces or thin water films. It was shown that the colloid retention mechanism in single-phase flow predicted well with the DLVO theory. In contrast, colloid retention on Air-Water interfaces involves additional force considerations (i.e., capillary forces) other than the DLVO forces. Significant colloid retention was observed for hydrophilic colloids due to Long-range or Short-Range

interaction between the colloids and Solid-Water Interface or other colloids. In contrast, hydrophobic colloid interactions were repulsive, resulting in effective transport through porous media. In soil porous media, hydrophobic colloids such as bacteria and viruses may transport deep into the groundwater reservoirs compared to hydrophilic colloids (i.e., clay colloids, iron oxides, etc.). Therefore, facilitated transport of contaminants via hydrophilic colloids may be insignificant compared to the hydrophobic colloids. Moreover, an increase in ionic strength or a decrease in pH reduces the mobility of hydrophobic colloids, whereas the impact of solution chemistry was insignificant for hydrophilic colloids. During drainage, the moving Air-Water Interface mobilize the deposited colloids, and the mobilization was greater for hydrophobic colloids, whereas hydrophilic colloids were redeposited on Air-Water Solid Interfaces or thin water films. However, with the increase in ionic strength or decrease in pH, both colloids exhibit strong interaction with Solid-Water Interface, and the mobilization by Air-Water Interfaces significantly reduced. This study also emphasizes the necessity to consider the coupled effects of solution chemistry and colloid hydrophobicity while studying the colloid transport mechanisms in porous media.

The important effect of colloid hydrophobicity on colloid mobilization from a Solid-Water Interface and Air-Water Interface was further shown in the micromodel, as explained in Chapter 5 during drainage and imbibition, respectively. The deposited colloids on Solid Water Interfaces mobilize during drainage and attached to Air-Water Interfaces. Hydrophilic colloids attach to Air-Water-Solid Interface or thin films in addition to the Air-Water Interfaces. Colloids on Air-Water Interface were transported through the porous media along with the moving interfaces leaving colloids only on a few air bubbles. Previous studies reported the cluster formation at the end of bubble dissolution. However, in this study, hydrophilic colloids redeposit on Solid-Water

Interfaces, whereas hydrophobic colloids form colloid aggregates on the interface during the bubble dissolution process. As the moving Air-Water Interfaces are common in subsurface porous media in continuous cycles of evaporation and infiltration events or capillary fringe fluctuations, the understanding of the release mechanisms would help to assess or predict the subsurface contamination followed by these events.

Colloid release behavior in response to the perturbations in flow rate and solution chemistry was investigated visually in a saturated micromodel, as illustrated in Chapter 6. Colloids with different favorability to the Solid-Water Interface was selected to observe different colloid deposition profile for each colloid. Colloid deposition on collector center via interception dominates for favorable interaction conditions whereas, under unfavorable conditions, colloids deposited mostly on Forward Flow Stagnation Zones. This study visually evidenced the release of colloids predominantly from the collector center than the flow stagnation zones as the hydrodynamic torque exceeds the adhesion forces with an increase in flow rate or solution pH and a decrease in solution ionic strength. Those colloids attached on Forward Flow Stagnation Zones were transferred to deep primary minima at a very short separation distance where the hydrodynamic drag forces are lower compared to collector centers. Therefore, a greater release of colloids under favorable conditions occur compared to unfavorable conditions.

REFERENCES

[1] S. Sirivithayapakorn, A. Keller, Transport of colloids in unsaturated porous media : A pore-scale observation of processes during the dissolution of air-water interface, 39 (2003). https://doi.org/10.1029/2003WR002487.

[2] J.T. Crist, Y. Zevi, J.F. Mccarthy, J.A. Throop, T.S. Steenhuis, Transport and Retention Mechanisms of Colloids in Partially Saturated Porous Media, 4 (2005) 184–195.

[3] S. Tao, D. Tang, H. Xu, S. Li, Y. Geng, J. Zhao, S. Wu, Q. Meng, X. Kou, S. Yang, Fluid velocity sensitivity of coal reservoir and its effect on coalbed methane well productivity: A case of Baode Block, northeastern Ordos Basin, China, J. Pet. Sci. Eng. 152 (2017) 229–237.

[4] W. Song, A.R. Kovscek, Functionalization of micromodels with kaolinite for investigation of low salinity oil-recovery processes, Lab Chip. 15 (2015) 3314–3325. https://doi.org/10.1039/C5LC00544B.

[5] K.R. Bradbury, M.A. Borchardt, M. Gotkowitz, S.K. Spencer, J. Zhu, R.J. Hunt, Source and transport of human enteric viruses in deep municipal water supply wells, Environ. Sci. Technol. 47 (2013) 4096–4103.

[6] C.K. Uejio, S.H. Yale, K. Malecki, M.A. Borchardt, H.A. Anderson, J.A. Patz, Drinking water systems, hydrology, and childhood gastrointestinal illness in Central and Northern Wisconsin, Am. J. Public Health. 104 (2014) 639–646.

[7] T.K. Sen, K.C. Khilar, Review on subsurface colloids and colloid-associated contaminant transport in saturated porous media, Adv. Colloid Interface Sci. 119 (2006) 71–96.

[8] K.-M. Yao, M.T. Habibian, C.R. O'Melia, Water and waste water filtration. Concepts and applications, Environ. Sci. Technol. 5 (1971) 1105–1112.

[9] S.A. Bradford, S.R. Yates, M. Bettahar, J. Simunek, Physical factors affecting the transport and fate of colloids in saturated porous media, Water Resour. Res. 38 (2002).

[10] S.A. Bradford, J. Simunek, M. Bettahar, M.T. van Genuchten, S.R. Yates, Modeling colloid attachment, straining, and exclusion in saturated porous media, Environ. Sci. Technol. 37 (2003) 2242–2250.

[11] Y.H. El-Farhan, N.M. DeNovio, J.S. Herman, G.M. Hornberger, Mobilization and transport of soil particles during infiltration experiments in an agricultural field, Shenandoah Valley, Virginia, Environ. Sci. Technol. 34 (2000) 3555–3559.

[12] J.T. Crist, Y. Zevi, J.F. McCarthy, J.A. Throop, T.S. Steenhuis, Transport and retention mechanisms of colloids in partially saturated porous media, Vadose Zo. J. 4 (2005) 184–195.

[13] Y. Zevi, A. Dathe, J.F. Mccarthy, B.K. Richards, T.S. Steenhuis, Distribution of colloid particles onto interfaces in partially saturated sand, Environ. Sci. Technol. 39 (2005) 7055–7064. https://doi.org/10.1021/es048595b.

[14] B. Gao, J.E. Saiers, J. Ryan, Pore-scale mechanisms of colloid deposition and mobilization during steady and transient flow through unsaturated granular media, Water Resour. Res. 42 (2006).

[15] B. Derjaguin, L. Landau, The theory of stability of highly charged lyophobic sols and coalescence of highly charged particles in electrolyte solutions, Acta Physicochim. URSS. 14 (1941) 58.

[16] J.T.G. Overbeek, E.J.W. Verwey, Theory of the Stability of Lyophobic Colloids: The interaction of Sol Particles Having an Electric Double Layer, 1948.

[17] J.T. Crist, J.F. McCarthy, Y. Zevi, P. Baveye, J.A. Throop, T.S. Steenhuis, Pore-

Scale Visualization of Colloid Transport and Retention in Partly Saturated Porous Media, Vadose Zo. J. 3 (2004) 444. https://doi.org/10.2136/vzj2004.0444.

[18] Q. Zhang, S.M. Hassanizadeh, B. Liu, J.F. Schijven, N.K. Karadimitriou, Effect of hydrophobicity on colloid transport during two-phase flow in a micromodel, Water Resour. Res. 50 (2014) 7677–7691.

[19] C.J. Van Oss, Interfacial forces in aqueous media, CRC press, 2006.

[20] J.N. Israelachvili, Intermolecular and surface forces, Academic press, 2011.

[21] B. Gao, T.S. Steenhuis, Y. Zevi, V.L. Morales, J.L. Nieber, B.K. Richards, J.F. McCarthy, J. Parlange, Capillary retention of colloids in unsaturated porous media, Water Resour. Res. 44 (2008).

[22] Y. Zevi, A. Dathe, B. Gao, B.K. Richards, T.S. Steenhuis, Quantifying colloid retention in partially saturated porous media, Water Resour. Res. 42 (2006).

[23] V. Lazouskaya, L.-P. Wang, H. Gao, X. Shi, K. Czymmek, Y. Jin, Pore-scale investigation of colloid retention and mobilization in the presence of a moving air–water interface, Vadose Zo. J. 10 (2011) 1250–1260.

[24] V. Lazouskaya, Y. Jin, D. Or, Interfacial interactions and colloid retention under steady flows in a capillary channel, J. Colloid Interface Sci. 303 (2006) 171–184. https://doi.org/https://doi.org/10.1016/j.jcis.2006.07.071.

[25] J. Wan, J.L. Wilson, Visualization of the role of the gas-water interface on the fate and transport of colloids in porous media, Water Resour. Res. 30 (1994) 11–23. https://doi.org/10.1029/93WR02403.

[26] V. Lazouskaya, Y. Jin, Colloid retention at air–water interface in a capillary channel, Colloids Surfaces A Physicochem. Eng. Asp. 325 (2008) 141–151. https://doi.org/https://doi.org/10.1016/j.colsurfa.2008.04.053.

[27] M. Auset, A.A. Keller, Pore-scale visualization of colloid straining and filtration in saturated porous media using micromodels, 42 (2006) 1–9. https://doi.org/10.1029/2005WR004639.

[28] M. Auset, A.A. Keller, Pore-scale processes that control dispersion of colloids in saturated porous media, 40 (2004). https://doi.org/10.1029/2003WR002800.

[29] S. Aramrak, M. Flury, J.B. Harsh, R.L. Zollars, Colloid mobilization and transport during capillary fringe fluctuations, Environ. Sci. Technol. 48 (2014) 7272–7279.

[30] Q. Zhang, A. Raoof, S.M. Hassanizadeh, Pore-scale study of flow rate on colloid attachment and remobilization in a saturated micromodel, J. Environ. Qual. 44 (2015) 1376–1383.

[31] Q. Zhang, S.M. Hassanizadeh, The role of interfacial tension in colloid retention and remobilization during two-phase flow in a polydimethylsiloxane micro-model, Chem. Eng. Sci. 168 (2017) 437–443.

[32] Y. Guo, J. Huang, F. Xiao, X. Yin, J. Chun, W. Um, Bead-Based Micro fl uidic Sediment Analogues: Fabrication and Colloid Transport, (2016). https://doi.org/10.1021/acs.langmuir.6b02184.

[33] Q. Zhang, S.M. Hassanizadeh, N.K. Karadimitriou, A. Raoof, B. Liu, P.J. Kleingeld, A. Imhof, Retention and remobilization of colloids during steady-state and transient two-phase flow, Water Resour. Res. 49 (2013) 8005–8016.

[34] V. Lazouskaya, L.-P. Wang, D. Or, G. Wang, J.L. Caplan, Y. Jin, Colloid mobilization by fluid displacement fronts in channels, J. Colloid Interface Sci. 406 (2013) 44–50.

[35] G.C. Agbangla, É. Climent, P. Bacchin, Experimental investigation of pore clogging by microparticles: Evidence for a critical flux density of particle

yielding arches and deposits, Sep. Purif. Technol. 101 (2012) 42–48.

[36] J. Jung, S. Cao, R. Al-Raoush, K. Alshibli, Fines migration and clogging behavior in methane hydratebearing sediments, Qatar Found. Annu. Res. Conf. Proc. 2018 (2018) EEPD710. https://doi.org/10.5339/qfarc.2018.EEPD710.

[37] J. Jung, S.C. Cao, Y.-H. Shin, R.I. Al-Raoush, K. Alshibli, J.-W. Choi, A microfluidic pore model to study the migration of fine particles in single-phase and multi-phase flows in porous media, Microsyst. Technol. (2017). https://doi.org/10.1007/s00542-017-3462-1.

[38] M. Auset, A.A. Keller, V. Lazarova, Intermittent filtration of bacteria and colloids in porous media, 41 (2005) 1–14. https://doi.org/10.1029/2004WR003611.

[39] H.M. Wyss, D.L. Blair, J.F. Morris, H.A. Stone, D.A. Weitz, Mechanism for clogging of microchannels, Phys. Rev. E. 74 (2006) 61402.

[40] E. Dressaire, A. Sauret, Clogging of microfluidic systems, Soft Matter. 13 (2017) 37–48.

[41] J. Argent, S. Torkzaban, S. Hubbard, H. Le, T. Amirianshoja, M. Haghighi, Visualization of Micro-Particle Retention on a Heterogeneous Surface Using Micro-models : Influence of Nanoscale Surface Roughness, Transp. Porous Media. 109 (2015) 239–253. https://doi.org/10.1007/s11242-015-0511-z.

[42] G. Chen, M. Flury, Retention of mineral colloids in unsaturated porous media as related to their surface properties, Colloids Surfaces A Physicochem. Eng. Asp. 256 (2005) 207–216.

[43] J. Wan, J.L. Wilson, T.L. Kieft, Influence of the Gas-Water Interface on Transport of Microorganisms through Unsaturated Porous Media, 0099 (1994) 509–516.

[44] P. Sharma, M. Flury, J. Zhou, Detachment of colloids from a solid surface by a moving air-water interface, J. Colloid Interface Sci. 326 (2008) 143–150. https://doi.org/10.1016/j.jcis.2008.07.030.

[45] Q. Zhang, N.K. Karadimitriou, S.M. Hassanizadeh, P.J. Kleingeld, A. Imhof, Journal of Colloid and Interface Science Study of colloids transport during two-phase flow using a novel polydimethylsiloxane micro-model, J. Colloid Interface Sci. 401 (2013) 141–147. https://doi.org/10.1016/j.jcis.2013.02.041.

[46] W. Song, A.R. Kovscek, Direct visualization of pore-scale fines migration and formation damage during low-salinity waterflooding, J. Nat. Gas Sci. Eng. 34 (2016) 1276–1283. https://doi.org/10.1016/j.jngse.2016.07.055.

[47] W. Song, T.W. de Haas, H. Fadaei, D. Sinton, Chip-off-the-old-rock: the study of reservoir-relevant geological processes with real-rock micromodels, Lab Chip. 14 (2014) 4382–4390.

[48] W. Wang, S. Chang, A. Gizzatov, Toward reservoir-on-a-chip: fabricating reservoir micromodels by in situ growing calcium carbonate nanocrystals in microfluidic channels, ACS Appl. Mater. Interfaces. 9 (2017) 29380–29386.

[49] Y.A. Alzahid, P. Mostaghimi, A. Gerami, A. Singh, K. Privat, T. Amirian, R.T. Armstrong, Functionalisation of Polydimethylsiloxane (PDMS)-Microfluidic Devices coated with Rock Minerals, Sci. Rep. 8 (2018) 15518.

[50] T. Amirian, M. Haghighi, P. Mostaghimi, Pore scale visualization of low salinity water flooding as an enhanced oil recovery method, Energy & Fuels. 31 (2017) 13133–13143.

[51] S.C. Cao, S. Dai, J. Jung, Supercritical CO2and brine displacement in geological carbon sequestration: Micromodel and pore network simulation studies, Int. J. Greenh. Gas Control. 44 (2016) 104–114.

https://doi.org/10.1016/j.ijggc.2015.11.026.

[52] B. Xu, W.-Q. Du, J.-W. Li, Y.-L. Hu, L. Yang, C.-C. Zhang, G.-Q. Li, Z.-X. Lao, J.-C. Ni, J.-R. Chu, High efficiency integration of three-dimensional functional microdevices inside a microfluidic chip by using femtosecond laser multifoci parallel microfabrication, Sci. Rep. 6 (2016) 19989.

[53] R. Hu, J. Wan, Y. Kim, T.K. Tokunaga, Wettability effects on supercritical CO2–brine immiscible displacement during drainage: Pore-scale observation and 3D simulation, Int. J. Greenh. Gas Control. 60 (2017) 129–139.

[54] M. Kim, A. Abedini, P. Lele, A. Guerrero, D. Sinton, Microfluidic pore-scale comparison of alcohol-and alkaline-based SAGD processes, J. Pet. Sci. Eng. 154 (2017) 139–149.

[55] Y.A. Alzahid, P. Mostaghimi, S.D.C. Walsh, R.T. Armstrong, Flow regimes during surfactant flooding: The influence of phase behaviour, Fuel. 236 (2019) 851–860.

[56] W. Stumm, Chemical interaction in particle separation, Environ. Sci. Technol. 11 (1977) 1066–1070.

[57] H.-J. Kim, T. Phenrat, R.D. Tilton, G. V Lowry, Effect of kaolinite, silica fines and pH on transport of polymer-modified zero valent iron nano-particles in heterogeneous porous media, J. Colloid Interface Sci. 370 (2012) 1–10. https://doi.org/https://doi.org/10.1016/j.jcis.2011.12.059.

[58] J.N. Ryan, M. Elimelech, R.A. Ard, R.W. Harvey, P.R. Johnson, Bacteriophage PRD1 and silica colloid transport and recovery in an iron oxide-coated sand aquifer, Environ. Sci. Technol. 33 (1999) 63–73.

[59] Y. Sun, B. Gao, S.A. Bradford, L. Wu, H. Chen, X. Shi, J. Wu, Transport, retention, and size perturbation of graphene oxide in saturated porous media:

effects of input concentration and grain size, Water Res. 68 (2015) 24–33.

[60] R.N. Jordan, D.R. Yonge, W.E. Hathhorn, Enhanced mobility of Pb in the presence of dissolved natural organic matter, J. Contam. Hydrol. 29 (1997) 59–80.

[61] A.D. Karathanasis, Subsurface migration of copper and zinc mediated by soil colloids, Soil Sci. Soc. Am. J. 63 (1999) 830–838.

[62] L.A. Sprague, J.S. Herman, G.M. Hornberger, A.L. Mills, Atrazine adsorption and colloid-facilitated transport through the unsaturated zone, J. Environ. Qual. 29 (2000) 1632–1641.

[63] M. Flury, J.B. Mathison, J.B. Harsh, In situ mobilization of colloids and transport of cesium in Hanford sediments, Environ. Sci. Technol. 36 (2002) 5335–5341.

[64] J.N. Ryan, T.H. Illangasekare, M.I. Litaor, R. Shannon, Particle and plutonium mobilization in macroporous soils during rainfall simulations, Environ. Sci. Technol. 32 (1998) 476–482.

[65] S. Torkzaban, S.S. Tazehkand, S.L. Walker, S.A. Bradford, Transport and fate of bacteria in porous media: Coupled effects of chemical conditions and pore space geometry, Water Resour. Res. 44 (2008).

[66] C.H. Bolster, A.L. Mills, G.M. Hornberger, J.S. Herman, Spatial distribution of deposited bacteria following miscible displacement experiments in intact cores, Water Resour. Res. 35 (1999) 1797–1807.

[67] S. Torkzaban, S.M. Hassanizadeh, J.F. Schijven, H.H.J.L. Van Den Berg, Role of air-water interfaces on retention of viruses under unsaturated conditions, Water Resour. Res. 42 (2006) 1–11. https://doi.org/10.1029/2006WR004904.

[68] V.I. Syngouna, C. V Chrysikopoulos, Experimental investigation of virus and clay particles cotransport in partially saturated columns packed with glass beads,

J. Colloid Interface Sci. 440 (2015) 140–150.

[69] J.M. Zachara, J. Markus Flury, Colloid Facilitated Migration of Radioelements-Mechanisms, Significance, and Needed Conditions, Clay Min. 43 (2002) 285–293.

[70] Y. Wang, S.A. Bradford, J. Simunek, Release of E. coli D21g with transients in water content, Environ. Sci. Technol. 48 (2014) 9349–9357.

[71] J. Zhuang, J.F. McCarthy, J.S. Tyner, E. Perfect, M. Flury, In situ colloid mobilization in Hanford sediments under unsaturated transient flow conditions: Effect of irrigation pattern, Environ. Sci. Technol. 41 (2007) 3199–3204. https://doi.org/10.1021/es062757h.

[72] D.I. Kaplan, P.M. Bertsch, D.C. Adriano, W.P. Miller, Soil-borne mobile colloids as influenced by water flow and organic carbon, Environ. Sci. Technol. 27 (1993) 1193–1200.

[73] J. Wan, T.K. Tokunaga, Partitioning of Clay Colloids at Air–Water Interfaces, J. Colloid Interface Sci. 247 (2002) 54–61. https://doi.org/https://doi.org/10.1006/jcis.2001.8132.

[74] S.A. Bradford, S. Torkzaban, A. Shapiro, A theoretical analysis of colloid attachment and straining in chemically heterogeneous porous media, Langmuir. 29 (2013) 6944–6952.

[75] R. Rajagopalan, C. Tien, Trajectory analysis of deep-bed filtration with the sphere-in-cell porous media model, AIChE J. 22 (1976) 523–533.

[76] W. Long, M. Hilpert, A correlation for the collector efficiency of Brownian particles in clean-bed filtration in sphere packings by a Lattice-Boltzmann method, Environ. Sci. Technol. 43 (2009) 4419–4424.

[77] N. Tufenkji, M. Elimelech, Correlation equation for predicting single-collector

efficiency in physicochemical filtration in saturated porous media, Environ. Sci. Technol. 38 (2004) 529–536.

[78] H. Ma, W.P. Johnson, Colloid retention in porous media of various porosities: Predictions by the hemispheres-in-cell model, Langmuir. 26 (2009) 1680–1687.

[79] K.E. Nelson, T.R. Ginn, New collector efficiency equation for colloid filtration in both natural and engineered flow conditions, Water Resour. Res. 47 (2011).

[80] J. Gregory, Approximate expressions for retarded van der Waals interaction, J. Colloid Interface Sci. 83 (1981) 138–145.

[81] J.N. Israelachvili, Intermolecular and surface forces, (1992).

[82] R. Hogg, D.S. Cahn, T.W. Healy, D.W. Fuerstenau, Diffusional mixing in an ideal system, Chem. Eng. Sci. 21 (1966) 1025–1038.

[83] S.A. Bradford, S. Torkzaban, Colloid transport and retention in unsaturated porous media: A review of interface-, collector-, and pore-scale processes and models, Vadose Zo. J. 7 (2008) 667–681.

[84] Y. Gu, D. Li, The ζ-Potential of Glass Surface in Contact with Aqueous Solutions, J. Colloid Interface Sci. 226 (2000) 328–339. https://doi.org/https://doi.org/10.1006/jcis.2000.6827.

[85] A. Sze, D. Erickson, L. Ren, D. Li, Zeta-potential measurement using the Smoluchowski equation and the slope of the current–time relationship in electroosmotic flow, J. Colloid Interface Sci. 261 (2003) 402–410.

[86] J.A. Redman, S.L. Walker, M. Elimelech, Bacterial adhesion and transport in porous media: Role of the secondary energy minimum, Environ. Sci. Technol. 38 (2004) 1777–1785.

[87] J.E. Saiers, J.J. Lenhart, Colloid mobilization and transport within unsaturated porous media under transient-flow conditions, 39 (2003).

https://doi.org/10.1029/2002WR001370.

[88] S. Bhattacharjee, J.Y. Chen, M. Elimelech, DLVO interaction energy between spheroidal particles and a flat surface, Colloids Surfaces A Physicochem. Eng. Asp. 165 (2000) 143–156.

[89] I.L. Molnar, W.P. Johnson, J.I. Gerhard, C.S. Willson, D.M. O'Carroll, Predicting colloid transport through saturated porous media: A critical review, Water Resour. Res. 51 (2015) 6804–6845.

[90] M. Elimelech, Kinetics of capture of colloidal particles in packed beds under attractive double layer interactions, J. Colloid Interface Sci. 146 (1991) 337–352.

[91] N. Tufenkji, M. Elimelech, Breakdown of colloid filtration theory: Role of the secondary energy minimum and surface charge heterogeneities, Langmuir. 21 (2005) 841–852.

[92] H.-J. Butt, A technique for measuring the force between a colloidal particle in water and a bubble, J. Colloid Interface Sci. 166 (1994) 109–117.

[93] W.A. Ducker, Z. Xu, J.N. Israelachvili, Measurements of hydrophobic and DLVO forces in bubble-surface interactions in aqueous solutions, Langmuir. 10 (1994) 3279–3289.

[94] A. Schäfer, H. Harms, A.J.B. Zehnder, Bacterial accumulation at the air− water interface, Environ. Sci. Technol. 32 (1998) 3704–3712.

[95] R.-H. Yoon, D.H. Flinn, Y.I. Rabinovich, Hydrophobic interactions between dissimilar surfaces, J. Colloid Interface Sci. 185 (1997) 363–370.

[96] E. Ruckenstein, D.C. Prieve, Adsorption and desorption of particles and their chromatographic separation, AIChE J. 22 (1976) 276–283.

[97] P.N. Mitropoulou, V.I. Syngouna, C. V. Chrysikopoulos, Transport of colloids in unsaturated packed columns: Role of ionic strength and sand grain size, Chem.

Eng. J. 232 (2013) 237–248. https://doi.org/10.1016/j.cej.2013.07.093.

[98] K.C. Khilar, H.S. Fogler, Migrations of fines in porous media, Springer Science & Business Media, 1998.

[99] T. Mahmood, A. Amirtharajah, T.W. Sturm, K.E. Dennett, A micromechanics approach for attachment and detachment of asymmetric colloidal particles, Colloids Surfaces A Physicochem. Eng. Asp. 177 (2001) 99–110.

[100] S.A. Bradford, S. Torkzaban, Colloid interaction energies for physically and chemically heterogeneous porous media, Langmuir. 29 (2013) 3668–3676.

[101] J.N. Ryan, P.M. Gschwend, Effects of ionic strength and flow rate on colloid release: Relating kinetics to intersurface potential energy, J. Colloid Interface Sci. 164 (1994) 21–34.

[102] S. Torkzaban, S.A. Bradford, Critical role of surface roughness on colloid retention and release in porous media, Water Res. 88 (2016) 274–284.

[103] S. Xu, J. Qi, X. Chen, V. Lazouskaya, J. Zhuang, Y. Jin, Coupled effect of extended DLVO and capillary interactions on the retention and transport of colloids through unsaturated porous media, Sci. Total Environ. 573 (2016) 564–572.

[104] P.G.T. Saffman, The lift on a small sphere in a slow shear flow, J. Fluid Mech. 22 (1965) 385–400.

[105] S. Torkzaban, S.A. Bradford, S.L. Walker, Resolving the coupled effects of hydrodynamics and DLVO forces on colloid attachment in porous media, Langmuir. 23 (2007) 9652–9660.

[106] J. Bergendahl, D. Grasso, Prediction of colloid detachment in a model porous media: hydrodynamics, Chem. Eng. Sci. 55 (2000) 1523–1532.

[107] M.E. O'neill, A sphere in contact with a plane wall in a slow linear shear flow,

Chem. Eng. Sci. 23 (1968) 1293–1298.

[108] S. Aramrak, M. Flury, J.B. Harsh, Detachment of deposited colloids by advancing and receding air-water interfaces, Langmuir. 27 (2011) 9985–9993. https://doi.org/10.1021/la201840q.

[109] J. Sur, H.K. Pak, Capillary force on colloidal particles in a freely suspended liquid thin film, Phys. Rev. Lett. 86 (2001) 4326.

[110] C. Gómez-Suárez, H.C. van der Mei, H.J. Busscher, Air bubble-induced detachment of polystyrene particles with different sizes from collector surfaces in a parallel plate flow chamber, Colloids Surfaces A Physicochem. Eng. Asp. 186 (2001) 211–219.

[111] C. Gómez Suárez, J. Noordmans, H.C. Van der Mei, H.J. Busscher, Removal of Colloidal Particles from Quartz Collector Surfaces As Stimulated by the Passage of Liquid− Air Interfaces, Langmuir. 15 (1999) 5123–5127.

[112] A.F.M. Leenaars, Particle removal from silicon substrates using surface tension forces, Philips J Res. 44 (1989) 183–209.

[113] H.-J. Butt, B. Cappella, M. Kappl, Force measurements with the atomic force microscope: Technique, interpretation and applications, Surf. Sci. Rep. 59 (2005) 1–152.

[114] S. Aramrak, M. Flury, J.B. Harsh, Detachment of deposited colloids by advancing and receding air–water interfaces, Langmuir. 27 (2011) 9985–9993.

[115] S.A. Bradford, S. Torkzaban, A. Wiegmann, Pore-scale simulations to determine the applied hydrodynamic torque and colloid immobilization, Vadose Zo. J. 10 (2011) 252–261.

[116] J. Bergendahl, D. Grasso, Colloid generation during batch leaching tests: mechanics of disaggregation, Colloids Surfaces A Physicochem. Eng. Asp. 135

(1998) 193–205.

[117] K.L. Johnson, K.L. Johnson, Contact mechanics, Cambridge university press, 1987.

[118] J. Shang, M. Flury, G. Chen, J. Zhuang, Impact of flow rate, water content, and capillary forces on in situ colloid mobilization during infiltration in unsaturated sediments, Water Resour. Res. 44 (2008) 1–12. https://doi.org/10.1029/2007WR006516.

[119] J.W. Bridge, S.A. Banwart, A.L. Heathwaite, High-resolution measurement of pore saturation and colloid removal efficiency in quartz sand using fluorescence imaging, Environ. Sci. Technol. 41 (2007) 8288–8294.

[120] A.K. Alhuraishawy, B. Bai, M. Wei, J. Geng, J. Pu, Mineral dissolution and fine migration effect on oil recovery factor by low-salinity water flooding in low-permeability sandstone reservoir, Fuel. 220 (2018) 898–907. https://doi.org/10.1016/j.fuel.2018.02.016.

[121] M.J. Barnaji, P. Pourafshary, M.R. Rasaie, Visual investigation of the effects of clay minerals on enhancement of oil recovery by low salinity water flooding, Fuel. 184 (2016) 826–835. https://doi.org/10.1016/j.fuel.2016.07.076.

[122] J. Zhuang, N. Goeppert, C. Tu, J. McCarthy, E. Perfect, L. McKay, Colloid transport with wetting fronts: Interactive effects of solution surface tension and ionic strength, Water Res. 44 (2010) 1270–1278.

[123] V.B. Pandya, S. Bhuniya, K.C. Khilar, Existence of a Critical Particle Concentration in Plugging of a Packed Bed, AIChE J. 44 (1998) 978–981. https://doi.org/10.1002/aic.690440424.

[124] H. Mahani, A.L. Keya, S. Berg, W.-B. Bartels, R. Nasralla, W.R. Rossen, Insights into the mechanism of wettability alteration by low-salinity flooding

(LSF) in carbonates, Energy & Fuels. 29 (2015) 1352–1367.

[125] C. Kim, J. Lee, Experimental study on the variation of relative permeability due to clay minerals in low salinity water-flooding, J. Pet. Sci. Eng. 151 (2017) 292–304. https://doi.org/10.1016/j.petrol.2017.01.014.

[126] N. Chatterjee, M. Flury, Effect of particle shape on capillary forces acting on particles at the air-water interface, Langmuir. 29 (2013) 7903–7911. https://doi.org/10.1021/la4017504.

[127] J.N. Ryan, M. Elimelech, Colloid mobilization and transport in groundwater, Colloids Surfaces A Physicochem. Eng. Asp. 107 (1996) 1–56.

[128] C. Shen, B. Li, Y. Huang, Y. Jin, Kinetics of coupled primary-and secondary-minimum deposition of colloids under unfavorable chemical conditions, Environ. Sci. Technol. 41 (2007) 6976–6982.

[129] A. Franchi, C.R. O'Melia, Effects of natural organic matter and solution chemistry on the deposition and reentrainment of colloids in porous media, Environ. Sci. Technol. 37 (2003) 1122–1129.

[130] M.W. Hahn, D. Abadzic, C.R. O'Melia, Aquasols: On the role of secondary minima, Environ. Sci. Technol. 38 (2004) 5915–5924.

[131] M.W. Hahn, C.R. O'Melia, Deposition and reentrainment of Brownian particles in porous media under unfavorable chemical conditions: Some concepts and applications, Environ. Sci. Technol. 38 (2004) 210–220.

[132] S. Kamrani, M. Rezaei, M. Kord, M. Baalousha, Transport and retention of carbon dots (CDs) in saturated and unsaturated porous media: Role of ionic strength, pH, and collector grain size, Water Res. 133 (2018) 338–347.

[133] B. Gao, J.E. Saiers, J.N. Ryan, Deposition and mobilization of clay colloids in unsaturated porous media, Water Resour. Res. 40 (2004).

[134] D. Langmuir, Aqueous environmental, Prentice Hall, 1997.

[135] X. Li, P. Zhang, C.L. Lin, W.P. Johnson, Role of hydrodynamic drag on microsphere deposition and re-entrainment in porous media under unfavorable conditions, Environ. Sci. Technol. 39 (2005) 4012–4020.

[136] M. Tong, W.P. Johnson, Excess colloid retention in porous media as a function of colloid size, fluid velocity, and grain angularity, Environ. Sci. Technol. 40 (2006) 7725–7731.

[137] Z.A. Kuznar, M. Elimelech, Direct microscopic observation of particle deposition in porous media: Role of the secondary energy minimum, Colloids Surfaces A Physicochem. Eng. Asp. 294 (2007) 156–162.

[138] C. Zhang, A. Yan, G. Wang, C. Jin, Y. Chen, C. Shen, Impact of flow velocity on transport of graphene oxide nanoparticles in saturated porous media, Vadose Zo. J. 17 (2018).

[139] J. Hou, M. Zhang, P. Wang, C. Wang, L. Miao, Y. Xu, G. You, B. Lv, Y. Yang, Z. Liu, Transport and long-term release behavior of polymer-coated silver nanoparticles in saturated quartz sand: The impacts of input concentration, grain size and flow rate, Water Res. 127 (2017) 86–95.

[140] H. Li, Y. Zhao, Z. Han, M. Hong, Transport of sucrose-modified nanoscale zero-valent iron in saturated porous media: role of media size, injection rate and input concentration, Water Sci. Technol. 72 (2015) 1463–1471.

[141] Y. Zevi, A. Dathe, B. Gao, W. Zhang, B.K. Richards, T.S. Steenhuis, Transport and retention of colloidal particles in partially saturated porous media: Effect of ionic strength, Water Resour. Res. 45 (2009).

[142] S.A. Bradford, M. Bettahar, J. Simunek, M.T. Van Genuchten, Straining and attachment of colloids in physically heterogeneous porous media, Vadose Zo. J.

3 (2004) 384–394.

[143] X. Li, C.-L. Lin, J.D. Miller, W.P. Johnson, Role of grain-to-grain contacts on profiles of retained colloids in porous media in the presence of an energy barrier to deposition, Environ. Sci. Technol. 40 (2006) 3769–3774.

[144] S.A. Bradford, J. Simunek, S.L. Walker, Transport and straining of E. coli O157: H7 in saturated porous media, Water Resour. Res. 42 (2006).

[145] A.A. Keller, S. Sirivithayapakorn, Transport of colloids in unsaturated porous media: Explaining large-scale behavior based on pore-scale mechanisms, Water Resour. Res. 40 (2004).

[146] Q. Zhang, S.M. Hassanizadeh, N.K. Karadimitriou, A. Raoof, B. Liu, P.J. Kleingeld, A. Imhof, Retention and remobilization of colloids during steady-state and transient two-phase flow, 49 (2013) 8005–8016. https://doi.org/10.1002/2013WR014345.

[147] S. Torkzaban, S.A. Bradford, J.L. Vanderzalm, B.M. Patterson, B. Harris, H. Prommer, Colloid release and clogging in porous media: Effects of solution ionic strength and flow velocity, J. Contam. Hydrol. 181 (2015) 161–171.

[148] S.A. Bradford, H. Kim, Causes and implications of colloid and microorganism retention hysteresis, J. Contam. Hydrol. 138 (2012) 83–92.

[149] Y. Liu, D. Janjaroen, M.S. Kuhlenschmidt, T.B. Kuhlenschmidt, T.H. Nguyen, Deposition of Cryptosporidium parvum oocysts on natural organic matter surfaces: microscopic evidence for secondary minimum deposition in a radial stagnation point flow cell, Langmuir. 25 (2009) 1594–1605.

[150] P.R. Johnson, M. Elimelech, Dynamics of colloid deposition in porous media: Blocking based on random sequential adsorption, Langmuir. 11 (1995) 801–812.

[151] C. Wang, A.D. Bobba, R. Attinti, C. Shen, V. Lazouskaya, L.-P. Wang, Y. Jin,

Retention and transport of silica nanoparticles in saturated porous media: effect of concentration and particle size, Environ. Sci. Technol. 46 (2012) 7151–7158.

[152] Y. Liang, S.A. Bradford, J. Simunek, H. Vereecken, E. Klumpp, Sensitivity of the transport and retention of stabilized silver nanoparticles to physicochemical factors, Water Res. 47 (2013) 2572–2582.

[153] X. Jiang, M. Tong, R. Lu, H. Kim, Transport and deposition of ZnO nanoparticles in saturated porous media, Colloids Surfaces A Physicochem. Eng. Asp. 401 (2012) 29–37.

[154] X. Jiang, M. Tong, H. Kim, Influence of natural organic matter on the transport and deposition of zinc oxide nanoparticles in saturated porous media, J. Colloid Interface Sci. 386 (2012) 34–43.

[155] J.J. Lenhart, J.E. Saiers, Colloid mobilization in water-saturated porous media under transient chemical conditions, Environ. Sci. Technol. 37 (2003) 2780–2787.

[156] T. Li, Y. Jin, Y. Huang, B. Li, C. Shen, Observed dependence of colloid detachment on the concentration of initially attached colloids and collector surface heterogeneity in porous media, Environ. Sci. Technol. 51 (2017) 2811–2820.

[157] L.M. McDowell-Boyer, J.R. Hunt, N. Sitar, Particle transport through porous media, Water Resour. Res. 22 (1986) 1901–1921.

[158] X. Li, T.D. Scheibe, W.P. Johnson, Apparent decreases in colloid deposition rate coefficients with distance of transport under unfavorable deposition conditions: A general phenomenon, Environ. Sci. Technol. 38 (2004) 5616–5625.

[159] N. Tufenkji, J.A. Redman, M. Elimelech, Interpreting deposition patterns of microbial particles in laboratory-scale column experiments, Environ. Sci.

Technol. 37 (2003) 616–623.

[160] S.A. Bradford, J. Simunek, M. Bettahar, M.T. Van Genuchten, S.R. Yates, Significance of straining in colloid deposition: Evidence and implications, Water Resour. Res. 42 (2006).

[161] S. Xu, B. Gao, J.E. Saiers, Straining of colloidal particles in saturated porous media, Water Resour. Res. 42 (2006).

[162] S. Xu, J.E. Saiers, Colloid straining within water-saturated porous media: Effects of colloid size nonuniformity, Water Resour. Res. 45 (2009).

[163] A.A. Porubcan, S. Xu, Colloid straining within saturated heterogeneous porous media, Water Res. 45 (2011) 1796–1806.

[164] M.Y. Lin, H. Lindsay, D.A. Weitz, R.C. Ball, R. Klein, P. Meakin, Universality in colloid aggregation, Nature. 339 (1989) 360.

[165] S. Jungblut, A. Eychmüller, Modeling nanoparticle aggregation, (2019).

[166] S. Lazzari, Modeling simultaneous deposition and aggregation of colloids, Chem. Eng. Sci. 155 (2016) 469–481.

[167] P. Sandkühler, M. Lattuada, H. Wu, J. Sefcik, M. Morbidelli, Further insights into the universality of colloidal aggregation, Adv. Colloid Interface Sci. 113 (2005) 65–83.

[168] S. Jungblut, J.-O. Joswig, A. Eychmüller, Diffusion-and reaction-limited cluster aggregation revisited, Phys. Chem. Chem. Phys. 21 (2019) 5723–5729.

[169] E. Rosenbrand, I.L. Fabricius, H. Yuan, Thermally induced permeability reduction due to particle migration in sandstones: the effect of temperature on kaolinite mobilisation and aggregation, in: Proc. Thirty-Seventh Work. Geotherm. Reserv. Eng. Stanford Univ. Stanford, California, Jan, 2012.

[170] M.Y. Lin, H.M. Lindsay, D.A. Weitz, R. Klein, R.C. Ball, P. Meakin, Universal

diffusion-limited colloid aggregation, J. Phys. Condens. Matter. 2 (1990) 3093.

[171] M.Y. Lin, H.M. Lindsay, D.A. Weitz, R.C. Ball, R. Klein, P. Meakin, Universal reaction-limited colloid aggregation, Phys. Rev. A. 41 (1990) 2005.

[172] S. Lin, M.R. Wiesner, Deposition of Aggregated Nanoparticles A Theoretical and Experimental Study on the Effect of Aggregation State on the Affinity between Nanoparticles and a Collector Surface, Environ. Sci. Technol. 46 (2012) 13270–13277.

[173] T. Cosgrove, Colloid science: principles, methods and applications, John Wiley & Sons, 2010.

[174] C. Garing, J.A. de Chalendar, M. Voltolini, J.B. Ajo-Franklin, S.M. Benson, Pore-scale capillary pressure analysis using multi-scale X-ray micromotography, Adv. Water Resour. 104 (2017) 223–241. https://doi.org/10.1016/j.advwatres.2017.04.006.

[175] P. Sharma, H.M. Abdou, M. Flury, Effect of the Lower Boundary Condition and Flotation on Colloid Mobilization in Unsaturated Sandy Sediments, Vadose Zo. J. 7 (2008) 930. https://doi.org/10.2136/vzj2007.0163.

[176] A.I. Abdel-Fattah, M.S. El-Genk, Sorption of hydrophobic, negatively charged microspheres onto a stagnant air/water interface, J. Colloid Interface Sci. 202 (1998) 417–429.

[177] A.A. Keller, M. Auset, A review of visualization techniques of biocolloid transport processes at the pore scale under saturated and unsaturated conditions, Adv. Water Resour. 30 (2007) 1392–1407.

[178] A.I. Abdel-Fattah, M.S. El-Genk, On colloidal particle sorption onto a stagnant air–water interface, Adv. Colloid Interface Sci. 78 (1998) 237–266.

[179] S. Torkzaban, S.A. Bradford, M.T. van Genuchten, S.L. Walker, Colloid

transport in unsaturated porous media: The role of water content and ionic strength on particle straining, J. Contam. Hydrol. 96 (2008) 113–127. https://doi.org/10.1016/j.jconhyd.2007.10.006.

[180] T. Knappenberger, M. Flury, E.D. Mattson, J.B. Harsh, Does Water Content or Flow Rate Control Colloid Transport in Unsaturated Porous Media?, Environ. Sci. Technol. 48 (2014) 3791–3799. https://doi.org/10.1021/es404705d.

[181] S. Sirivithayapakorn, A. Keller, Transport of colloids in unsaturated porous media: A pore-scale observation of processes during the dissolution of air-water interface, Water Resour. Res. 39 (2003). https://doi.org/10.1029/2003WR002487.

[182] S.S. Thompson, M. V Yates, Bacteriophage inactivation at the air-water-solid interface in dynamic batch systems, Appl. Environ. Microbiol. 65 (1999) 1186–1190.

[183] J. Thompson, Prison theatre: Perspectives and practices, Jessica Kingsley Publishers London, 1998.

[184] J. Wan, T.K. Tokunaga, Film Straining of Colloids in Unsaturated Porous Media: Conceptual Model and Experimental Testing, Environ. Sci. Technol. 31 (1997) 2413–2420. https://doi.org/10.1021/es970017q.

[185] S. Veerapaneni, J. Wan, T.K. Tokunaga, Motion of particles in film flow, Environ. Sci. Technol. 34 (2000) 2465–2471.

[186] S.B. Roy, D.A. Dzombak, Colloid release and transport processes in natural and model porous media, Colloids Surfaces A Physicochem. Eng. Asp. 107 (1996) 245–262.

[187] T. Tosco, A. Tiraferri, R. Sethi, Ionic strength dependent transport of microparticles in saturated porous media: Modeling mobilization and

immobilization phenomena under transient chemical conditions, Environ. Sci. Technol. 43 (2009) 4425–4431.

[188] S. Torkzaban, H.N. Kim, J. Simunek, S.A. Bradford, Hysteresis of colloid retention and release in saturated porous media during transients in solution chemistry, Environ. Sci. Technol. 44 (2010) 1662–1669.

[189] J.J. Sheng, Critical review of low-salinity waterflooding, J. Pet. Sci. Eng. 120 (2014) 216–224.

[190] Z. Mesticou, M. Kacem, P. Dubujet, Influence of ionic strength and flow rate on silt particle deposition and release in saturated porous medium: experiment and modeling, Transp. Porous Media. 103 (2014) 1–24.

[191] S.A. Bradford, S. Torkzaban, H. Kim, J. Simunek, Modeling colloid and microorganism transport and release with transients in solution ionic strength, Water Resour. Res. 48 (2012).

[192] P. Bedrikovetsky, A. Zeinijahromi, F.D. Siqueira, C.A. Furtado, A.L.S. de Souza, Particle detachment under velocity alternation during suspension transport in porous media, Transp. Porous Media. 91 (2012) 173–197.

[193] C. Shen, V. Lazouskaya, H. Zhang, F. Wang, B. Li, Y. Jin, Y. Huang, Theoretical and experimental investigation of detachment of colloids from rough collector surfaces, Colloids Surfaces A Physicochem. Eng. Asp. 410 (2012) 98–110.

[194] Y. Du, C. Shen, H. Zhang, Y. Huang, Effects of flow velocity and nonionic surfactant on colloid straining in saturated porous media under unfavorable conditions, Transp. Porous Media. 98 (2013) 193–208.

[195] C. Lu, Y. Wu, S. Hu, M.A. Raza, Y. Fu, Mobilization and transport of metal-rich colloidal particles from mine tailings into soil under transient chemical and physical conditions, Environ. Sci. Pollut. Res. 23 (2016) 8021–8034.

[196] G. Bin, X. Cao, Y. Dong, Y. Luo, L.Q. Ma, Colloid deposition and release in soils and their association with heavy metals, Crit. Rev. Environ. Sci. Technol. 41 (2011) 336–372.

[197] O.H. Jacobsen, P. Moldrup, C. Larsen, L. Konnerup, L.W. Petersen, Particle transport in macropores of undisturbed soil columns, J. Hydrol. 196 (1997) 185–203.

[198] T. Tosco, J. Bosch, R.U. Meckenstock, R. Sethi, Transport of ferrihydrite nanoparticles in saturated porous media: role of ionic strength and flow rate, Environ. Sci. Technol. 46 (2012) 4008–4015.

[199] S.B. Roy, D.A. Dzombak, Sorption nonequilibrium effects on colloid-enhanced transport of hydrophobic organic compounds in porous media, J. Contam. Hydrol. 30 (1998) 179–200.

[200] D. Grolimund, M. Borkovec, Long-term release kinetics of colloidal particles from natural porous media, Environ. Sci. Technol. 33 (1999) 4054–4060.

[201] J.E. Saiers, G.M. Hornberger, The influence of ionic strength on the facilitated transport of cesium by kaolinite colloids, Water Resour. Res. 35 (1999) 1713–1727.

[202] C. Kjaergaard, P. Moldrup, L.W. De Jonge, O.H. Jacobsen, Colloid mobilization and transport in undisturbed soil columns. II. The role of colloid dispersibility and preferential flow, Vadose Zo. J. 3 (2004) 424–433.

[203] E. Pazmino, J. Trauscht, W.P. Johnson, Release of colloids from primary minimum contact under unfavorable conditions by perturbations in ionic strength and flow rate, Environ. Sci. Technol. 48 (2014) 9227–9235.

[204] W.P. Johnson, M. Hilpert, Upscaling colloid transport and retention under unfavorable conditions: Linking mass transfer to pore and grain topology, Water

Resour. Res. 49 (2013) 5328–5341.

[205] W.P. Johnson, X. Li, M. Tong, H. Ma, Comment on “Transport and fate of bacteria in porous media: Coupled effects of chemical conditions and pore space geometry” by Saeed Torkzaban et al., Water Resour. Res. 45 (2009).

[206] S. Torkzaban, S.A. Bradford, J. Wan, T. Tokunaga, A. Masoudih, Release of quantum dot nanoparticles in porous media: role of cation exchange and aging time, Environ. Sci. Technol. 47 (2013) 11528–11536.

[207] N. Tufenkji, M. Elimelech, Deviation from the classical colloid filtration theory in the presence of repulsive DLVO interactions, Langmuir. 20 (2004) 10818–10828.

[208] Y. Yang, F.D. Siqueira, A.S.L. Vaz, Z. You, P. Bedrikovetsky, Slow migration of detached fine particles over rock surface in porous media, J. Nat. Gas Sci. Eng. 34 (2016) 1159–1173. https://doi.org/10.1016/j.jngse.2016.07.056.

[209] L. Chequer, A. Vaz, P. Bedrikovetsky, Injectivity decline during low-salinity waterflooding due to fines migration, J. Pet. Sci. Eng. (2018) 1–19. https://doi.org/10.1016/j.petrol.2018.01.012.

[210] F. Huang, Y. Kang, Z. You, L. You, C. Xu, Critical conditions for massive fines detachment induced by single-phase flow in coalbed methane reservoirs: modeling and experiments, Energy & Fuels. 31 (2017) 6782–6793.

[211] V.L. Morales, B. Gao, T.S. Steenhuis, Grain surface-roughness effects on colloidal retention in the vadose zone, Vadose Zo. J. 8 (2009) 11–20.

[212] C. Jin, T. Glawdel, C.L. Ren, M.B. Emelko, Non-linear, non-monotonic effect of nano-scale roughness on particle deposition in absence of an energy barrier: Experiments and modeling, Sci. Rep. 5 (2015) 17747.

[213] R.D. Duffadar, J.M. Davis, Interaction of micrometer-scale particles with

nanotextured surfaces in shear flow, J. Colloid Interface Sci. 308 (2007) 20–29.

[214] R.D. Duffadar, J.M. Davis, Dynamic adhesion behavior of micrometer-scale particles flowing over patchy surfaces with nanoscale electrostatic heterogeneity, J. Colloid Interface Sci. 326 (2008) 18–27.

[215] E. Pazmino, J. Trauscht, B. Dame, W.P. Johnson, Power law size-distributed heterogeneity explains colloid retention on soda lime glass in the presence of energy barriers, Langmuir. 30 (2014) 5412–5421.

[216] W.P. Johnson, A. Rasmuson, E. Pazmiño, M. Hilpert, Why variant colloid transport behaviors emerge among identical individuals in porous media when colloid–surface repulsion exists, Environ. Sci. Technol. 52 (2018) 7230–7239.

[217] R. Duffadar, S. Kalasin, J.M. Davis, M.M. Santore, The impact of nanoscale chemical features on micron-scale adhesion: Crossover from heterogeneity-dominated to mean-field behavior, J. Colloid Interface Sci. 337 (2009) 396–407.

[218] K.C. Khilar, H.S. Fogler, The existence of a critical salt concentration for particle release, J. Colloid Interface Sci. 101 (1984) 214–224.

[219] T. Russell, D. Pham, M.T. Neishaboor, A. Badalyan, A. Behr, L. Genolet, P. Kowollik, A. Zeinijahromi, P. Bedrikovetsky, Effects of kaolinite in rocks on fines migration, J. Nat. Gas Sci. Eng. 45 (2017) 243–255. https://doi.org/10.1016/j.jngse.2017.05.020.

[220] A. Zeinijahromi, R. Farajzadeh, J. Bruining, P. Bedrikovetsky, Effect of fines migration on oil-water relative permeability during two-phase flow in porous media, Fuel. 176 (2016) 222–236. https://doi.org/10.1016/j.fuel.2016.02.066.

[221] C. Kim, J. Lee, Experimental study on the variation of relative permeability due to clay minerals in low salinity water-flooding, J. Pet. Sci. Eng. 151 (2017) 292–304.

[222] F. Hussain, A. Zeinijahromi, P. Bedrikovetski, A. Badalyan, T. Carageorgos, Y. Cinar, Enhanced Oil Recovery Through Low Salinity Fines-Assisted Waterflooding: Laboratory and Mathematical Modelling, SPE Asia Pacific Oil Gas Conf. Exhib. (2014). https://doi.org/10.2118/171525-MS.

[223] A.K. Alhuraishawy, B. Bai, M. Wei, J. Geng, J. Pu, Mineral dissolution and fine migration effect on oil recovery factor by low-salinity water flooding in low-permeability sandstone reservoir, Fuel. 220 (2018) 898–907. https://doi.org/10.1016/j.fuel.2018.02.016.

[224] B.A. Macler, J.C. Merkle, Current knowledge on groundwater microbial pathogens and their control, Hydrogeol. J. 8 (2000) 29–40.

[225] S.A. Bradford, S. Torkzaban, Determining parameters and mechanisms of colloid retention and release in porous media, Langmuir. 31 (2015) 12096–12105.

[226] S.A. Bradford, S. Torkzaban, Colloid adhesive parameters for chemically heterogeneous porous media, Langmuir. 28 (2012) 13643–13651.

[227] S.A. Bradford, S. Torkzaban, J. Simunek, Modeling colloid transport and retention in saturated porous media under unfavorable attachment conditions, Water Resour. Res. 47 (2011).

[228] S.A. Bradford, S. Torkzaban, S.L. Walker, Coupling of physical and chemical mechanisms of colloid straining in saturated porous media, Water Res. 41 (2007) 3012–3024.

[229] J. Zhuang, J.S. Tyner, E. Perfect, Colloid transport and remobilization in porous media during infiltration and drainage, J. Hydrol. 377 (2009) 112–119. https://doi.org/10.1016/j.jhydrol.2009.08.011.

[230] J.E. Saiers, G.M. Hornberger, D.B. Gower, J.S. Herman, The role of moving air-

water interfaces in colloid mobilization within the vadose zone, Geophys. Res. Lett. 30 (2003).

[231] J. Noordmans, P.J. Wit, H.C. Van Der Mei, H.J. Busscher, Detachment of polystyrene particles from collector surfaces by surface tension forces induced by air-bubble passage through a parallel plate flow chamber, J. Adhes. Sci. Technol. 11 (1997) 957–969.

[232] C.G. Suárez, J. Noordmans, H.C. van der Mei, H.J. Busscher, Detachment of colloidal particles from collector surfaces with different electrostatic charge and hydrophobicity by attachment to air bubbles in a parallel plate flow chamber, Phys. Chem. Chem. Phys. 1 (1999) 4423–4427.

[233] F.P. Bretherton, The motion of long bubbles in tubes, J. Fluid Mech. 10 (1961) 166–188.

[234] M.T. Kreutzer, F. Kapteijn, J.A. Moulijn, J.J. Heiszwolf, Multiphase monolith reactors: chemical reaction engineering of segmented flow in microchannels, Chem. Eng. Sci. 60 (2005) 5895–5916.

[235] D. Quéré, Fluid coating on a fiber, Annu. Rev. Fluid Mech. 31 (1999) 347–384.

[236] P. Kralchevsky, K. Nagayama, Particles at fluid interfaces and membranes, Elsevier Science Amsterdam, 2001.

[237] P.A. Kralchevsky, V.N. Paunov, I.B. Ivanov, K. Nagayama, Capillary meniscus interaction between colloidal particles attached to a liquid—fluid interface, J. Colloid Interface Sci. 151 (1992) 79–94.

[238] J. Shang, M. Flury, J.B. Harsh, R.L. Zollars, Comparison of different methods to measure contact angles of soil colloids, J. Colloid Interface Sci. 328 (2008) 299–307.

[239] T. Cheng, J.E. Saiers, Mobilization and transport of in situ colloids during

drainage and imbibition of partially saturated sediments, Water Resour. Res. 45 (2009) 1–14. https://doi.org/10.1029/2008WR007494.

[240] L. Chen, D.A. Sabatini, T.C.G. Kibbey, Role of the air–water interface in the retention of TiO2 nanoparticles in porous media during primary drainage, Environ. Sci. Technol. 42 (2008) 1916–1921.

[241] H.L. Weissberg, Effective diffusion coefficient in porous media, J. Appl. Phys. 34 (1963) 2636–2639.

[242] N. Otsu, A threshold selection method from gray-level histograms, IEEE Trans. Syst. Man. Cybern. 9 (1979) 62–66.

[243] A. Asundi, Z. Wensen, Fast phase-unwrapping algorithm based on a gray-scale mask and flood fill, Appl. Opt. 37 (1998) 5416–5420.

[244] E. Joseph, G. Singhvi, Multifunctional nanocrystals for cancer therapy: a potential nanocarrier, in: Nanomater. Drug Deliv. Ther., Elsevier, 2019: pp. 91–116.

[245] A. Kumar, C.K. Dixit, Methods for characterization of nanoparticles, in: Adv. Nanomedicine Deliv. Ther. Nucleic Acids, Elsevier, 2017: pp. 43–58.

[246] P. Zhang, B. Bai, S. Jiang, P. Wang, H. Li, Transport and deposition of suspended particles in saturated porous media: effect of hydrodynamic forces and pore structure, Water Sci. Technol. Water Supply. 16 (2016) 951–960.

[247] W.P. Johnson, X. Li, G. Yal, Colloid retention in porous media: Mechanistic confirmation of wedging and retention in zones of flow stagnation, Environ. Sci. Technol. 41 (2007) 1279–1287.

[248] L. Chequer, P. Bedrikovetsky, T. Carageorgos, A. Badalyan, V. Gitis, Mobilization of Attached Clustered Colloids in Porous Media, Water Resour. Res. 55 (2019) 5696–5714.

[249] J.N. Israelachvili, Intermolecular and surface forces, Academic press, 2015.

[250] M.L. Fielden, R.A. Hayes, J. Ralston, Surface and capillary forces affecting air bubble− particle interactions in aqueous electrolyte, Langmuir. 12 (1996) 3721–3727.

[251] D.J. Johnson, N.J. Miles, N. Hilal, Quantification of particle–bubble interactions using atomic force microscopy: A review, Adv. Colloid Interface Sci. 127 (2006) 67–81.

[252] B. Albijanic, O. Ozdemir, A. V Nguyen, D. Bradshaw, A review of induction and attachment times of wetting thin films between air bubbles and particles and its relevance in the separation of particles by flotation, Adv. Colloid Interface Sci. 159 (2010) 1–21.

[253] M. Flury, S. Aramrak, Role of air-water interfaces in colloid transport in porous media: A review, Water Resour. Res. 53 (2017) 5247–5275.

[254] P. Knüpfer, J. Fritzsche, T. Leistner, M. Rudolph, U.A. Peuker, Investigating the removal of particles from the air/water-interface–Modelling detachment forces using an energetic approach, Colloids Surfaces A Physicochem. Eng. Asp. 513 (2017) 215–222.

[255] N. Ishida, Direct measurement of hydrophobic particle–bubble interactions in aqueous solutions by atomic force microscopy: effect of particle hydrophobicity, Colloids Surfaces A Physicochem. Eng. Asp. 300 (2007) 293–299.

[256] D.F. Williams, J.C. Berg, The aggregation of colloidal particles at the air—water interface, J. Colloid Interface Sci. 152 (1992) 218–229.

[257] D. Ershov, J. Sprakel, J. Appel, M.A.C. Stuart, J. van der Gucht, Capillarity-induced ordering of spherical colloids on an interface with anisotropic curvature, Proc. Natl. Acad. Sci. 110 (2013) 9220–9224.

[258] S. Das, J. Koplik, R. Farinato, D.R. Nagaraj, C. Maldarelli, P. Somasundaran, The Translational and Rotational Dynamics of a Colloid Moving Along the Air-Liquid Interface of a Thin Film, Sci. Rep. 8 (2018) 8910.

[259] J. Shang, M. Flury, Y. Deng, Force measurements between particles and the air-water interface: Implications for particle mobilization in unsaturated porous media, Water Resour. Res. 45 (2009).

[260] S. Aramrak, M. Flury, J.B. Harsh, R.L. Zollars, H.P. Davis, Does colloid shape affect detachment of colloids by a moving air-water interface?, Langmuir. 29 (2013) 5770–5780. https://doi.org/10.1021/la400252q.

[261] B.H.-P. Cheong, T.W. Ng, Y. Yu, O.W. Liew, Using the meniscus in a capillary for small volume contact angle measurement in biochemical applications, Langmuir. 27 (2011) 11925–11929.

[262] E. Al-Zaidi, X. Fan, Effect of aqueous electrolyte concentration and valency on contact angle on flat glass surfaces and inside capillary glass tubes, Colloids Surfaces A Physicochem. Eng. Asp. 543 (2018) 1–8.

[263] B. Wei, J. Ning, J. He, L. Lu, Y. Wang, L. Sun, Relation between brine-crude oil-quartz contact angle formed on flat quartz slides and in capillaries with brine composition: Implications for low-salinity waterflooding, Colloids Surfaces A Physicochem. Eng. Asp. 555 (2018) 660–667.

[264] A.L. Herring, F.J. Gilby, Z. Li, J.E. McClure, M. Turner, J.P. Veldkamp, L. Beeching, A.P. Sheppard, Observations of nonwetting phase snap-off during drainage, Adv. Water Resour. 121 (2018) 32–43.

[265] L. Yu, N.C. Wardlaw, The influence of wettability and critical pore-throat size ratio on snap—off, J. Colloid Interface Sci. 109 (1986) 461–472.

[266] H. Auld, D. MacIver, J. Klaassen, Heavy rainfall and waterborne disease

outbreaks: the Walkerton example, J. Toxicol. Environ. Heal. Part A. 67 (2004) 1879–1887.

[267] F.C. Curriero, J.A. Patz, J.B. Rose, S. Lele, The association between extreme precipitation and waterborne disease outbreaks in the United States, 1948–1994, Am. J. Public Health. 91 (2001) 1194–1199.

[268] A.B. Kenst, E. Perfect, S.W. Wilhelm, J. Zhuang, J.F. McCarthy, L.D. McKay, Virus transport during infiltration of a wetting front into initially unsaturated sand columns, Environ. Sci. Technol. 42 (2008) 1102–1108.

[269] M. Elimelech, C.R. O'Melia, Kinetics of deposition of colloidal particles in porous media, Environ. Sci. Technol. 24 (1990) 1528–1536.

[270] N. Tufenkji, M. Elimelech, Spatial distributions of Cryptosporidium oocysts in porous media: Evidence for dual mode deposition, Environ. Sci. Technol. 39 (2005) 3620–3629.

APPENDIX

Description of the Supplementary material

Movie 1.avi: shows the mobile colloids interacting with GWI and attachment occur due to hydrophobic interaction. The effect of hydrodynamics near GWI on colloid movement near GWI is visible from the distracted colloids due to flow reversal near the solid phase.

Movie 2.avi: shows the detachment of deposited colloids by the moving GWI and subsequently retained on GWI, GWSI, and thin films.

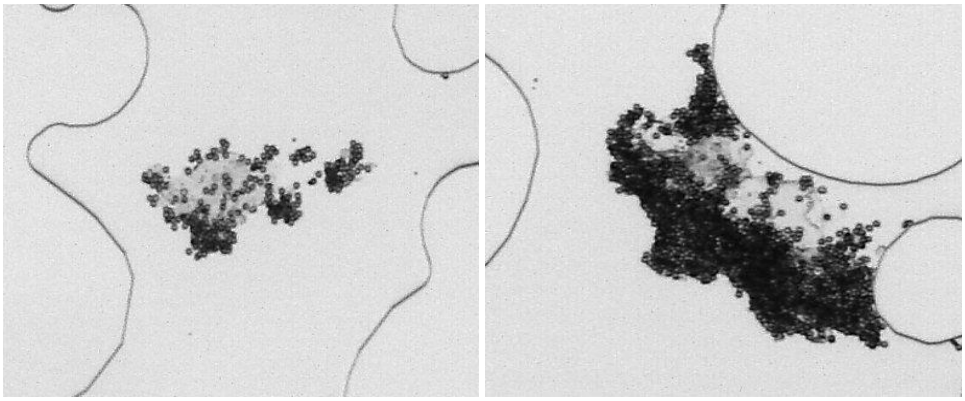

Figure A1: Colloids favorably attached to the surface heterogeneity formed by the presence of impurities in the micromodel during the experiment (dust or other suspended particles other than colloids in the injecting solution).

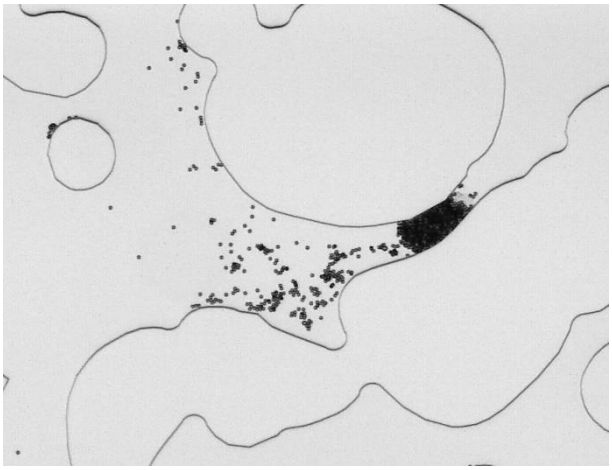

Figure A2: Colloid deposition in the micromodel at low-flow zones (created by pore-blocking) for PS_100mM.

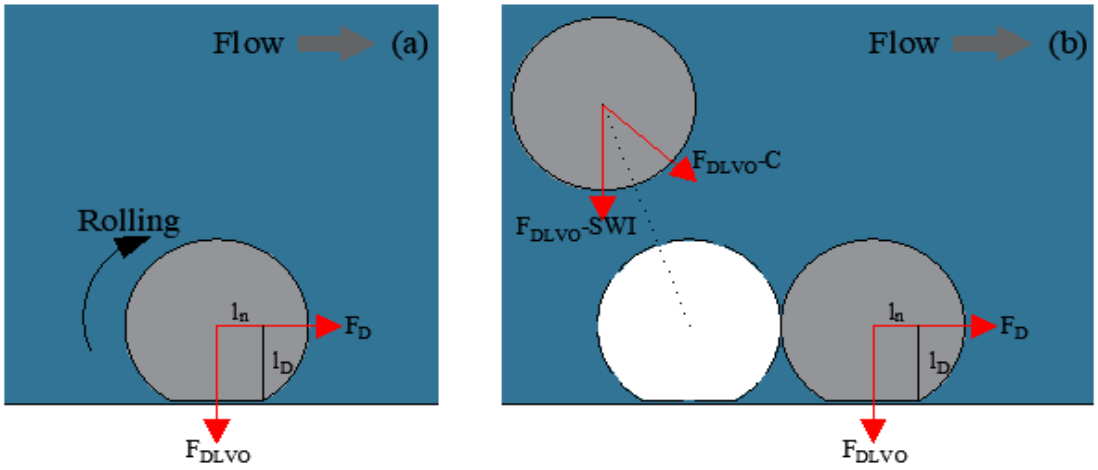

Figure A3: (a) Schematic of attachment and detachment forces acting on a single colloid and the lever arms, (b) attachment of the second colloid under colloid-colloid attraction condition

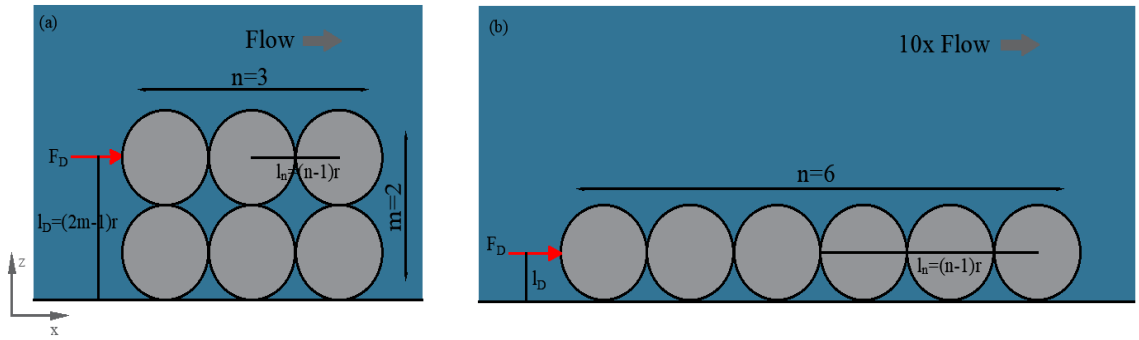

Figure A4: (a) Mechanical equilibrium of the attached multilayer cluster of colloids, (b) re-alignment of the clusters in response to 10x increase in flow velocity to reduce the detachment torque

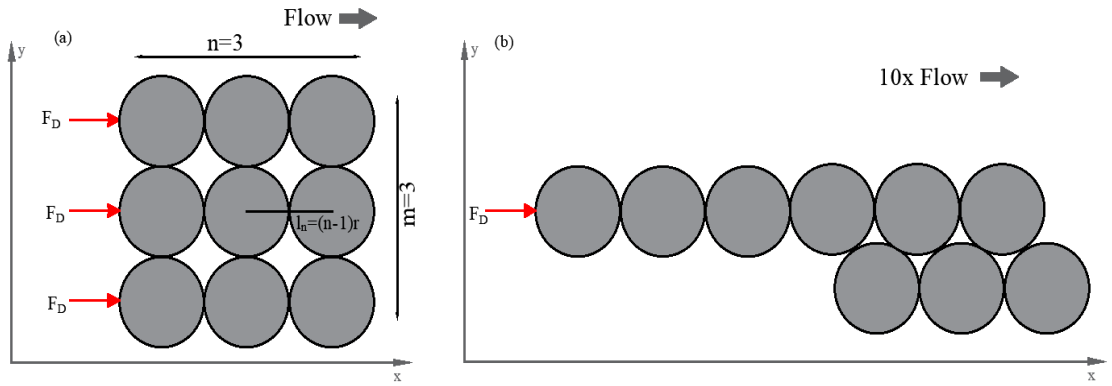

Figure A5: (a) Mechanical equilibrium of the attached monolayer cluster of colloids, (b) re-alignment of the clusters in response to 10x increase in flow velocity to reduce the detachment torque